Evolution and development in Spiralia: Early progeny of the mesodermal lineage in the leech *Helobdella* sp. (Austin)

By

Stephanie Eve Gline

A dissertation submitted in partial satisfaction of the

requirements for the degree of

Doctor of Philosophy

in

Molecular and Cell Biology

in the

Graduate Division

of the

University of California, Berkeley

Committee in charge:

Professor David A. Weisblat, Chair
Professor Sharon Amacher
Professor Karsten Weis
Professor Britt Glaunsinger

Spring 2010

Abstract

Evolution and development in Spiralia: Early progeny of the mesodermal lineage in the leech *Helobdella* sp. (Austin):

By

Stephanie Eve Gline

Doctor of Philosophy in Mollecular and Cell Biology

University of California, Berkeley

Professor David A. Weisblat, Chair

One of the major questions in evolutionary biology is, how changes in development over time result in diversity of adult body plans. Spiralia are a highly diverse group of protostome taxa, in terms of their adult body plans, but which nonetheless share a highly conserved pattern of early cell divisions, called spiral cleavage. Thus, in the early embryos of spiralian taxa, homologous blastomeres are identifiable on the basis of their embryonic origins and their subsequent fates in later development. One of the best-known examples of such homologous blastomeres are the precursors of left and right mesoderm, which arise from the bilateral division of a cell classically known as micromere 4d. Given the dramatic differences among body plans of various spiralian species (consider the mesoderm of an unsegmented mollusk and that of a segmented annelid, such as the leech, for example), it is obvious that the 4d lineages must diverge at some point in development of different species.

In the leech *Helobdella,* a clitellate annelid, the homolog of the cell 4d is called DM" and its bilateral division gives rise to two large stem cells (M teloblasts) whose iterated divisions yield precursors (m blast cells) of segmental mesoderm. In this work I present new plasmid driven high-resolution cell lineage tracing techniques. Using high-resolution tracers in conjunction with standard tracers, I have been able to study the early progeny of the M teloblasts in great detail. I have found that each M teloblast produces six precursors of non-segmental mesoderm, prior to initiating the production of purely segmental blast cells. While all segmental blast cells undergo identical stereotyped early divisions and give rise to homologous definitive pattern elements, the early clonal distributions of the first six cells, as well as their definitive contributions differ from each other and from the segmental blast cells. The early mesodermal progeny make major contributions to anterior non-segmental mesoderm especially throughout the head and the muscular proboscis, an eversible, specialized feeding apparatus.

Collaborative work with Ayaki Nakamoto on more detailed analysis of the 4d lineage in the oligochaete *Tubifex* revealed that, in this annelid too, the 4d lineage makes contributions to anterior non-segmental mesoderm. However, unlike *Helobdella*, *Tubifex* ingest sediments and are filter feeders, and thus have different head and foregut morphology. In accord with these differences, I find that the anterior contributions of the M lineage differ between these two

annelids. These differences illustrate that the 4d lineage exhibits evolutionary plasticity and that potentially small changes in the developmental program of the M teloblasts can result in a diversity of adult body plans.

Acknowledgements

Many thanks to all of the Weisblat lab members, Foster Gonsalves, Ajna Rivera, Deidre Lyons, Dian-Han Kuo, Sung-Jin Cho and Yvonne Valles who answered my countless, and often repeated questions, helped me make sense of my data and with troubleshooting. Thank you to Sung-Jin for collaborating with me and helping me find molecular markers for cells in the proboscis and for doing difficult fluorescent in situs. Dian-Han, thank you for being endlessly patient, knowing everything there is to know about leeches and biology, for answering my questions even if you were in the middle of an experiment, helping me clone tricky genes, troubleshoot and for editing all of my writing. Dede thank you for knowing all things spiralian and for being able to explain it all to me over and over again. Thanks to Ayaki Nakamoto for a terrific collaboration. I am constantly amazed by your ability to handle and inject *Tubifex* embryos. Thanks to the Levine lab for very generously letting me use the confocal for hours and hours. Thanks to all my friends without whom I would be way crazier than I already am! Jasmine, thanks for keeping me sane during hours and hours and hours of thesis writing, Roberta thanks for motivating me to exercise especially up many hills and taking me in for dinner on nights I would have otherwise just eaten eggs…again. Thanks to my family who always came to visit me, took me to all the restaurants I had been wanting to go to and who saw me through much science and health related frustrations. I could not have gotten through this without you. David, thanks for introducing me to the fascinating leech embryo and for making me a much better speaker (and for helping me lose the upspeak), writer, critical thinker and flat tire fixer and for putting my bike up every day.

TABLE OF CONTENTS

Chapter 1: Introduction

Introduction	**1**
Figures	**10-12**

Chapter 2: High-resolution cell lineage tracing reveals developmental variability in leech

Introduction	**13**
Results	**14**
Discussion	**20**
Figures	**23-36**

Chapter 3: Early progeny of the mesodermal lineage in the leech *Helobdella* sp. (Austin) and the oligochaete *Tubifex tubifex*

Introduction	**37**
Results	**38**
Discussion	**51**
Figures	**54-78**

Chapter 4: Notch signaling during leech development

Introduction	**79**
Results	**81**
Discussion	**84**
Figures	**85-96**

Materials and methods **97-101**

References **102-110**

LIST OF FIGURES

1.1. Summary of relevant aspects of leech development. **10**

1.2. Schematic showing the tissue organization of the proboscis in the stage 10 embryo and adult in *Helobdella*. **12**

2.1. Early divisions in the O lineage. **23**

2.2. Expression of H2B:GFP in the DNOPQ^{x} and DM^{x} lineages. **24**

2.3. Range of mosaicism of pEF-H2B:GFP expression in the NOPQ lineage. 26

2.4. Expression of pEF-H2B:GFP in the O lineage. 29

2.5. Frames from time-lapse movies capturing divisions of primary p and q.f blast cells. 31

2.6. Stereotyped development in the early O lineage. 32

2.7. Variability in the o.appl/m lineage. 33

2.8. Comparison of transcript distributions resulting from plasmid and mRNA injections. 34

2.9. Plasmid-driven transgene expression in a micromere lineage. 36

3.1. Distributions of individual sm cell clones. 54

3.2. Mesodermal lineage during cleavage and segmentation stages. 56

Figure 3.3. Blastocoel deformation of the M teloblasts during early blast cell production. 58

Figure 3.4. DM" makes large contributions to the prostomium of the late stage embryo. 60

Figure 3.5. DM" contributions in relation to the body segments. 61

Figure 3.6. Mesodermal and ectodermal lineages begin segmental blast cell production at approximately the same time. 62

Figure 3.7. Six cells are born from each M teloblast prior to stage 6b. 64

Figure 3.8. Clonal distributions of early m lineages. 66

Figure 3.9. Proliferation rates of early mesodermal lineages at 2 and 3 days clonal age. 68

Figure 3.10. The early mesodermal lineages make unique definitive contributions. 69

Figure 3.11. Similar to that of sm cells, the primary division of em6 is bilateral. 71

Figure 3.12. Alignment of segmentally contributing ectodermal and mesodermal lineages during development. 73

Figure 3.13. The DM" lineage contributes to the proboscis as well as to musculature throughout the proboscis sheath. 74

Figure 3.14. Morphology of late stage *Tubifex* embryos. 76

Figure 3.15. 4d lineage in *Tubifex* throughout development. 77

Figure 4.1. Alignment of conserved domains of hairy and Enhancer of split related family members. 85

Figure 4.2. *Hau-hes* expression during stage 8. 87

Figure 4.3. Developmental RT-PCR for Notch pathway members at stages 1-10. 88

Figure 4.4. Nucleotide and protein sequence of *Hau-hes2*. 89

Figure 4.5. Expression of *Hau-hes2* during stages 8 and 9. 90

Figure 4.6. Nucleotide and protein sequence of *Hau-hey*. 91

Figure 4.7. Expression of *Hau-hey* during development. 92

Figure 4.8. Early *Hau-hey* expression in the segmental precursors is first restricted to the N lineage and then expands to the other ectodermal lineages during stage 8-9. 93

Figure 4.9. Expression of *Hro-notch* during stages late 7 to late 8. 94

Figure 4.10. *Hau-suH*, *Hau-ser* and *Hau-notch* show similar domains of expression during late stage 7 through stage 8. 95

LIST OF TABLES

Table 2.1: I-SceI digestion increases mosaicism of plasmid-driven transgene expression. 28

Table 4.1 Notch pathway members found in the *H. robusta* genome sequence. 86

CHAPTER ONE

Introduction

Metazoan animals develop from single-cell zygotes. Thus, the diversity of adult body plans reflects the accumulation of differences in developmental programs across taxa over evolutionary time. To understand these changes it is important to compare the development of diverse animals in their phylogenetic context.

A paradox in evolutionary developmental biology is that while animals exhibit vast morphological diversity, they all share similar complements of genes. Moreover, recent phylogenetic studies using molecular datasets have upended many long-held hypotheses on the relationships among animals (Halanych et al., 1995; Aguinaldo, 1997; Dunn et al., 2008). The emerging consensus is that bilaterally symmetric animals fall into three major superphyla; one clade of moulting animals, uniting arthropods and nematodes (Ecdysozoa), one grouping lophophorates, mollusks and annelids together (Lophotrochozoa) and one uniting chordates, echinoderms and hemichordates (Deuterostomia). Each of these three super-phyla include both segmented and unsegmented members, raising more questions concerning the origins of segmentation than resolving previous ones.

Compared to Deuterostomia and Edysozoa, Lophotrochozoa, a highly diverse and successful group, remain understudied. Many of the lophotrochozoan taxa are characterized by a homologous early cleavage program called spiral cleavage, now hypothesized to be the ancestral mode of embryonic development of this group, with presumed losses among several phyla (Dunn et al., 2008). Spiralians include mollusks, annelids, polyclad turbellarians, nemerteans and entoprocts, which share strikingly similar early blastomere geometries. Typical spiralian embryos are analyzed in terms of four quadrants (A, B, C and D), each of which is defined as comprising the progeny of the eponymous blastomere in the four-cell embryo. The A and C quadrants commonly give rise to left lateral and right lateral tissue respectively, while B and D quadrants often make ventral anterior and dorsal posterior contributions respectively (Henry and Martindale, 1999). In particular, at sixth cleavage, the D quadrant of virtually all spiralian embryos yields a cell classically known as micromere 4d, which is the precursor of the bilaterally symmetric mesoderm, and is a an example of homology at the cellular level, without parallel in the rest of metazoan development. The 4d lineage is central to my dissertation and will be discussed in detail below.

The spiral cleavage mode of early development is characterized by asymmetric cell divisions at oblique angles, with quartets of smaller, animal, daughter cells (micromeres) alternatively born in clockwise, and counterclockwise directions with respect to the underlying vegetal sister cells (macromeres). These cleavages are highly stereotyped within species, however there is interspecies variation among spiralians including, in the degree of asymmetry, the direction (initially clockwise vs. counterclockwise) as well as the timing, of the divisions (Boyer et al., 1998; Lambert, 2010). Therefore, while the lineages of spiralians are homologous based on cell position and fate, the embryos can look fairly dissimilar. Despite morphological differences amongst spiralian embryos, their high conservation of stereotyped cleavages has resulted in the development of a standard nomenclature used to identify homologous lineages in this diverse group (Conklin, 1897; Costello and Henley, 1976).

Coupled with the tremendous diversity of adult morphologies, the conserved early cleavage patterns of spiralian embryos provides a powerful system for comparing development in homologous lineages and thus determining the developmental sources of adult body plan diversity. As more comparative lineage tracing is being done across spiralians, it is becoming abundantly clear that there is extensive variation across homologous lineages (Boyer et al., 1998; Dohle, 1999; Henry and Martindale, 1999). Therefore, spiralians are an ideal group of organisms in which to ask how changes in development over time lead to diversity of adult body plans. Here I will be focusing on the lineage analysis of cell 4d (known as DM" in leech) across spiralians in order to elucidate changes in this lineage during evolution that are reflected in the diversity seen across spiralian taxa. My major finding was that in addition to giving rise to all the segmental mesoderm, the DM" lineage also makes major contributions to mesoderm throughout the head of the leech *Helobdella*. Additionally I have shown that the homologous lineage in the segmented oligochaete worm *Tubifex* also makes anterior prostomial contributions though strikingly different in final morphology than those in the leech. Therefore the 4d lineage exhibits evolutionary plasticity even within the clitellate annelids.

Stereotyped lineage-driven segmentation in the leech

The leech *Helobdella*, is a representative annelid model, useful in understanding the process of lineage-driven segmentation and in making comparisons among segmented animals across the phylogenetic tree. It is also useful for comparing development among spiralians. Developmental mechanisms underlying segmentation vary greatly across bilaterians. Idealized generalizations describe three basic modes of segmentation: simultaneous segmentation, sequential segmentation and combinations of the two. In simultaneous segmentation, as classically described in *Drosophila*, all segments along the anterior posterior axis are specified at once. In addition to these different temporal modes of segmentation, we can also distinguish two different models for generating the spatial repeating morphology associated with segmentation, namely boundary-driven and lineage-driven segmentation. In boundary-driven segmentation, typified by vertebrate somitogenesis, an apparently homogenous field of cells is divided into discrete units. Once the boundaries are in place, the resulting body plan is recognized as segmented if a similar morphogenetic program unfolds within each unit. In addition to vertebrates, many arthropods also exhibit boundary driven segmentation.

In contrast, the leech *Helobdella* is a model example of lineage-driven segmentation. In *Helobdella*, each segmental lineage produces a column (bandlet) of cells (blast cells). The lineage of origin dictates the early division patterns and definitive contributions of the blast cells. Each blast cell within a bandlet, behaves identically, dividing at a precise clonal age, undergoing identical division patterns, and generating a similar clone of definitive progeny, whose position along the anterior-posterior axis is determined by the birth order of its blast cell of origin. Repeating such stereotyped lineages along the A-P axis generates morphologically recognizable segments, even though adjacent clones interdigitate (see Figure 3.1 for an example of this in the M lineage).

Summary of leech development

Early leech development proceeds via a modified version of spiral cleavage (Whitman, 1878; Bissen and Weisblat, 1989; Dohle, 1999) that generates 25 micromeres, 3 macromeres and 10 segmentation stem cells (teloblasts; Fig. 1.1). Micromere lineages contribute progeny to prostomial tissue and to provisional and definitive epidermis (Weisblat et al., 1984; Nardelli-Haefliger and Shankland, 1993; Huang et al., 2002). Segmental ectoderm, and mesoderm are derived from the five bilateral pairs of teloblasts (Fig. 1.1A; Weisblat et al., 1980; Shankland and Savage, 1997); each teloblast lineage contributes a stereotyped, segmentally iterated complement of progeny. Teloblasts undergo iterated highly asymmetric divisions with cell cycle durations of about 75 to 120 minutes, depending on the lineage, to produce columns of segmental founder cells (blast cells), which coalesce ipsilaterally to form germinal bands (Fig. 1.1). The left and right germinal bands join at their anterior ends and move over the surface of the embryo, coalescing into a bilaterally symmetric germinal plate, from which the segmental tissues differentiate (Fig. 1.1A). In *Helobdella*, the early blastomeres are amenable to microinjection and with few exceptions, early development proceeds via determinate lineages (Bissen and Weisblat, 1989; Smith and Weisblat, 1994; Huang et al., 2002).

The mesodermal precursor 4d (DM") and its specification across spiralians

One of the most strikingly similar, and well-studied, of the conserved lineages amongst spiralians is the one that will give rise to the majority of the mesoderm. This lineage is commonly derived from the 4th micromere born from the D quadrant, classically called 4d (macromere DM" in *Helobdella*). In diverse spiralians, this cell is the first to undergo an equal and bilateral division to give rise to the left and right mesodermal precursor cells, which produce bands of smaller cells that contribute visceral mesodermal organs and muscles (Lambert, 2007). In mollusks, nemerteans and polyclad turbellarians, 4d is referred to as the mesentoblast, because in addition to mesoderm, it also gives rise to endoderm (intestine) (Boyer et al., 1998; Henry and Martindale, 1998; Hejnol, 2007). However this lineage has not been shown to contribute to endoderm in those annelids in which it has been studied with the one exception, the polychaete, *Platynereis dumerilii* (Ackermann et al., 2005). Interestingly however, in both *Helobdella* and *Tubifex*, there are segmental clusters of M derived neurons, therefore, while this lineage mainly contributes to mesoderm in these annelids, it could be considered mesectoderm (Weisblat and Shankland, 1985; Goto et al., 1999a; Goto et al., 1999b). Mesoderm derived from other micromere lineages is called ectomesoderm.

The 4d precursor of the mesoderm arises from the D quadrant. However, not all spiralians specify their D quadrant through the same mechanism, and because of this, specification of the mesodermal precursor occurs at different stages in development depending on the species. There are two general ways in which the D quadrant can be specified, which are known as equal cleavage and unequal cleavage. In equal cleavage, the four blastomeres arising at second cleavage can be demonstrated experimentally to share the same developmental potential to become the D quadrant (and are usually the same size); in such embryos, it is only at a later stage, usually in the interval between fifth and sixth cleavage, that one of the third order macromeres interacts with the overlying first quartet micromeres, and is induced to become 3D, and thus the precursor of the mesentoblast (van den Biggelar, 1977; van den biggelaar and Guerrier, 1979; Henry, 2002). In unequal cleavers, by contrast, D quadrant specification is achieved through segregating determinants to one of the blastomeres during the first two unequal

cell divisions and thus is complete by the end of second cleavage (Freeman and Lundelius, 1992). This segregation of determinants can be accomplished through two general mechanisms. One involves formation of a polar lobe, an enucleate membrane bound protrusion, which fuses with only one of the four blastomeres (Freeman and Lundelius, 1992). The other involves eccentric placement of the spindle, resulting in asymmetic cytokinesis with specialized determinants shunted to the larger cell, which will become the D quadrant (Freeman and Lundelius, 1992). It is assumed that equal cleavage represents the ancestral mode of D quadrant specification (Freeman and Lundelius, 1992).

Therefore, in equal cleavers, D quadrant specification occurs much later than it does in unequal cleavers. Even within equal cleavers there is a range of stages in which the D quadrant is specified due to differences in timing of cell divisions of the animal micromeres relative to the vegetal macromeres (van den Biggelaar and Haszprunar, 1996). What is the evolutionary benefit of acceleration of D quadrant specification? The D quadrant is specified early through asymmetric cleavages and segregation of determinants both in the leech *Helobdella* and the oligochaete worm *Tubifex*. Since these annelids are direct developers, and thus do not go through larval stages, it has been proposed that their heterochronic shift to precocious D quadrant specification is a reflection of a need for shortened development, in contrast to those annelids, which have later D quadrant specification, as well as intermediate larval forms (Freeman and Lundelius, 1992).

The mesodermal precursor as the organizer

It has been shown in various spiralians that, once the 3D macromere is specified, it acts as an organizer, signaling to the overlying micromeres, whose fates are determined according to their position relative to 3D. The organizer activity of 3D has been illustrated through deletion experiments. In embryos in which 3D has been deleted, lineage tracing experiments have shown that not only are the fates of those cells derived from 3D missing, but also those of micromere lineages, especially lineages on the dorsal side closest to 3D, indicating that 3D is inductively signaling (Clement, 1962; van den Biggelaar, 1977; Martindale, 1986). Additionally, experiments in the mollusk *Ilyanassa*, have shown that later ablations of cell 3D yielded fairly well-organized larva, whereas earlier deletions resulted in more extensive developmental defects. Furthermore, the earlier in development the 3D cell is specified, the sooner its organizer activity can occur. Therefore even subtle heterochronic shifts in the specification of 3D, can potentially have major influences on early development (van den Biggelaar and Haszprunar, 1996).

Originally it had been believed that once 3D divided to form 4D and 4d, the mesodermal precursor, its organizer activity was completed. However, several studies have illustrated embryos whose 4d cell continued the organizer activity of 3D (Rabinowitz et al., 2008) or performed the organizer activity rather than 3D, such as in the snail *Crepidula*. In *Crepidula*, deletions of 4d radialize the embryo, (Henry et al., 2006) suggesting that in this mollusk 4d is functioning as the embryonic organizer rather than 3D. Recent experiments in *Ilyanassa* have shown that 4d is also involved in organizer signaling, and that when deleted larva are deficient not only in 4d derivatives but also show foot structure abnormalities (Rabinowitz et al., 2008).

MAPK signaling and the organizer

Recent molecular data from several spiralians corroborates cell deletion results and indicates that the Erk1-2 mitogen activated protein kinase (MAPK) signaling pathway is associated with the organizer activity of 3D and/or its daughter cell 4d (Lambert, 2008). In *Ilyanassa*, activated MAPK signaling (visualized through double phosphorylated MAPK antibody staining) is initiated specifically in 3D. Furthermore, this has since been shown to be the case in several other mollusks (Lambert, 2008). In *Ilyanassa*, activated MAPK signaling subsequently spreads to overlying micromeres in an expanding dorsal vegetal crescent of cells (Lambert and Nagy, 2001). In those embryos whose 3D cell was ablated, MAPK activation was no longer seen in the micromeres, and treatment of embryos with the MAPK inhibitor U0126 resulted in phenotypes resembling those of early 3D ablated embryos (Lambert and Nagy, 2001).

While MAPK activation in 3D has been reported in a number of other mollusks, secondary activation in the micromeres has not been observed (Lambert and Nagy, 2003). These results suggest that MAPK activation in 3D is the more evolutionarily conserved aspect of this process. Additionally, in the equal cleaving polychaete *Hydroides*, activated MAPK signaling is seen only in the 4d cell, suggesting a heterochronic shift to this lineage as the main organizer (Lambert and Nagy, 2003). The signal(s) activating MAPK remain unidentified.

In the snail *Crepidula* deletion experiments indicate that the 4d cell, not 3D, is acting as the organizer, and patterns of embryonic MAPK activation are complicated. Early MAPK signaling is seen in a subset of animal micromeres derived from the first quartet, and later activated MAPK signaling is also seen in both 3D and 4d (Henry and Perry, 2008). Inhibition of MAPK signaling through early UO126 treatment radializes the embryo, while later treatment starting one hour before the birth of 4d does not seem to affect the organizer activity of 4d (Henry and Perry, 2008). Therefore in *Crepidula*, MAPK signaling may be necessary in early micromeres for specification of the D quadrant but not in D quadrant organizer activity.

There is some data illustrating organizer activity of the D quadrant in *Helobdella*. In normal development, the A and B macromeres fuse after they have each made three micromeres. Subsequently the AB cell then fuses with the C macromere to form the endodermal precursor, part of the yolk syncytium, which will later form the lining of the gut. Biochemical arrest of either cell D', or both of its daughters before, (DM and DNOPQ) or after (DM' and DNOPQ'), they have each made one micromere, prevents fusion of the A and B macromeres. This illustrates that the fusion is regulated by cells that do not themselves undergo the fusion (Isakesen et al., 1999). It would therefore be interesting to look at the affects of UO126 treatment on AB fusion to test whether MAPK signaling is involved in D quadrant induction of macromere fusion.

There is dynamic MAPK signaling in the two-cell leech embryo and it has been implicated in regulation of Notch transcript stability (Gonsalves and Weisblat, 2006). These results are provocative and together with other data highlighting dynamic expression of Wnt ligands and other transcripts at the two-cell stage (Huang et al., 2001; Cho et al., 2010; SJC unpublished data) suggest that early signaling may be involved in D quadrant specification. At later stages, staining for activated MAPK shows diffuse cytoplasmic staining throughout the blast cells of all lineages (Gonsalves PhD thesis, 2006). While inhibition of MAPK signaling starting from early stages has a phenotype of delayed cleavage of OP into the O/P teloblasts, all other cleavages proceeded normally, though later defects in epiboly were seen (Gonsalves thesis, 2006). However, early dynamic signaling in the two-cell leech embryo, including MAPK signaling, could be involved in accelerated D quadrant specification. Furthermore, the involvement of MAPK signaling in D quadrant induction of AB fusion remains to be tested.

Variations in the 4d lineage among spiralians

While there is extensive observational evidence from multiple species to support the assertion that cell 4d divides bilaterally to give rise to the precursors of the majority of the mesoderm across diverse spiralians, subsequent divisions and fates of cells in the sublineages arising from 4d have not been well characterized. Such information is essential for understanding how developmental variations in the 4d lineage manifest in morphological diversity across spiralian taxa. However, available data suggest that the 4d lineage exhibits significant variation among spiralians. For example, in some flatworms, formation of M_L and M_R occurs one generation later than is the standard in annelids and mollusks; the 4d cell first divides in the plane of the animal vegetal axis before the animal daughter, then divides bilaterally to give rise to the left and right mesodermal precursors (Van den Biggelar, 1997). There are many other examples of deviations from standard division patterns in the mesodermal lineage. In the leech *Erpodella octoculata*, after 4d divides into M_L and M_R, the mesodermal precursors undergo multiple rounds of equal cleavages and with no identifiable smaller bandlets of mesodermal progeny, until later stages (Dohle, 1999). In the earthworm *Eisenia*, after 4d divides equally into the two M-cells, these cells each give rise to abortive "enteroblasts" and then several cells described as "migratory mesoblats" and only later can mesodermal bandlets be discerned (Dohle, 1999). In the snail *Ilyanassa* there are clearly two large mesentoblasts born from 4d, each of which undergoes several asymmetric divisions to give rise to smaller precursors of mesendoderm. In this species, however, the orientation of successive mesentoblast divisions changes such that no columns of mesodermal blast cells are seen (Rabinowitz et al., 2008). While there are many examples of the 4d lineage giving rise to bilateral bands of mesodermal precursors (Zackson, 1982; Henry and Martindale, 1998; Goto et al., 1999a; Hejnol et al., 2007) the notion of a very stereotyped and conserved lineage may instead yield to one in which greater variation and evolutionary plasticity is acknowledged.

Questions addressed in this thesis (1): How to get a head

Much of the focus on leech development has revolved around understanding the process of segmentation. This bias is understandable given the inherent interest in lineage-driven segmentation as exemplified by leech, combined with the interest in making evolutionary comparisons between segmentation in Lophotrochozoa and Ecdysozoa and the experimental accessibility of the segmentation stem cells, (teloblasts) and their progeny. However, this interest in segmentation means that other lineages are often understudied, including those contributing to the anterior non-segmental head, notwithstanding two careful studies of micromere lineages (Smith and Weisblat, 1994; Huang et al., 2002). Previous work implicated the early mesodermal lineages in prostomial contributions in the leech *Helobdella triserialis* (Zackson, 1982) and a somewhat more detailed analysis of contributions of the first several m blast cells to the head and proboscis was undertaken in the leech *Theromyzon rude* (Gleizer and Stent, 1993). However, since these publications, anterior contributions from DM" remained largely forgotten and were not explored any further.

The problem of defining and understanding the head, especially the vertebrate head (as it is particularly interesting to ponder one's own head), has intrigued and confused scientists for

over a century. While it is fairly well understood what comprises a segmental unit in the vertebrate trunk (although extensive debate around this topic still continues, eg. Budd, 2002), determining what exactly is considered "head" and whether or not it is actually made up of specialized segments is not simple. Prior to the discovery of the neural crest and their cranial derivatives, it was believed by some scientists that the vertebrate head was segmented, with repeating units homologous to modified or specialized vertebrae (Noden and Schneider, 2006). Additionally during the 1870s, when the Articulata Hypothesis was in favor (which stated that annelids and arthopods were closely related and that vertebrates evolved from these more primitive segmented animals), it was believed that vertebrates evolved ***from*** annelids, which provided a predisposition to consider the head as comprising iterated structures. Segmentation in mesodermal head cavities of fish as well as in cranial nerves and pharyngeal arches, were all seen as supporting the notion that the vertebrate head was made of repeating units. Attempts were even made to correlate segments in the head with equivalents of somites worth of mesoderm (Noden and Schneider, 2006).

Similar debates have also been ongoing concerning arthropod heads and the number and nature of the segments comprising them (Scholtz and Edgecombe, 2006). Trunks of arthropods are made up of repeated units associated with structures derived from mesoderm, ectoderm and endoderm such as, ganglia, coelomic cavities and muscle. Additionally, arthropod segments often have modifications such as specialized appendages or lack of appendages. The organization of the arthropod head region is even more confusing, and debates surrounding what portions of the head represent hypothetical ancestral segments continue. The Articulata Hypothesis also biased the way scientists viewed arthropod head segmentation and led to the belief that arthropod and annelid heads were homologous. In annelids, the primary non-segmental portion of the body was known as the acron, which housed the brain, and until recently was believed to be homologous to the anterior portion of the arthropod head. Therefore various pre-oral structures in arthropods were considered non-segmental, although this was complicated by pre-oral appendages such as antennae, which would make the arthropod "acron" more like a segment with a specialized modification (Scholtz and Edgecombe, 2006). But now the ecdysozoa hypothesis makes an arthropod "acron" seem less likely. However there is still debate over the nature of the pre-oral region in arthropods. Additionally, in many arthropods, such as the crustacean *Parhyale hawaiensis*, anterior segments are formed differently than more posterior ones, which further complicates the problem of defining the anterior boundary of the first segment (Price et al., 2009).

Stent (1999) made the point that, given the lineage-dependent mode of segmentation seen in leech the problem of segmentation for this animal is "solved" as soon as the teloblasts form their columns of blast cell progeny, and in a sense this is true. The stereotyped cell lineages characteristic of development in leech and other clitellate annelids should also make the "head problem" more tractable as well. It has been shown that in clitellate embryos, all segmental tissue arises sequentially in anteroposterior progression from five pairs of segmentation stem cells (the teloblasts). This result leads understandably to the simplifying assumption that the earliest born progeny of each teloblast should contribute progeny to the first segment and that tissues anterior to the first segment should arise from non-segmental progenitors, i.e., the micromeres (and/or macromeres in principle). The inadequacy of this assumption is revealed by previous studies detailing the contributions of the frankly non-segmental micromere lineages, which leave much of the head region unaccounted for (Huang et al., 2002). Moreover, other

work has yielded the problematic result that the anterior borders of the various lineages are not coincident and thus could not define a clear border between segmental and non-segmental tissues; in particular, it has been shown unambiguously that the first cell arising from each N teloblast divides differently from the standard n blast cells and that these cells contribute progeny to the head region that have no obvious homologues in the unambiguous segments of the mid-body (Zhang, 2005). Other, less complete observations suggest that the M teloblast lineages also contribute to non-segmental tissues of the head. In Chapter 3 of this thesis, I present work detailing the M-derived progeny responsible for these anteriormost tissues.

Questions addressed in this thesis (2): Origins of the foregut in clitellate annelids

In leeches the foregut is defined as the portion of the digestive tract from the mouth opening through the esophagus, which connects to the midgut (Kang et al., 2003). Leeches feed on a variety of hosts and this is reflected in the diversity of both specialized mouthparts and foreguts. "True leeches" are divided into two major groups: the Rhynchobdellida or jawless leeches which have an eversible muscular proboscis; and the Arhynchobdellida, which do not have a proboscis and may or may not have jaws. Within the Arhynchobdellida are the Gnathobdella, or jawed leeches, whose jaws which display a range of size, shape and number of "teeth", are used to facilitate "grasping, rasping and tearing" (Sawyer, 1986 pg. 457), when bloodsucking on a variety of hosts from amphibians to mammals (Sawyer, 1986). Previously Gnathobdellids were found with either two or three jaws containing varying numbers of teeth depending on the species. Recently a new genus and species of leech, *Tyrannobdella rex*, was discovered, which has a single jaw containing 8 teeth (Phillips et al., 2010).

Among the Rhynchobdellida, the proboscises are generally organized into three layers; inner, middle and outer, all of which are encased by a muscular sheath (Fig. 1.2). Rhynchobdellida leeches as a group feed on a wide range of hosts; individual species which have specialized to feed on one or more of the five classes of vertebrates, as well as a variety of invertebrates. Specializations of their proboscises reflect their diverse feeding practices. Among the Rhynchobdellida, there is variation in terms of proboscis location. In *Helobdella*, which practices liquidosomatophagous predation on snails, the proboscis everts from the mouthpore, which is located on the head near the eyespots dorsal to the anterior sucker. In *Glossiphonia complananta*, which also feeds on invertebrates, the proboscis emerges from the center of the anterior sucker. In *Haementeria ghilianii*, which feeds on amphibians and mammals, the proboscis emerges from the anterior rim of the sucker. Another example of morphological specialization in the feeding structures of this group is the Japanese *Ancyrobdella biwae*, which has three hook-like structures at the anterior tip of its proboscis (Sawyer, 1986).

In Chapter 3 of this thesis, I show that, in addition to its other contributions to the head, the DM" (4d) lineage in the leech *Helobdella* also makes the majority of the musculature in the proboscis and the proboscis sheath. Moreover, through collaborative work with Ayaki Nakamoto, I have re-examined anterior contributions of the 4d lineage in the oligochaete *Tubifex tubifex*. Through careful analysis, we also see contribution from the 4d lineage to head mesoderm in *Tubifex*. However, unlike *Helobdella*, *Tubifex* ingests sediments and are filter feeders, and has a different foregut morphology. Therefore it is not unexpected that the anterior contributions of this lineage in these two annelids are different. These differences illustrate that the 4d lineage

exhibits evolutionary plasticity and that potentially small changes in the developmental program of the M teloblasts can result in a diversity of adult body plans.

Questions addressed in this thesis (3): DNA based lineage tracers.

Knowing the normal patterns of embryonic cell proliferation, migration, and differentiation is a cornerstone for understanding development. Yet for most species, the precision with which embryonic cell lineages can be determined is limited by technical considerations (the large numbers of cells, extended developmental times, opacity of the embryos), and the lineage tracers available. For example, standard dextran-based cytoplasmically distributed tracers cannot achieve cellular resolution when lineages are comprised of cells which are small, numerous, contiguous and in different layers. Additionally, the inherent variability of the lineages themselves exacerbates their tracing. In Chapter 2, I describe an improved method of cell lineage tracing in the leech *Helobdella*, driving the expression of a nuclearly localized histone H2B:GFP (green fluorescent protein) fusion protein in selected lineages by microinjection of a plasmid vector. This construct generates a long lasting and minimally mosaic signal with single cell resolution, and does not disrupt the development of most lineages tested. I have validated this technique by elucidating details of cell lineages contributing to segmental and prostomial tissues that could not be observed with standard dextran lineage tracers.

Questions addressed in this thesis (4): Notch signaling during leech development.

Recently the whole genome of *Helobdella robusta* was sequenced. This has allowed for characterization of signaling pathways throughout development in far greater detail than previously possible (eg., see Cho et al., 2010). In Chapter 4, in addition to re-examining the expression of previously cloned Notch pathway members, I have taken advantage of the whole genome sequence to clone and characterize the expression of additional homologues of Notch pathway members including a ligand, co-activator and several potential bHLH downstream targets, during stages late 7 through 9. While I had originally chose the Notch signaling pathway with the expectations that it was involved in segmentation, many of the pathway members that I characterized, showed strongest expression in anterior non-segmental cells. I saw *Hro-Notch*, *Hau-ser* and *Hau-suH* expression in overlapping populations of cells anterior to the germinal plate, as is necessary for Notch signaling to function in a cell-cell signaling network. However, all of the potential bHLH targets of Notch signaling examined showed largely non-overlapping expression patterns with each other and with the Notch receptor and ligand, suggesting their expression is regulated independently of Notch signaling.

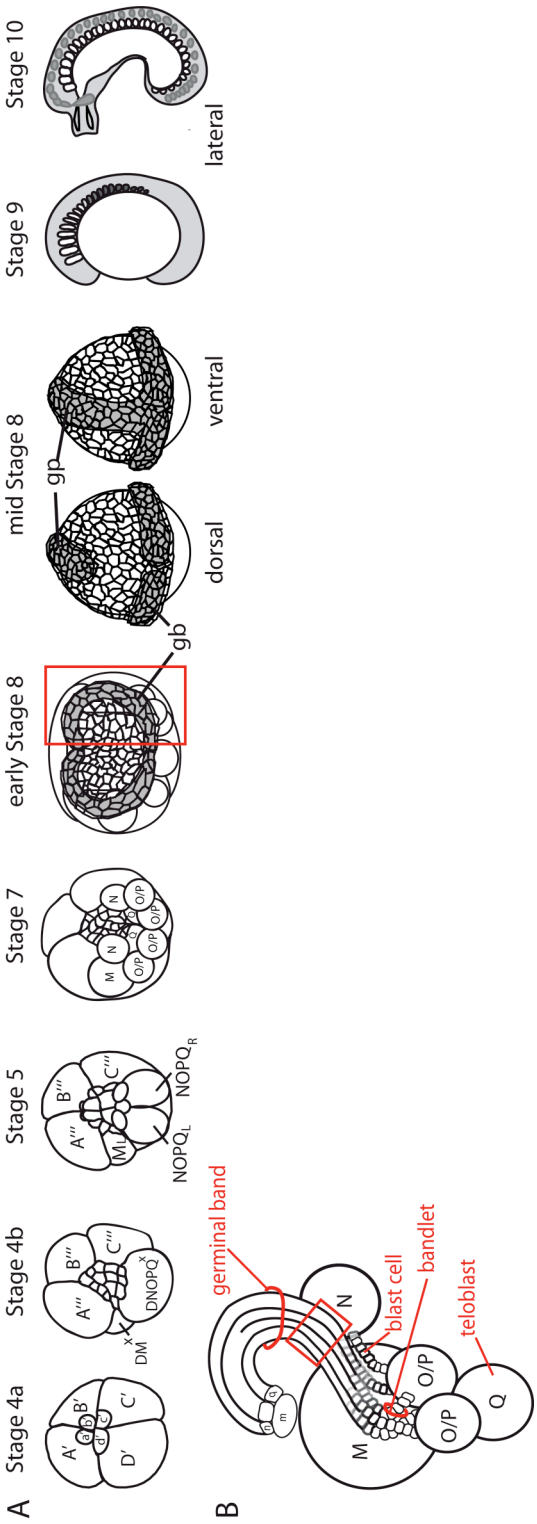


Figure 1.1. Summary of relevant aspects of leech development.

Figure 1.1. Summary of relevant aspects of leech development. A. Diagrammatic representations of selected stages (animal pole views unless otherwise indicated). In the 8-cell embryo (stage 4a), the D quadrant has cleaved to form micromere d' and macromere D', the teloblast precursor. At stage 5, macromere D' has given rise to left and right mesodermal and ectodermal precursors (M teloblasts and NOPQ proteloblasts, respectively, the right M teloblast is out of view at the vegetal pole). At stage 7, all five pairs of teloblasts are present. At early stage 8, teloblasts have produced columns of segmental founder cells called germinal bands (gb, grey; see panel B for details); germinal bands and the territory between them are covered with a provisional epithelium generated by micromeres. At mid stage 8, the lengthening germinal bands have begun to coalesce along the prospective ventral midline to form the germinal plate (gp), from which segmental mesoderm and ectoderm arise. During stages 9 and 10, segments differentiate and the germinal plate expands from ventral to dorsal territory, displacing the micromere-derived epithelium (not shown at these stages). B. Schematic of a stage 8 embryo, corresponding to the boxed section in panel (A), showing the relationships of teloblasts, blast cells, bandlets, and germinal band. Teloblasts mark the posterior growth zone and the older, more distal blast cells contribute to more anterior segments.

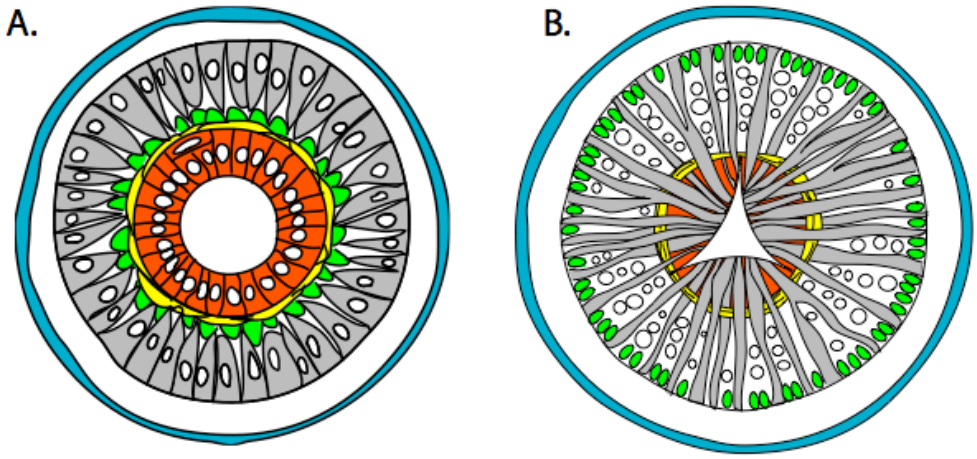


Figure 1.2. Schematic showing the tissue organization of the proboscis in the stage 10 embryo and adult in *Helobdella*. Schematic of a transverse cross-section of the proboscis from an early stage 10 embryo (A) and an adult leech (B). A. Proboscis sheath, derived from multiple lineages, is shown in blue, presumptive radial muscle fibers derived from DM" in grey, longitudinal muscles from the first quartet in green, circumferential muscle fibers derived from dm' and c"' in yellow, and the inner ring derived from DM" in red. B. The organization of the adult proboscis drastically changes compared to that of the stage 10 embryo. Colors correspond to hypothetical cells of origin in A. In the adult, the proboscis is tri-radiate. Radial muscle fibers (grey) extend from the lumen to the outer edge of the proboscis and are opposed by a belt of circumferential muscle fibers (yellow). Longitudinal muscles are arranged around the periphery of the proboscis. We predict that the cells of the inner ring shown in A. (red) are either interspersed among the extended radial muscle fibers within the ring of circumferential muscle fibers, or form a lining facing the lumen. Salivary gland ductules (open circles) are distributed between the longitudinal muscle fibers. The origin of the cells comprising the ductules is not known.

CHAPTER TWO

High-resolution cell lineage tracing reveals developmental variability in leech embryos

Introduction

Cell lineage-dependent patterning processes are broadly implicated in metazoan development. In the nematode *Caenorhabditis elegans*, for example, all 1090 somatic cells in the adult hermaphrodite arise by essentially invariant lineages (Sulston et al., 1983). Skilled observers can complete precise lineage analyses for *C. elegans* by direct observation, thanks to the rapid development (less than 15 hours from zygote to hatching), small number of cells and transparency of its embryos (Sulston et al., 1983). In most animals, however, embryonic cell lineages can be observed and described with only limited precision and completeness.

In the leech *Helobdella* for example, embryogenesis takes about 10 days and its large yolky embryo poses significant challenges for visualization, compounded by the fact that *Helobdella* generates juveniles containing over 50,000 cells. Even such moderately complex embryos provide a technical challenge in analyzing cell lineages, and thus in establishing the extent to which cell lineages are determinate. To circumvent these problems, embryonic cell lineages in *Helobdella* and other systems have been studied using microinjected intracellular lineage tracers (Weisblat et al., 1978; Zhang and Weisblat, 2005). Here, I present a modified cell lineage tracing technique based on plasmid injection, which provides a significant improvement on previous methods in *Helobdella* and one that I anticipate will be of use in other cellularly complex embryos.

As a glossiphoniid leech, *Helobdella* is a segmented representative of the superphylum Lophotrochozoa. Segmental mesoderm and ectoderm arise from a posterior growth zone (PGZ) comprising five bilateral pairs of lineage-restricted stem cells (M, N, O/P, O/P and Q teloblasts), and the initial divisions of the teloblast progeny (the m, n, o, p and q blast cell clones) are highly stereotyped (Fig.1; Zackson, 1984; Shankland, 1987a, b; Bissen and Weisblat, 1989; Zhang and Weisblat, 2005). Intracellularly injected lineage tracers were first developed for use on *Helobdella* embryos, including HRP (Weisblat et al., 1978), fluorescently modified peptides (Weisblat et al., 1980) and the now standard fluorescent dextrans (Gimlich and Braun, 1985). More recently, nuclear localized fluorescent proteins (nXFPs) expressed from injected mRNAs have been used for cell lineage analysis in this system (Zhang and Weisblat, 2005). nXFPs are useful because they permit more precise determination of cell position and cell number than can be achieved with tracers distributed throughout the cytoplasm, especially as the cellular complexity of the embryo increases during development (Zhang and Weisblat, 2005). However degradation of injected mRNAs leads to decreasing levels of even the relatively stable XFP proteins in older embryos (Zhang and Weisblat, 2005). Moreover, nXFPs disperse as the nuclear envelope breaks down during mitosis, impeding the analysis of complex lineages.

Plasmid DNA may be more stable than mRNA and can be continuously transcribed in those cells that inherit it. Plasmid injections into nuclei of post-mitotic cells have been used in late stage embryos of the medicinal leech *Hirudo* to express reporter constructs as well as for functional studies (Baker and Macagno, 2006; Shefi et al., 2006; Baker and Macagno, 2007; Baker et al., 2008). Previous attempts to drive ectopic gene expression in the early *Helobdella*

embryo using plasmid injections were problematic, however; expression was highly mosaic (i.e., was seen in only a few of the progeny of the injected cell) and the injected lineage developed abnormally independent of the expression of the transgene

In the experiments reported here, I have used an improved plasmid construct in which leech EF1alpha promoter (Pilon and Weisblat, 1997) drives the expression of a leech histone2B fused to green fluorescent protein (pEF-H2B:GFP). Cloning of leech histone2B and construction of the pEF-H2B:GFP construct was done performed by Dian-Han Kuo, a post doctoral fellow in the lab. Injection of this construct resulted in long-lasting, robust expression of the transgene in the progeny of injected cells. Plasmid injection and expression of H2B:GFP transgene did not appear to disrupt normal development in most lineages, although some lineages were more sensitive to plasmid injections than others.

Using this construct in conjunction with a standard cytoplasmic lineage tracer rhodamine dextran (RDA), I was able to follow an o blast cell sublineage (o.app), which contributes a clone of purely epidermal progeny (Shankland, 1987a), from its birth through differentiation. While the first division in this sub-lineage is as stereotyped as those leading up to it, subsequent divisions are not, consistent with a transition from tightly regulated cell divisions in early development to a more stochastic process as cellular complexity increases.

Results

pEF-H2B:GFP drives transgene expression in proteloblast lineages

Previous plasmid injections in *Helobdella* were found to disrupt development of the injected lineage (Pilon and Weisblat, 1997). Here, the DNA concentrations (96 ng/microliter) used are 40-fold lower than in previous experiments (Pilon and Weisblat, 1997) and an intron between the promoter and reporter gene in the previous construct has been deleted (see Experimental Procedures). To test the effects of pEF-H2B:GFP on development, we first injected it into the ectodermal proteloblast (i.e., cell DNOPQ, DNOPQ', DNOPQ'' or DNOPQ'''', designated collectively as $DNOPQ^{x}$, in embryos ranging from 12 to 20 hours after zygotic deposition (AZD) during stage 4; see Fig. 1.1A). These cells were chosen because deviations in their normal cleavage patterns would be obvious. Co-injecting rhodamine dextran amine (RDA) with the plasmid allowed us to assess the mosaicism of the plasmid-driven gene expression, by comparing the distributions of RDA- and GFP-labeled cells. Embryos at mid stage 8 (78 to 120 hours post-injection) were scored for normal development, as judged by the presence of the normal complement of 8 ectoteloblasts, blast cell progeny arranged into left and right germinal bands and by the blast cell division patterns within individual lineage as revealed by the expression of the H2B:GFP transgene (Fig. 2.2A, B).

By these criteria, the success of the injections varied. Pooling the seven most successful of ten experimental clutches, 80% of the embryos (63/79 embryos) developed normally, while in the other three clutches, only 31% of the injected embryos (47/152 embryos) developed normally; typically, success rates of 90% or more are achieved when RDA alone is injected. Most of the RDA-labeled cells in the normally developing embryos exhibited robust GFP fluorescence in their nuclei, indicative of H2B:GFP expression and localization (Fig. 2.2A, B). The spatial distributions and size differences of GFP-labeled nuclei in the individual ectodermal bandlets also corresponded to previous descriptions of blast cell division patterns (Fig. 2.1B, Fig.

2.2B; Zackson, 1984; Shankland, 1987a, b; Bissen and Weisblat, 1989), indicating that the plasmid injection and consequent expression of the H2B:GFP transgene had not significantly perturbed development.

The success rate of the plasmid injections varied in a stage-dependent manner. For example, none of the experiments in which zygotes (stage 1) were injected yielded normal embryos (data not shown), whereas, the majority of embryos (66/78 or 85% overall in 5 experiments) developed normally for injections of the unilateral ectodermal precursors $NOPQ^x$ (i.e. cell NOPQ, NOPQ' or NOPQ") at stage 5 (Fig. 1.1A, Fig. 2.3, Table 2.1).

Closer inspection of the plasmid-injected embryos revealed that the H2B:GFP signal was not uniform in all the RDA-labeled progeny of the injected blastomere (Fig. 2.2). Moreover, in some embryos, one or more of the RDA-labeled ectodermal lineages showed low or no transgene expression, indicative of mosaic expression of the injected plasmid (Fig. 2.2, Fig. 2.3, and data not shown). Curiously, the mosiaicism of transgene expression was increased, rather than decreased when the plasmid was digested with I-SceI meganuclease prior to injection (Fig. 2.3; Table 2.1).

To compare the efficacy of transgene expression in segmental mesoderm with that observed in the ectodermal lineages, I injected the mesodermal precursor DM, DM' or DM" (collectively designated DM^x) with a mixture of RDA and pEF-H2B:GFP. As with $DNOPQ^x$, injecting plasmid into the DM^x proteloblasts disrupted development of the mesodermal lineage to a somewhat greater extent than did standard lineage tracers; 72% (33/46 embryos in 3 experiments) had developed normally when scored 4-5 days post injection. As with the $NOPQ^x$ vs. $DNOPQ^x$ comparisons, plasmid injection into individual M teloblasts was less disruptive of normal development than injection into DM^x; 88% of M-injected embryos (46/52 embryos in 3 experiments) developed normally.

Expression of the transgene was robust in the mesodermal lineage (Fig. 2.2C) and exhibited a range of mosaicism similar to experiments in which pEF-H2B:GFP was injected into the ectodermal proteloblasts. Expression of the transgene was most likely to be mosaic or absent in the cells arising early on in the M lineage, including a group of non-segmental, mesenchymal "freckle cells", which lie between the germinal bands at early stage 8 and arise from cells born early on in the mesodermal lineage (Fig. 2.2C, D; Zackson, 1982; Nelson and Weisblat, 1991; Nelson and Weisblat, 1992; Chi, 1996). The transgene lineage tracer revealed another set of M-derived non-segmental cells that have not been previously described: large cells with flattened nuclei at the anterior lateral portion of the left and right mesodermal germinal bands (Fig. 2.2C; S.E.G. unpublished observations).

Transgene expression and perdurance in teloblast lineages

A major goal of this work was to develop a technique that would facilitate determination of the complete lineages of the identifiable neurons comprising the segmental nervous system of the leech (Muller et al., 1981). For this purpose, long-lasting non-disruptive expression of the fluorescent, nuclearly localized transgene product and compatibility with time lapse imaging are key features.

Using plasmid-driven expression of H2B:GFP as the lineage tracer, I was able to make time-lapse videos of sufficiently high frame rate and long duration to capture sequential divisions of o blast cells (Fig. 2.4A). With the H2B:GFP reporter I could follow chromatin morphology

throughout highly asymmetric divisions; intriguingly, asymmetries in chromatin volume between the cells o.a and o.p were evident before the nuclei had reformed (Fig. 2.4A).

Similar time-lapse videos were made focusing on the p and q lineages, capturing primary divisions of p blast cells and a q.f cell respectively. Late mitotic chromatin morphology was used as an indicator of spindle positioning in analyzing the movies. Unlike in the o lineage, p primary blast cells undergo nearly symmetric initial divisions. These divisions are parallel to the AP axis of the bandlet, whereas in the o lineage the late mitotic spindle is positioned at an angle predictive of the position of the daughter cells (Fig. 2.5A). Interestingly while time-lapse movies of the o lineage show that the daughter cells o.a and o.p are born at and remain at an angle to the bandlet, in the p lineage, time-lapse imaging illustrates that the spindle is positioned along the AP axis and that the daughter cells p.a and p.p rotate clockwise soon after chromatin decondensation is complete. However, p.a and p.p will subsequently rotate counterclockwise to reposition themselves 180 degrees from one another to form a column of cells of nearly equivalent nuclear volume that is classically indicative of p lineage morphology (Bissen and Weisblat, 1989; Kuo and Shankland, 2004). The initial division of the q.f cell was also captured in time-lapse imaging. q.f divides asymmetrically to give rise to a smaller q.fa cell and a larger q.fp cell (Fig. 2.5B; Bissen and Weisblat, 1989). Similar to the primary division of the o blast cells, the late mitotic spindle of q.f is positioned at an angle predictive of the positions of the daughter cells which do not show subsequent rotations as in the p lineage.

To test the perdurance of plasmid-driven H2B:GFP expression in teloblast lineages, I injected individual teloblasts with pEF-H2B:GFP and tested for normal development of the labeled lineages by comparing the patterns of labeled nuclei with expectations based on numerous previous studies. Here, I focused on the O lineage because the O-derived pattern elements have been described previously and are relatively easy to identify (Shankland and Weisblat, 1984; Weisblat and Blair, 1984; Zackson, 1984; Shankland, 1987a).

I injected individual O/P teloblasts in numerous embryos and fixed samples at times ranging from 3 to 10 days post injection. The majority of all batches injected exhibited normal development, as judged by the timing and orientation of inferred blast cell divisions at about 3 days post-injection (Fig. 2.4B; Fig. 2.6) and by the distribution of RDA- and GFP-labeled progeny at 6 to 10 days post-injection (Fig. 2.4C-E).

The one exception to the essentially non-mosaic expression in these experiments was in embryos in which the first blast cell clone labeled with RDA showed very low levels of H2B:GFP expression, compared to the rest of the injected lineage (Fig. 2.5C; Fig. 2.7C). The occasional failure of transgene expression in the clone of the first blast cell produced after injection was consistent with the expected differences in diffusional mobility between the plasmid (2000 kDa) and the RDA (10 kDa on average). Thus, when teloblasts were, by chance, injected late in the cell cycle, the cytokinetic furrow would have closed off the nascent blast cell before the larger molecule could diffuse from the site of injection into the nascent blast cell.

For embryos fixed at stage 8 and beyond, it is possible to dissect the germinal bands and/or germinal plate from the yolk, for analysis by confocal microscopy. In such preparations, pattern elements corresponding to previously described clusters of segmentally iterated cells could be identified. For example, in stages 9-11, the O lineage in each segment includes differentiated neurons in anterior dorsal (AD), crescent-shaped (CR) and posterior ventral (PV) clusters within the segmental ganglion plus three peripheral neurons (oz1, oz2 and LD2) and a lateral skin dot (LSD) (Fig. 2.4E; Shankland, 1987a). As embryos reach the juvenile stage,

H2B:GFP fluorescence declines and autofluorescence increases, perhaps in association with the emergence of differentiating pigment cells in the body wall. In these older animals, I was still able to generate a strong signal for the expressed transgene product by immunostaining for GFP (Fig. 2.4D).

Inter-species difference and intra-species variation in blast cell division and differentiation patterns

The discrete nuclear localization of H2B:GFP fluorescence makes it possible to identify and count cells in individual pattern elements with a precision not previously available. Here, I have used this technique to determine the extent to which the stereotyped early blast cell division patterns persist later in development. Previous studies showed that cell o.app, a great-granddaughter of the o blast cell, gives rise to a clone comprising exclusively squamous epidermal cells in the posterior mediolateral portion of each segment in the congeneric species *H. triserialis* (see Fig. 2.1B for cell nomenclature; Shankland, 1987a). In contrast, cell o.aa contributes a clone of mixed cell types including a separate, smaller patch of epidermis that eventually merges with the larger o.app clone from the next anterior segment (Fig. 2.5B, E; Weisblat and Shankland, 1985; Shankland, 1987a); thus, in any given segment, these two patches of O-derived epidermis arise from two different blast cell clones. The further divisions within the o.app and o.aa clones have not been examined previously, because it was not possible to distinguish epidermal cell boundaries using cytoplasmic lineage tracers. Using H2B:GFP expression in conjunction with RDA as lineage tracers, I was able to identify and count the epidermal contributions from the O lineage in each segment at a variety of developmental times. For this purpose, the germinal plates were dissected from embryos fixed at various time points post injection and examined by confocal microscopy.

The mediolaterally oriented division of cell o.app to form cells o.appl and o.appm was first described in *Helobdella triserialis* (Shankland, 1987a), where it occurs at about 40 hours clonal age (cl.ag.), i.e., 40 hours after the birth of the o blast cell from which the o.app in question derives. I found that the homologous o.app cell in *H.* sp. (Austin) undergoes an equivalent division, but significantly later than in *H. triserialis*. For example, in one experiment, only 5 of 13 embryos fixed 72 hours after injections contained segments in which o.app had divided. In one of these embryos o.app had divided in the first five labeled segments, suggesting that the anteriormost labeled o.app had divided at about 66 hours cl.ag. in that embryo. Yet in sibling embryos, that division had not yet occurred at 72 hours cl.ag. At the next time point from this experiment, 87 hours after injection, all 12 embryos fixed contained multiple segments in which o.app had divided. Thus, we estimate that the time window during which the o.app division occurs can be more than five hours among embryos of a single clutch and that o.app divides no earlier than 66 hours cl.ag., roughly 30 hours later than in *H. triserialis*. This interspecies difference is consistent with previously observed retardation of about 24 hours for primary blast cell cycles in *H. robusta* and this sibling species relative to *H. triserialis* (Bissen and Weisblat, 1989; Zhang and Weisblat, 2005).

Notwithstanding the differences in cell division times between species, and to a lesser extent among embryos of a given species, divisions of primary blast cells and their early progeny in any given embryo correlate closely with the order in which the blast cells arise from the parent teloblast; occasional cases are observed in which blast cells divide out of birth order, i.e. a more

posterior cell divides before its anterior counterpart (Fig. 2.4B; Zackson, 1984). Consistent with these previous findings, in just one of the five embryos fixed 72 hours post-injection, I observed an o.app that had divided slightly "out of order". That is, the o.app cell in one segment had already completed its division while o.app in the next anterior segment was still in metaphase (Fig. 2.4B). The labeled O lineage of a sibling embryo from the same batch, also fixed at the 72 hours post-injection, looks identical to the embryo in Fig. 2.4B, except that the anteriormost o.app cell has divided to form o.appl/m. Comparing the O lineage in these embryos illustrates the high degree of stereotyped development in this lineage at this stage; in both embryos o.apa cells at the same clonal age (69.5 hours) are in telophase giving rise to o.apaa and o.apap (Fig. 2.6). In contrast to the small range of variation in timing of divisions in the o blast cell clones up to that of o.app, however, we observed considerably larger variability in the subsequent patterns of cell division and differentiation within the o.app clones, even in individual embryos, as detailed below.

Cells o.appl/m have a relatively long cell cycle (>35 hours) during which they undergo morphological differentiation. Differentiation of the first O-derived epidermal cells was judged by their large nuclear profile and flattened morphology (Fig. 2.4E and Fig. 2.7). These two epidermal cells then further proliferate (Fig. 2.7) and the timing of their subsequent divisions is no longer tightly linked to birth order. By their positions and by comparison with previous studies we interpreted these cells as morphologically differentiated o.appl and o.appm cells. Epidermal differentiation was observed as early as 88 hours cl.ag. in some segments (not shown), but there was considerable variability in the timing of the differentiation. For example, in one batch of embryos fixed 99 hours post injection, some embryos contained as few as three and others as many as nine segments with pairs of labeled, differentiated epithelial cells (Fig. 2.7B).

The rate of cell proliferation in the o.app clones was also variable. For example, in one embryo, only two morphologically differentiated epidermal cells could be seen in each of 15 segments (cl.ag.124-141.5 hours), and hence neither o.appl nor o.appm had divided; but in another embryo from a separate batch, three epidermal cells in an o.app clone were observed as early as 105.5 hours cl.ag. Even within individual embryos, the number of o.app descendents did not increase monotonically with o blast cell clonal age (Fig. 2.7B). While we observed a general trend of increasing cell number among the o.app progeny in older clones (Fig. 2.7, clonal age did not reliably predict the number of cells in the o.app clone and embryos were commonly seen with multiple segments containing greater epidermal cell counts than their anterior neighboring segment (Fig. 2.7). Thus, by this point in development of the o.app clones, the timing of cell divisions had become decoupled from the birth order of the parent blast cells.

In contrast to the o.app-derived epidermal clone, morphological differentiation of the laterally situated o.aa-derived epidermal cell (which generates the lateral skin dot; LSD) was first observed at clonal age 125 hours, and we never observed more than a single labeled o.aa-derived epidermal cell at clonal ages up to 144 hours (Fig. 2.4E). Even in the most advanced embryos examined, corresponding to cl.ag. 204 hours, a maximum of three o.aa-derived epidermal cells were observed in the first labeled segment, where the separate contributions of o.aa and o.app-derived epidermal cells could be unambiguously distinguished (Fig. 2.4D).

Long lasting expression reflects ongoing transcription from the injected plasmid

The perduring expression we observed from injecting pEF-H2B:GFP into precursors of diverse lineages in the *Helobdella* embryo might represent either transcription of the transgene throughout the injected lineage, and/or inheritance of protein and/or mRNA produced in an early burst within the injected cell and its immediate progeny. To distinguish the relative contributions of these possibilities, we injected plasmid encoding nGFP driven by the EF1-alpha promoter (pEF-nGFP) into the N teloblast lineage and then, after culturing the embryos for various periods of time, processed them by in situ hybridization for *gfp* transcripts. For comparison, we injected N teloblasts in sibling embryos with nGFP mRNA and processed them in parallel with plasmid-injected embryos (Zhang and Weisblat, 2005).

The results showed that transcription of the transgene occurred throughout the progeny of the injected cell. Transcript was readily detected in the plasmid-injected embryos by 21 hours post-injection, but at this time transcript levels were clearly lower than in mRNA-injected embryos (Fig. 2.8A). Moreover, in contrast with the mRNA-injected embryos, transcript levels in plasmid-injected specimens were higher in the blast cells than in the injected teloblast itself, as judged by the intensity of the in situ staining (Fig. 2.8A). Consistent with previous results, (Zhang and Weisblat, 2005), the decreased intensity of in situ staining was evident throughout the labeled lineage in mRNA-injected embryos as early as 71 hours post-injection. In contrast, the in situ signal in plasmid-injected embryos increased until around 90 hours post injection. After this time, a decrease in staining intensity was first evident in anterior territory, spreading posterior at later times as in mRNA-injected embryos (Fig. 2.8A).

While *gfp* in situ staining was generally homogenous in intensity throughout the mRNA-injected lineage, clear variations in staining intensity were evident among cells in the plasmid-injected lineages. This reflects variation in transcript accumulation between cells, possibly due to differential inheritance or expression of the plasmid (Fig. 2.8B). Control experiments using sense probe for the in situs showed no staining (data not shown), which confirmed that the in situ protocol was not detecting plasmid DNA. Comparisons of GFP fluorescence in plasmid-injected versus mRNA-injected lineages further confirmed the differences seen at the protein level. By six days post-injection, expression was clearly stronger in the plasmid-injected lineages than those injected with mRNA, as judged by GFP fluorescence (Fig. 2.8C). Thus, while, mRNA injections are preferable for studies requiring gene expression within less than two days post-injection, plasmid injections are apt to be preferable for studies involving lineage tracing or ectopic gene expression at later time points.

pEF-H2B:GFP drives transgene expression in micromere lineages

To test expression of the transgene in non-teloblast lineages, we also injected pEF-H2B:GFP and RDA into the d' micromere (Fig. 1.1A), one of 25 small cells arising during cleavage which contribute to various non-segmental tissues of the embryo and adult (Smith and Weisblat, 1994; Huang et al., 2002). Cell cycle compositions and cell division patterns in the early micromere lineages have been described (Smith and Weisblat, 1994; Huang et al., 2002). Previous studies have shown that its early divisions in the d' lineage are unequal and stem cell-like (Huang et al., 2002). The d' lineage contributes progeny to the supraesophageal ganglion, definitive prostomial epidermis, proboscis muscle fibers and sheath, and to the epithelium of the provisional integument (Weisblat et al., 1984; Huang et al., 2002).

We injected the d' micromere with pEF-H2B:GFP and RDA soon after its birth (7.5 hours AZD) and fixed embryos at various time points post injection. At 48 hours post injection, the stem cell-like divisions of the labeled micromeres were evidenced by a column of smaller cells extending vegetally from a larger cell, comparable to our previous findings using RDA lineage tracers alone (Fig. 2.9A; Huang et al., 2002); by 72 hours, the d' clones comprised roughly 20 contiguous cells (Fig. 2.9B)

By 98 hours post-injection, two distinct populations of cells were evident within the d' clone. One population, previously identified as epithelial cells of the provisional integument, comprised about two dozen superficial cells with large, flattened nuclei, left of the midline, outside the expanding margins of the germinal plate in dorsal territory (Fig. 2.9C; Weisblat et al., 1984). The other population comprised about 30 densely packed, deeper cells with small, spherical nuclei, left of the midline and anterior to the germinal plate, partially covered by the d'-derived epithelial cells (Fig. 2.9C); we interpreted these cells as precursors of definitive prostomial tissues (Weisblat et al., 1984; Nardelli-Haefliger and Shankland, 1993; Huang et al., 2002). Within this anterior population were two seemingly distinct sub-populations of smaller cells as judged by cell morphology and nuclear arrangement (Fig. 2.9C).

By 120 hours post-injection, differences in nuclear diameters and cell density between the prostomial contributors and the larger epithelial cells were more apparent, and the epithelial cells no longer overlay the deeper cells at the anterior. The prostomial cells were more closely packed, and clearly separated into two distinct populations, while the epithelial cells had undergone few cell divisions and were continuing to spread into dorsal territory (Fig. 2.9D). By 144 hours post-injection, the two anterior populations of prostomial cells had become physically separate (Fig. 2.9E), and the epithelial cells were further away from both populations of anterior cells (Fig. 2.9E). At 168 hours post injection, the anterior prostomial populations had further subdivided into several discrete populations of cells. The provisional epithelial cells were constricted towards the dorsal midline, ceding territory to the expanding germinal plate (Fig. 2.9F).

Discussion

In the work presented here, we have explored the uses of plasmid-driven gene expression as a technique for tracing embryonic cell lineages in the leech *Helobdella*. Microinjecting circular plasmid, in which expression of a histone2B:GFP fusion protein is driven by a putative EF1-alpha enhancer, yielded robust expression of the transgene with unexpectedly low mosaicism, and with no obvious disruption of normal development in most experiments. Transgene transcript was detected throughout the labeled lineages for up to 5 days post injection and protein was readily detected immunohistochemically at 10 days post injection. Variation in transcript levels detected between blast cell progeny suggests differences in rates of transgene transcription. Additionally, transcription is not limited to the parent teloblast, in which case we would expect to see uniform staining in all blast cells and darker staining in the teloblasts as in mRNA injections. Surprisingly, injecting the plasmid as the I-SceI meganuclease restriction digest (Fig. 2.3, Table 1) resulted in a dramatically reduced proportion of cells in the descendant clone expressing the transgene, which is contrary to results reported from other systems. No stable expression of the transgene was observed in any of the animals recovered in these experiments.

Interestingly, I saw a cell type-dependent sensitivity to plasmid injections. Injections into zygotes never yielded normally developing embryos, and injections into the proteloblasts DM^x and $DNOPQ^x$ resulted in higher percentages of abnormal development of the injected lineage than injections into d', the proteloblast $NOPQ^x$ or individual meso- and ecto-teloblasts. Expression of transgene after injecting the large yolky proteloblasts (DM^x, $DNOPQ^x$ and $NOPQ^x$) was typically more mosaic than after injecting individual teloblasts, and micromeres. This is most likely because the large sizes and the short cell cycles of these blastomeres make it more difficult for the slowly diffusing plasmid to distribute evenly in the cell prior to the first division after injection.

Comparisons with other microinjection-based lineage tracing methods

Conventional lineage tracers such as RDA or other derivatized dextrans are distributed throughout the cytoplasm, which makes it difficult to resolve boundaries between adjacent labeled cells, especially when the progeny of the injected cell are small, densely packed and contain very little cytoplasm.

In contrast, the plasmid and mRNA injection techniques offer the advantage of expressing markers targeted to a specific sub-cellular organelle, which facilitates enumerating individual cells even within clusters of labeled cells. In the examples presented here, nuclear localization of the H2B:GFP made it possible to count individual cells within O-derived clusters of epidermal progeny, identify unique cells at the anterior end of the mesodermal germinal bands and allowed us to determine that the anterior portion of the d' micromere lineage comprised many small cells instead of a few large ones.

Compared to the direct injection of mRNAs, the plasmid-injection method provides for longer lasting and temporally more uniform transcript levels. Injected mRNA is being degraded continuously from the time of injection, and compensating for this by injecting more mRNA disrupts normal development (Fig. 2.8; Zhang and Weisblat, 2005). In contrast, mRNA levels build up and decline more gradually after plasmid injection, which is useful for long term experiments.

Disadvantages of the plasmid injection method include the delayed onset of expression compared to previous methods and varying degrees of mosaicism. The earliest detection of the expressed marker was between 14-48 hours post-injection depending on the lineage injected, and at these early times, the level of expression was often lower than that obtained with mRNA injections. Mosaicism of transgene expression was observed when plasmid was injected into early blastomeres. However, this is not a major problem for cell lineage analysis in the leech, since progeny of these cells, such as micromeres and teloblasts, are amenable for microinjection and mosaicism is minimal when individual micromeres or teloblasts are injected.

Another consideration concerning the use of the plasmid-driven lineage tracing is the possibility of developmental disruptions. The risk of disrupting development is inherent in any experiment involving microinjection, but is compounded to the extent that the cells' metabolism is taken over to express exogenous genes. Our results suggest that for *Helobdella*, the large yolky blastomeres are particularly susceptible to developmental disruptions at the earliest stages of zygotic development and become progressively more resistant to such disruptions at later stages with the exception of the small and yolk-deficient first quartet micromeres.

Origins of cell lineage variability

Previous studies in *Helobdella* and related species (Zackson, 1982; Zackson, 1984; Bissen and Weisblat, 1989), building on the pioneering studies of annelid development carried out by E.B. Wilson (1892) and C.O. Whitman (1878), have illustrated that the early leech embryo exhibits stereotyped patterns of cell divisions comparable to those described for the nematode *Caenorhabditis elegans* (Sulston et al., 1983). Subsequent studies of leech development have focused largely on the segmental ganglia of the ventral nerve cord; in the first approximation, each adult ganglion contains about 200 pairs of individually identifiable neurons (Macagno, 1980), each of which is believed to arise by an invariant pattern of cell divisions from one of the five teloblast lineages during embryogenesis (Kramer and Weisblat, 1985; Weisblat and Shankland, 1985).

However, while the *C. elegans* larva hatches with precisely 558 cells, *Helobdella* contains roughly 50,000 cells as a juvenile; moreover, many non-neuronal cell types (e.g., muscles, epidermis, mesenchyme) continue proliferating post-embryonically, so that the adult probably comprises several hundred thousand cells. It is implausible that such large numbers of apparently interchangeable cells would arise by fixed lineages, especially in light of the developmental plasticity inherent in the capacities for indeterminate growth, regeneration and vegetative reproduction that are present in most annelid taxa. Even in *C. elegans*, significant variation is seen in cell cycle durations and in the positions of "identical" cells among embryos (Schnabel et al., 1997).

Thus, cell lineage variability in the *Helobdella* embryo is to be expected. Desjeux and Price (1999) documented variability in the production of supernumerary blast cells from teloblasts, and we have previously documented variability in cell cycle composition for specific micromere lineages (Huang et al., 2002). Here, I used expression from injected plasmid to study variability in the o.app lineage, which gives rise only to epithelial cells (Shankland, 1987a). I find that the stereotypy of the o.app lineage breaks down some time after its division into o.appl and o.appm. Cells o.appl and o.appm both exhibit prolonged cell cycles, however the subsequent divisions in the o.app clone are variable in timing, resulting in variation in the number of o.app-derived epithelial cells among different segments of the same individual at the juvenile stage. I have not excluded the possibility that the variability observed here in the o.app lineage reflects a cell-specific disruption of an otherwise stereotyped lineage by expression of the transgene or even the RDA itself. But given the normal development of the other O-derived sublineages in these same experiments, this possibility seems unlikely. Instead, I speculate that the o.aa lineage exhibits less variability than o.app due to constraints associated with the more tightly regulated production of specific neural cell phenotypes.

In conclusion, this study demonstrates the practicality of using plasmid injections to introduce persistent transgene expression in embryos of the leech *Helobdella*. Though I have exclusively focused on its use in cell lineage analysis here, this plasmid-based transgene expression method can be further adopted for gene *cis*-regulation analysis and for driving ectopic gene expression in functional analysis of developmental genes.

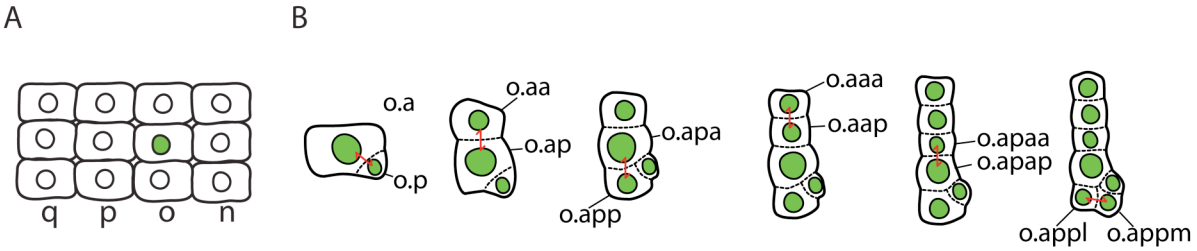


Figure 2.1. Early divisions in the O lineage. A. Arrangement of undivided ectodermal blast cells within the germinal band, corresponding to the boxed section of panel B in Figure 1.1; a single o blast cell is highlighted with a green nucleus. The mesodermal bandlet lies beneath the ectoderm and is not shown. B. Schematics showing the first six divisions of an o blast cell clone in the right germinal band; at each division the sister cells are named by adding a letter to indicate their relative positions at the end of cytokinesis, a = anterior, p = posterior, l = lateral, m = medial (lateral and medial are designated with respect to the position of the clone at the end of gastrulation). In each panel, sister cells of the most recent division are indicated by red double arrows.

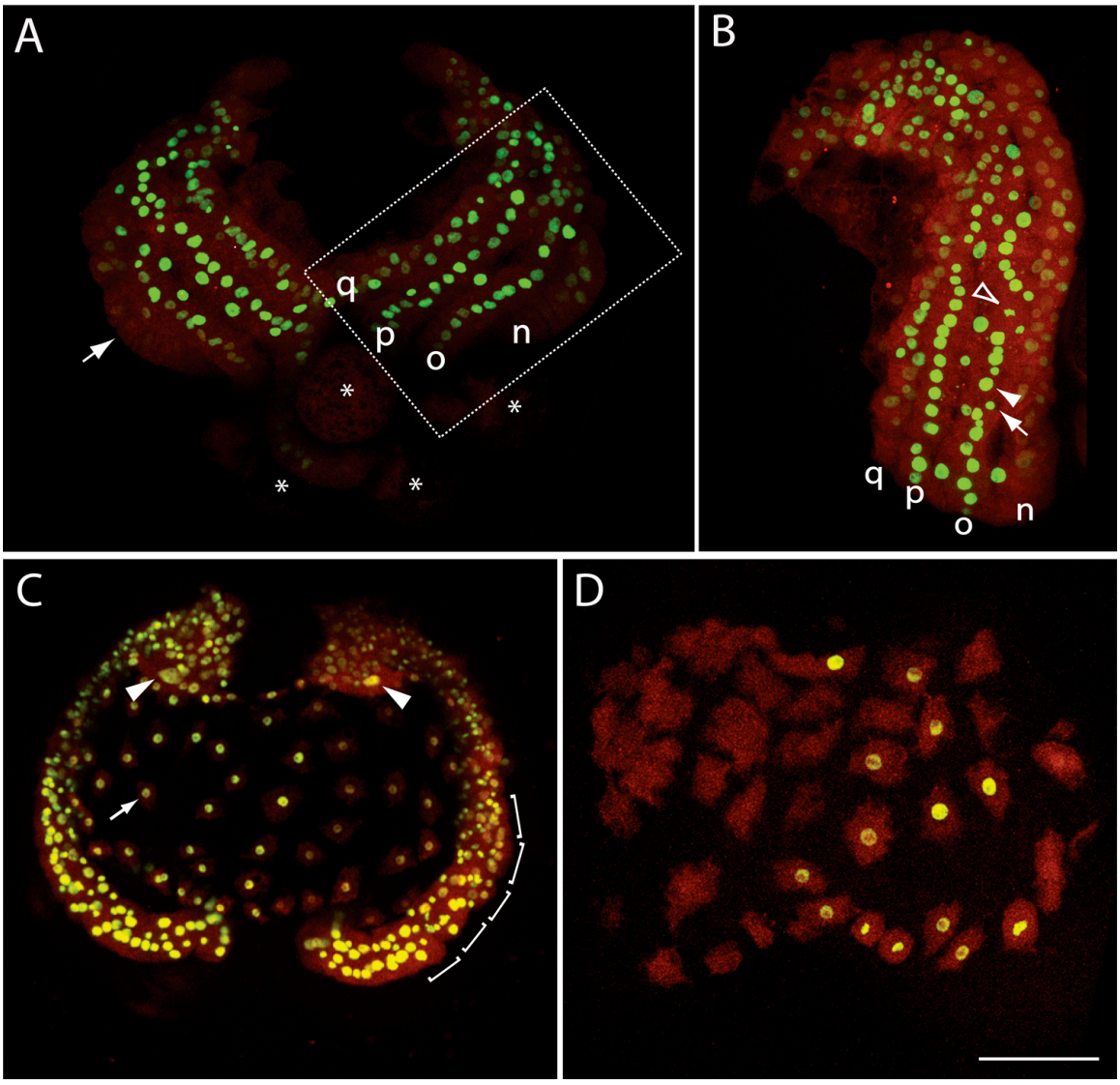


Figure 2.2. Expression of H2B:GFP in the DNOPQ^{x} and DM^{x} lineages.

Figure 2.2. Expression of H2B:GFP in the DNOPQ^{x} and DM^{x} lineages. In this and all figures, anterior is up, cytoplasmic RDA lineage tracer is red, nuclear H2B:GFP is green, and images are maximum projections of stacks of confocal images, unless otherwise noted. A. Animal pole view of an embryo whose DNOPQ^{x} had been injected with RDA and pEF-H2B:GFP 78 hours prior to fixation at early stage 8 (see Fig. 1.1A, B). This image shows blast cell bandlets in the left and right germinal bands (labeled in the right germinal band) and some teloblasts (asterisks); not all labeled cells are visible because the stack does not extend through the entire embryo. Note the reduced levels of transgene expression in the left n bandlet (arrow). B. Animal view of a sibling embryo fixed 96 hours post injection, showing the right germinal band, comparable to the region enclosed in the dotted box in panel (A). Normal divisions of blast cells in the o bandlet are indicated by the presence of identifiable cells including o.p (white arrow), o.a (white arrowhead) and a mitotic o.a cell (open arrowhead). C. An embryo whose DM^{x} was injected with RDA and pEF-H2B:GFP four days before fixation at early stage 8. Within the germinal bands, proliferation of individual m blast cell clones produce developing hemi-somites (brackets). In the region between the germinal bands, migratory, non-segmental freckle cells derived from the mesodermal lineage are evident (arrow) and additional non-segmental cells with exceptionally broad nuclei (arrowheads) are seen at the anterior of the left and right germinal bands. D. Higher magnification image of freckle cells in a sibling embryo showing mosaic transgene expression. Scale bar: 100 μm in A,C, 50 μm in B, 75 μm in D.

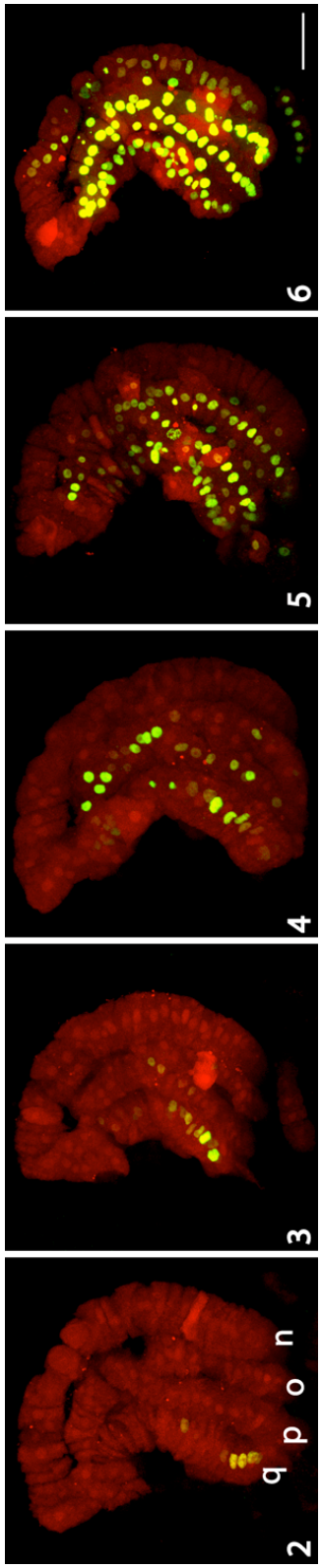


Figure 2.3. Range of mosaicism of pEF-H2B:GFP expression in the NOPQ lineage.

Figure 2.3. Range of mosaicism of pEF-H2B:GFP expression in the NOPQ lineage. Images of embryos fixed 72 hours after NOPQ^{x}, was injected with RDA and pEF-H2B:GFP, with or without I-SceI digestion. Categories of mosaicism are indicated by numbers as defined in Table 2.1, except that category 1 (no transgene expression) and category 7 (abnormal development) are not illustrated. Scale bar: 50 μm.

Table 2.1: I-SceI digestion increases mosaicism of plasmid-driven transgene expression.

Category	1	2	3	4	5	6	7
- *I-SceI* n=78	1 (1%)	6 (8%)	6 (8%)	6 (8%)	29 (37%)	18 (23%)	12 (15%)
+ *I-SceI* n=76	6 (8%)	23 (30%)	20 (26%)	9 (12%)	5 (7%)	0 (0%)	13 (17%)

Proteloblast NOPQ^{x} of stage 5 embryos was injected with pEF-H2B:GFP and RDA; the injected embryos were scored 3 days later at early stage 8, and the range of expression observed was divided into categories as defined below (see Figure 2.3 for examples): 1) No detectable expression. 2) Expression detected in several cells but not throughout any entire lineage. 3) Expression detected throughout one lineage as well as possibly in several other cells. 4) Expression detected throughout two lineages as well as possibly in several other cells. 5) Expression detected throughout three lineages as well as possibly in several other cells. 6) Expression detected throughout four lineages as well as possibly in a portion of, or all of the micromere lineages. 7) Abnormal development. For each experimental condition (- *I-SceI* or + *I-SceI*), data were pooled from five separate experiments.

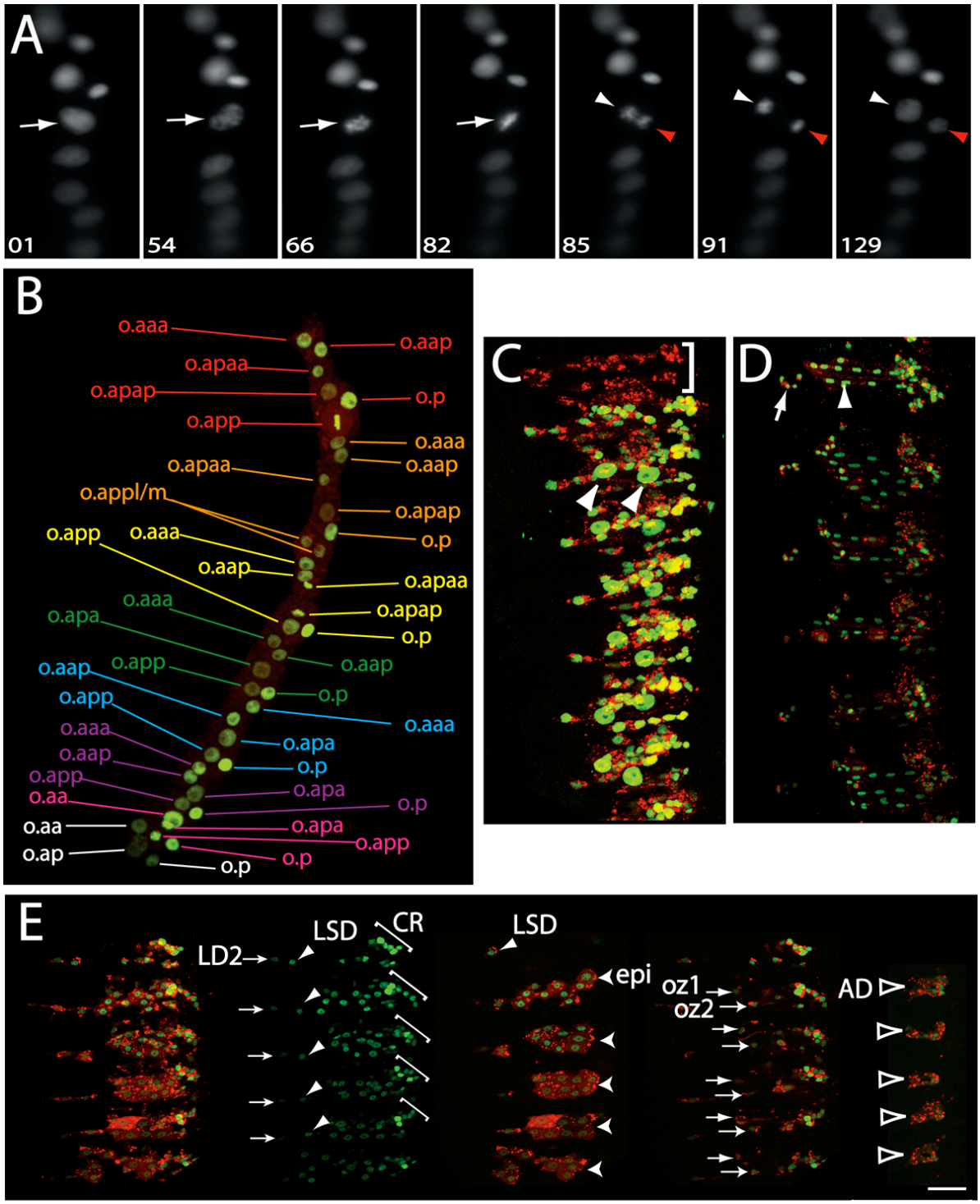


Figure 2.4. Expression of pEF-H2B:GFP in the O lineage.

Figure 2.4. Expression of pEF-H2B:GFP in the O lineage. A. Frames from a time-lapse video (one image per minute, 199 minutes total duration) showing the division of a primary o blast cell (white arrow) to form sister cells o.a (white arrowhead) and o.p (red arrowhead). In this field of view, two pairs of o.a and o.p sister cells are visible (see Fig. 2.1B), slightly out of focus, anterior to the dividing cell, and undivided primary blast cells lie posterior to it. Elapsed time (minutes since the start of imaging) is indicated in bottom left hand corner. B-E. Maximal projections of confocal stacks of O lineages labeled with RDA and pEF-H2B:GFP in embryos fixed at various time points post injection. B. 72 hours post injection; anterior portion of the o bandlet. Early progeny of the o clones are indicated, with distinct colors for each clone (cell nomenclature as in Fig. 2.1C). C. 144 hours post injection; anterior portion of a dissected germinal plate. Bracket marks progeny of first labeled blast cell clone, which is not expressing the transgene. Differentiated epidermal cells can be distinguished by their broadened nuclei (arrowheads) and by their superficial location. D. 206 hours post injection; anterior portion of the germinal plate. By this time, GFP transgene expression was no longer visible by direct fluorescence. This embryo was visualized by fluorescent immunostaining against GFP (green). E. Labeled O pattern elements. Views of six segments from the anterior portion of a germinal plate dissected from an embryo fixed 144 hours post injection. The two left-hand panels are maximal projections from the complete stack of confocal images; the second panel shows GFP signal only, to better visualize the nuclei corresponding to the secondary lateral dopaminergic cell (LD2), the o.aa-derived lateral skin dot (LSD) and the ganglionic crescent (CR). The three right-hand panels show partial stacks corresponding to superficial (ventral surface), medial and deep optical sections, highlighting o.app–derived epidermal cells (epi), O-derived peripheral neurons (oz1 and oz2) and a group of anterodorsal ganglionic cells (AD), respectively. Note that in the anteriormost segment the o.app-derived epidermis, oz1 and AD neurons are not labeled, because they are contributed to by the next anterior, unlabeled o blast cell clone (Weisblat and Shankland, 1985). Scale bar 10 μm in A,B; 33 μm in C, 37 μm in D, and 35 μm in E.

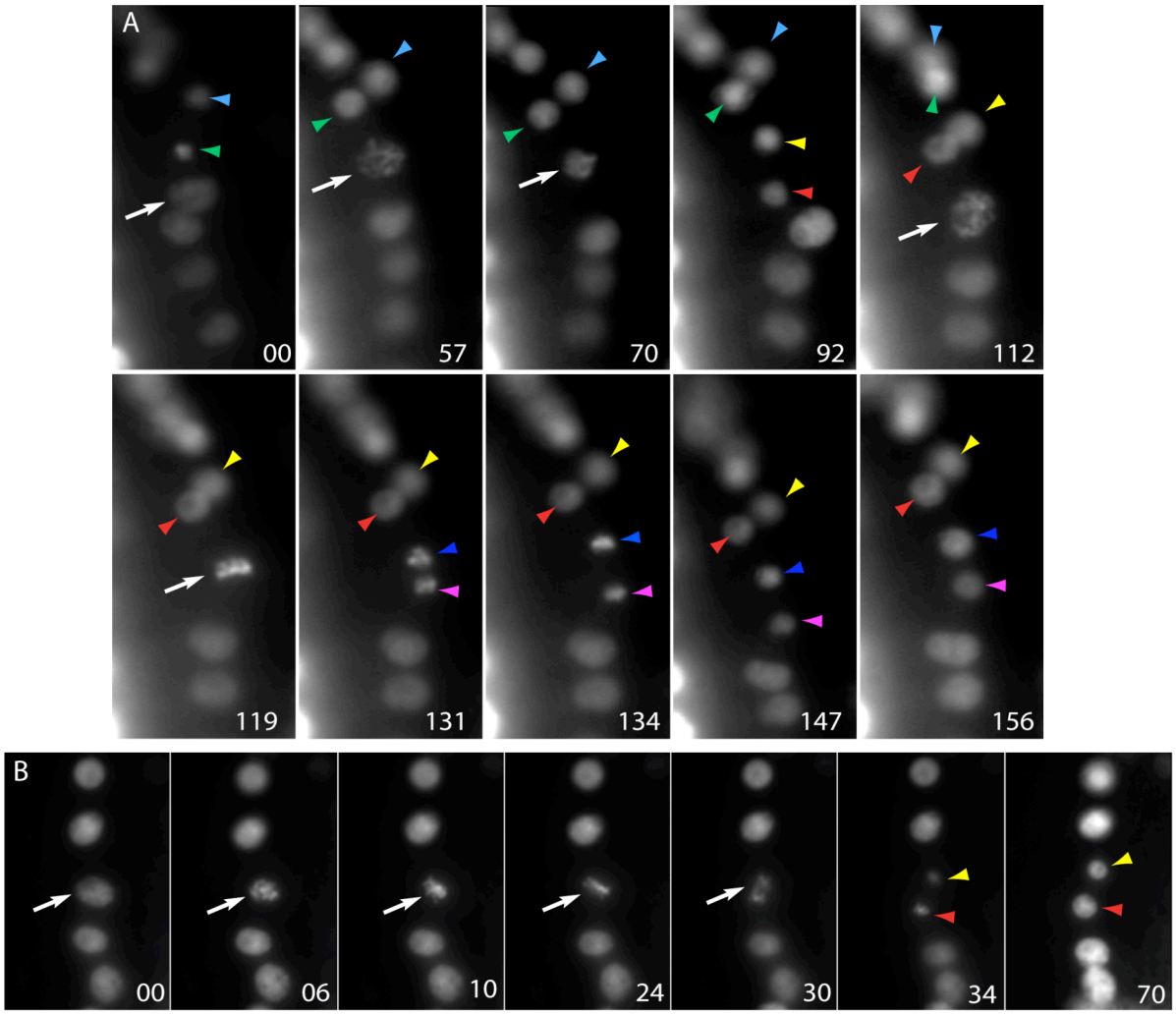


Figure 2.5. Frames from time-lapse movies capturing divisions of primary p and q.f blast cells. P or Q teloblasts were injected with pEF:H2B:GFP. Images were taken 2 days post injection (one image per minute). Number in the lower right corner indicate minutes elapsed. A. p blast cells (white arrows) undergo a nearly symmetric primary division to give rise to cells p.a and p.p (eg. blue and green arrowheads respectively). New colored pairs of arrowheads indicate a recently born pair of p.a and p.p cells. While born along the AP axis of the bandlet, the p.a and p.p cells, undergo a clockwise rotation before subsequently reorienting along the plane of the bandlet (see position of colored pairs of arrowheads relative to one another). B. A q.f blast cell (arrow) dividing asymmetrically to give rise to a smaller q.fa cell (yellow arrowhead) and a larger q.fp cell (red arrowhead).

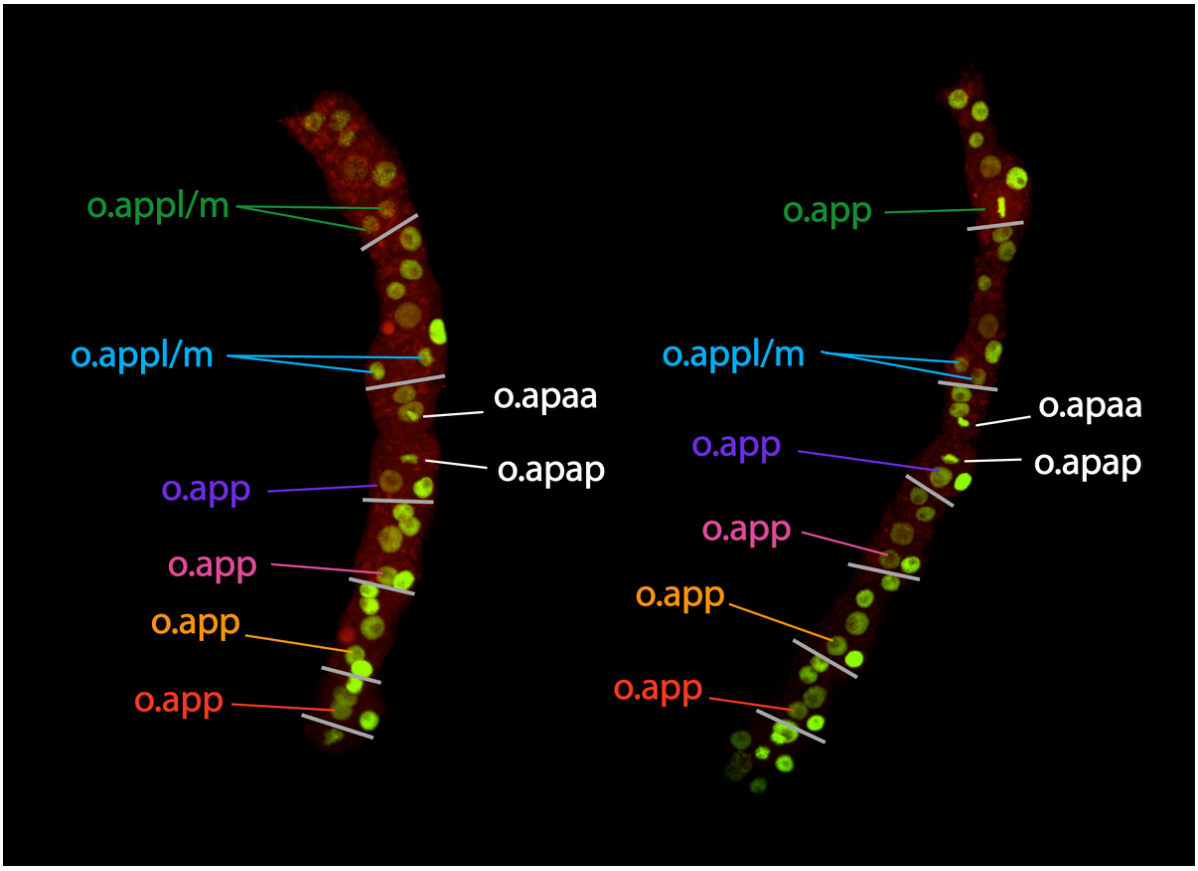


Figure 2.6. Stereotyped development in the early O lineage. Sibling embryos fixed 72 hours after injection of the O teloblast with RDA and pEF:H2B:GFP. The o.app cell and its progeny are labeled in each embryo, colors mark o.app lineages of the same clonal age. White horizontal lines mark the boundary between blast cell clones. The timing of division patterns in these two embryos is so similar that in both o.apaa and o.apap cells of the same clonal age are being born (labeled in white). The only difference in the lineages shown is that in the embryo on the right, the anteriormost o.app cell has not yet completed mitosis while in the embryo on the left it has.

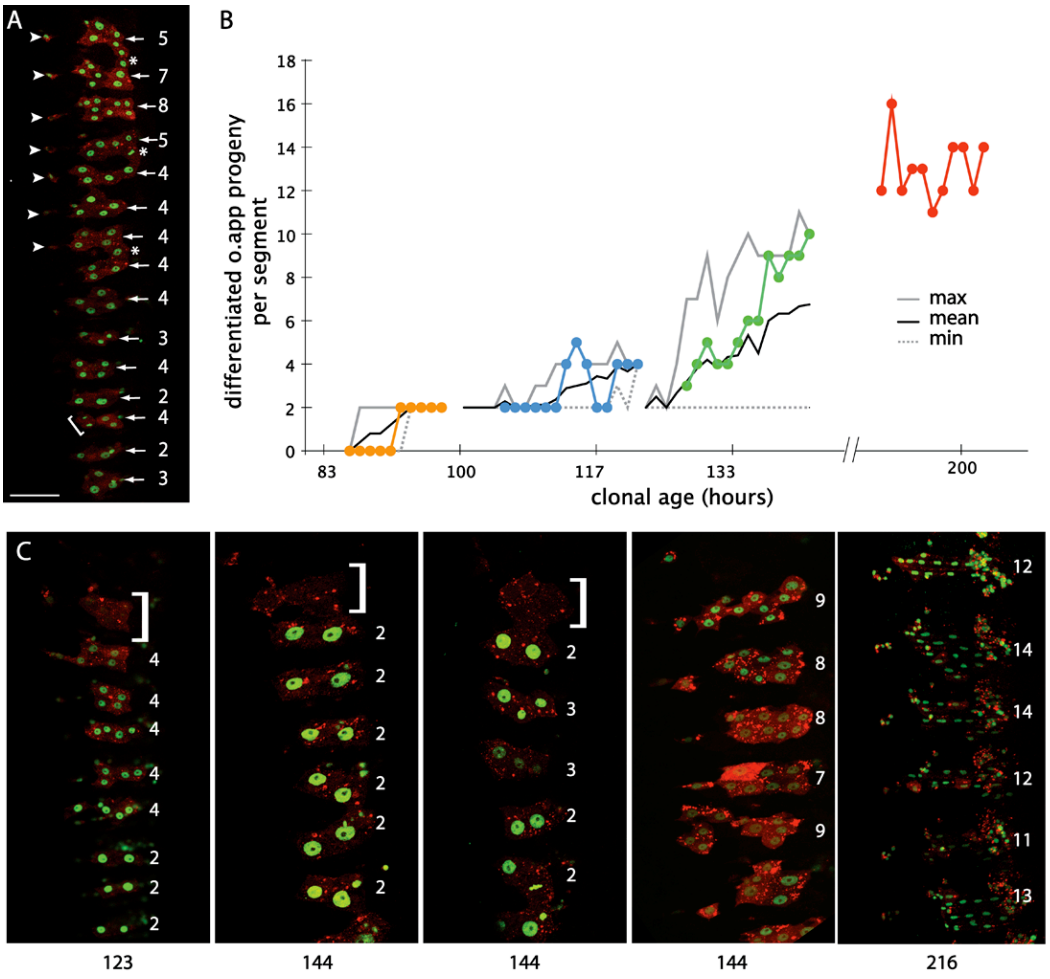


Figure 2.7. Variability in the o.appl/m lineage. A. Partial confocal stack showing the ventral-most aspect of a dissected germinal plate, to highlight epidermal cells derived from o.aa (arrowheads) and o.aap (arrows) in an embryo fixed 144 hours after injection of the parent teloblast with RDA and pEF-H2B:GFP. In this partial stack, o.aa-derived epidermal cells are not visible in posterior segments due to the curvature of the embryo. Numbers refer to count of o.app progeny per segment. Asterisks indicate the merger of o.app-derived epidermal clusters between neighboring segments. Proliferation of morphologically differentiated epidermal cells is evidenced by cells dividing in the plane of the epithelium (bracket and middle asterisk). B. Graphical representation of segment-by-segment o.app-derived epidermal cell counts vs. clonal age in 21 embryos fixed at various time points. Grey and black lines indicate the maximum, minimum and mean values obtained for each clonal age for which multiple specimens were examined. We did not interpolate between batches. Colored lines and dots represent data obtained from four individual specimens spanning various age ranges. C. Additional ventral projections similar to that shown in A, of embryos fixed at various time points post injection indicated in hours at the bottom of each panel. White numbers indicate cell counts for progeny of o.app, brackets indicate progeny of the first blast cell clone born after injection not expressing the transgene. Scale bar: 25 μm.

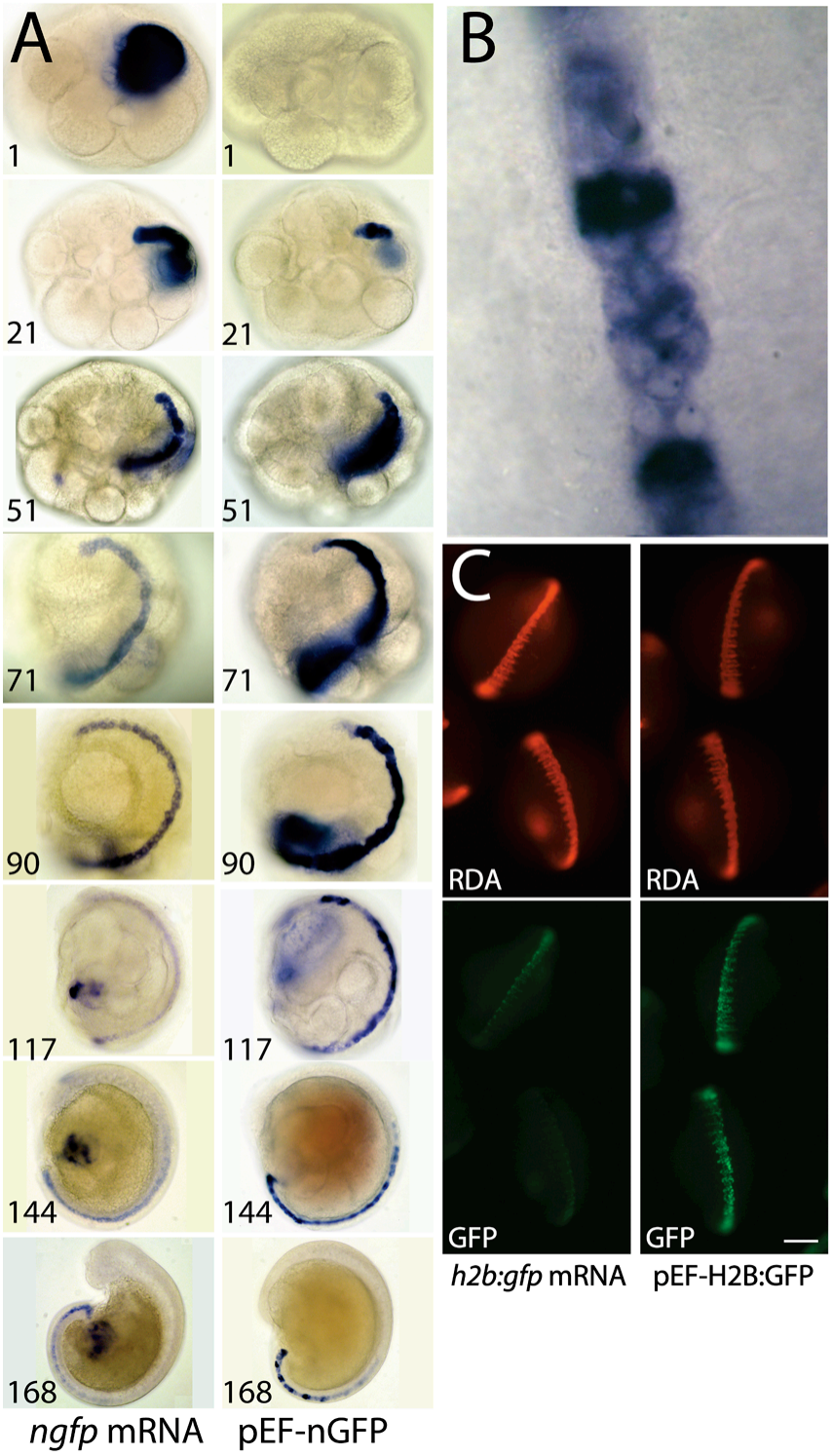


Figure 2.8. Comparison of transcript distributions resulting from plasmid and mRNA injections.

Figure 2.8. Comparison of transcript distributions resulting from plasmid and mRNA injections. Right N teloblasts of stage 6a embryos were injected with RDA and either mRNA or plasmid encoding the same transcript, and examined at various time points post injection (1-168 hours). A. Brightfield images of embryos injected with *ngfp* mRNA or pEF-nGFP plasmid, fixed at the times indicated (hours post injection) and processed for GFP in situ hybridization; animal pole views are shown for embryos fixed 1-51 hours post injection and lateral views for embryos fixed 71-168 hours post injection. B. High power image of a portion of a bandlet in the posterior germinal plate of an embryo processed for nGFP in situ 96 hours after plasmid injection shows non-uniform distribution of transcript. C. Epifluorescent images of embryos injected with RDA and either *h2b:gfp* mRNA or pEF-H2B:GFP plasmid, and fixed 144 hours post injection. RDA signals are comparable, but the GFP signal has largely disappeared from the mRNA-injected embryos. Scale bar: 100 μm in A, C; 8 μm in B.

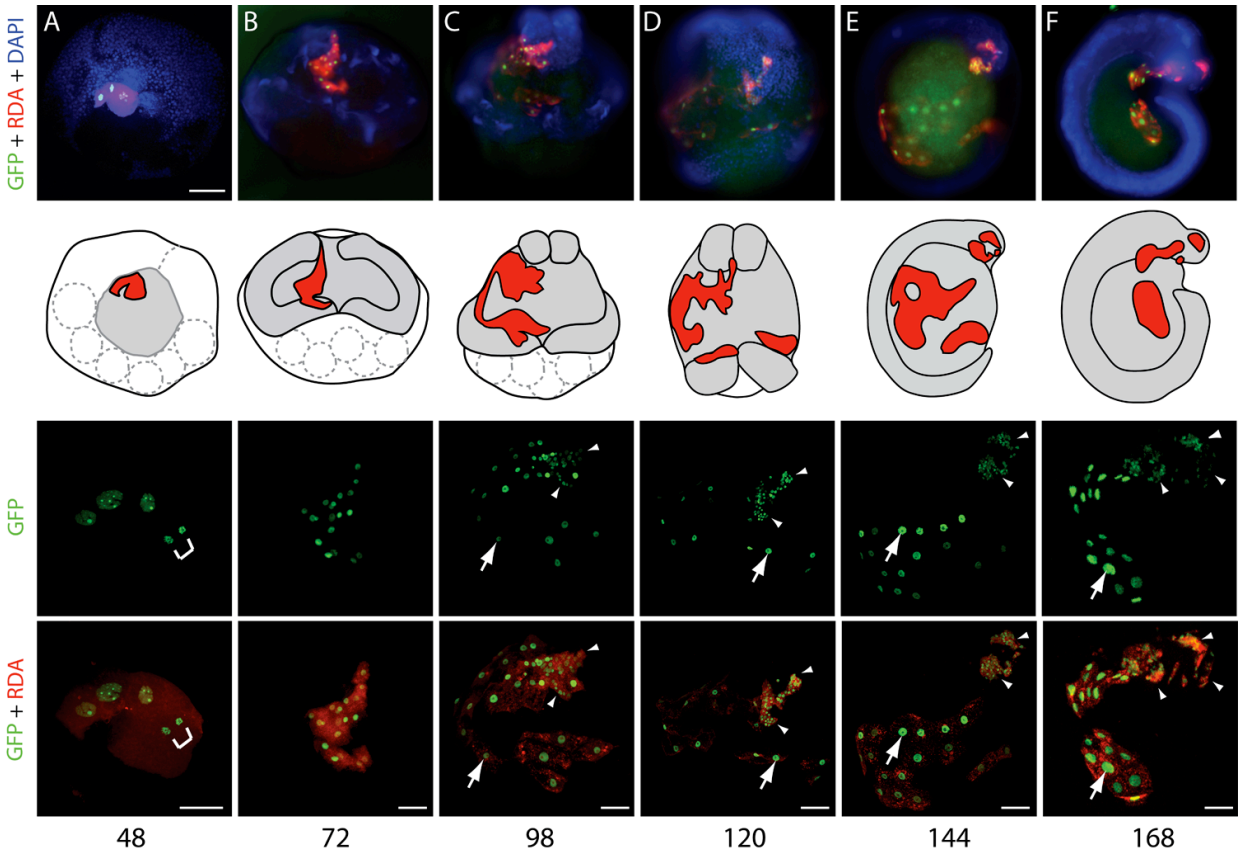


Figure 2.9. Plasmid-driven transgene expression in a micromere lineage. Images of embryos in which micromere d' was injected at approximately 15 minutes after its birth with RDA and pEF-H2B:GFP; injected embryos were fixed at a range of time points post injection (48-168 hours, as indicated below each panel). In each panel, the topmost images are a low power epifluorescence image of the entire embryo (RDA, red; H2B:GFP, green; DAPI counterstain, blue, except that in panel (A), the blue color is autofluorescence) and a cartoon representation of that image to show the location of the labeled d' clone. The two lower images in each panel are maximum projection confocal stacks as in other figures. A. The d' lineage undergoes early stem-cell like divisions, and in this embryo the parental "stem cell" was captured completing mitosis (white bracket). B-F. At later time points, the d' comes to comprise a mixed population of cells including provisional epithelial cells (arrows) and prostomial cells (arrowheads) that are readily distinguished based on differences in location, nuclear size, and cell morphology. Scale bar: 100 μm in upper panels; 20 μm in lower panels.

CHAPTER THREE

Early progeny of the mesodermal lineage in the leech *Helobdella* sp. (Austin) and the oligochaete *Tubifex tubifex*

Introduction

One of the major questions in evolutionary biology is how changes in developmental processes have enabled the evolution of the wide range of adult body plans seen in extant animals. The Spiralia comprise numerous protostome taxa, including Mollusca, Annelida, Platyhelminthes, Nemertea, Echiura, Sipunculida etc., which share a characteristic early embryonic cell division pattern, called spiral cleavage. Spiral cleavage is now regarded as an ancestral character of the lophotrochzoan superphylum (Dunn et al., 2008; Hejnol et al., 2009). Homologous blastomeres are identifiable among spiralian species by their cell lineage, position and fates, notwithstanding hundreds of millions of years of evolutionary divergence among spiralian taxa. Most prominently, the bilateral division of a cell known as micromere 4d yields left and right mesodermal precursors (mesoblasts). However, the mesoderm of an unsegmented mollusk is quite different from that of a segmented annelid, such as the leech, so at some point, the mesodermal lineages must have diverged among these distantly related spiralian species. Thus, comparing more complete characterizations of the 4d lineage (cell divisions patterns and definitive contributions to the larval and/or adult body plan) across spiralian taxa should permit us to eludicate the developmental changes underlying the morphological diversity of mesodermal structures.

In the leech *Helobdella,* a clitellate annelid, the homolog of the cell 4d is called DM", and its bilateral division gives rise to two large stem cells (M teloblasts), whose iterated divisions yield precursors (m blast cells) of all of the segmental mesoderm. Beyond the regular segmental contribution, it was previously shown that early cells derived from the M teloblasts contribute to non-segmental regions, including the anterior unsegmented tissues known as the prostomium. However due to technical reasons the prostomial contribution of M lineage was poorly defined in these early studies (Zackson, 1982). It was also shown that the "supernumerary m blast cells" (defined as the blast cells arising from the M teloblasts after it has produced the complete complement of segmental blast cells) are variable in number and eventually fuse with other lineages to form the yolk syncytium, which will ultimately comprise the endoderm (Zackson, 1982; Desjeux and Price, 1999).

Using new high-resolution cell lineage tracing techniques, I have developed, I have been able to study the early progeny of the M teloblasts in greater detail than previously possible. I have found that each M teloblast produces six early mesodermal cells (em cells), precursors of non-segmental mesoderm, prior to initiating the production of purely segmental m blast cells (sm cells). All sm cells undergo identical stereotyped early divisions and give rise to homologous sets of pattern elements whose position along the anterior/posterior axis is determined by the birth order of their blast cell of origin (Fig. 3.1; Weisblat and Shankland, 1985). In contrast, the early cell division patterns of the six em cells differ from each other and from the standard sm cells. Additionally, each of the em cells makes unique definitive contributions to the later embryo including the mesenchyme lining the gut and the majority of mesoderm in the head including

muscle throughout the proboscis, a specialized feeding apparatus representing the foregut of the rhynchobdellid leeches.

A more detailed re-examination of the 4d lineage in the oligochaete *Tubifex* revealed that in this annelid there is also contribution from 4d to anterior non-segmental tissue. In contrast to the predatory feeding behavior of *Helobdella*, *Tubifex* ingests sediments as a filter feeder; these differences in feeding behavior are reflected in different foregut morphologies and the anterior 4d contributions in *Tubifex* are dissimilar to those in *Helobdella*. Even among those leeches whose DM" lineage has been carefully studied thus far, (*Theromyzon* and *Helobdella*; current study), the anterior contributions of DM" (4d) vary somewhat (Gleizer and Stent, 1993). Thus, as anticipated these differences illustrate that changes in the developmental program of the teloblasts can result in diversity of adult body plans.

Results

Summary of leech development highlighting events in the mesodermal lineage

Cleavage stages:
Leech development proceeds via a modified version of spiral cleavage that generates 25 micromeres, three macromeres and five pairs of segmentation stem cells (teloblasts). The teloblasts are derived from the D quadrant, which is formed during the first two cleavages through an asymmetric cleavage resulting in segregation of yolk free cytoplasm determinants (teloplasm) first to cell CD (Ren and Weisblat, 2006) and then to the larger D cell (Lyons and Weisblat, 2009). The mesodermal precursor, DM" is born at 6^{th} zygotic cleavage, corresponding to the 4^{th} cleavage within the D quadrant lineage. In spiralians, the precursor of the majority of the mesoderm is classically designated as micromere 4d, due to its animal position relative to its vegetal sibling 4D. Mesoderm derived from other lineages is often referred to as ectomesoderm. The DM" cell in *Helobdella* is much larger than the dm" micromere, and is born vegetally. Therefore, DM" would classically be called 4D if based solely on position and size rather than fate. However since DM" undergoes an equal, bilateral division to give rise to the left and right mesoteloblasts (M_L and M_R) it is considered the homolog of 4d (Fig. 3.2A,B; Sandig and Dohle, 1988).

To visualize the early development of the DM" lineage, DM" was injected with the fluorescent lineage tracer RDA. Embryos were then fixed at various time points post-injection, processed for nuclear counterstaining using fluorescent anti-histone immunostaining and imaged using confocal microscopy. DM" divides bilaterally to give rise to M_L and M_R, which are immediately in apposition, with their nuclei eccentrically localized toward the interface with each other (Fig3.2B; Fernandez and Stent, 1980). After the M teloblasts undergo their initial asymmetric division, their smaller daughter cells (blast cells), make contact (Fig. 3.2C; Fernandez and Stent, 1980). This contact, which marks the anterior of the lineage, remains for over a day, even after proliferation of the blast cell clones has begun in the anteriormost portion of the lineage (Fig. 3.2E; Zackson, 1982). At this stage, although cell distribution patterns in the anterior M-derived blast cell clones are already distinct from each other, the posterior portion consists of a column of undivided primary blast cells, morphologically indistinguishable from one another (Fig. 3.2E).

It should be noted that confocal analysis also revealed that during early blast cell production the shape of the mesodermal teloblasts is not perfectly spherical due to deformation by a blastocoel, which is positioned between them and the ectodermal precursors (Fig. 3.3).

Production of segmental precursors:

Segmentation in the leech is a stereotyped, lineage-driven process. All 32 segments arise from serially homologous complements of mesodermal and ectodermal blast cell clones, deriving from 5 pairs of teloblasts. Four pairs of teloblasts (N, O, P and Q) give rise to the segmental ectoderm and one pair (M) gives rise to the segmental mesoderm. All teloblasts undergo iterated, asymmetric divisions producing columns (bandlets) of blast cells. In normal development, the position of the clonal contribution from a given blast cell along the A/P axis is determined by its birth order; earlier-born, older blast cells make more anterior contributions while later-born younger blast cells contribute progressively more posterior clones. Blast cells undergo lineage-specific stereotyped division patterns and contribute serially homologous pattern elements. Each ipsilateral segmental complement consists of cells derived from one m, o and p primary blast cell. For the N and Q lineages, however, two successive, non-identical blast cells, designated ns, nf, qs and qf are required to generate one segmental complement (Weisblat and Shankland, 1985). Moreover, each segmentally repeated clone spreads across segment boundaries so that repeated pattern elements from multiple blast cells interdigitate within a single morphological hemisegment (Fig. 3.1C-H).

In accord with the general description above, the sm cell gives rise to one segment's worth of mesodermal pattern elements including muscle cells (both provisional and definitive), nephridia, and, more surprisingly, several ganglionic neurons (Kramer and Weisblat, 1985; Gleizer and Stent, 1993; Weisblat and Huang, 2001). Similar to the segment-specific patterning seen in other segmented species, not all pattern elements are present in all segments of *Helobdella*; nephridia are restricted to midbody segments M2-M5 and M8-M18. Primordial germ cells (pgcs) are have also been shown to arise from the sm cells, but these are restricted to segments M6 (for female pgcs) and M8-M18 (for male pgcs) (Kang et al., 2002; Cho et al., in preparation). Ablation studies have shown that, the fate of a mesodermal blast cell is determined at or very soon after its birth (Gleizer and Stent, 1993). Therefore, the segmental identity of a mesodermal blast cell is largely cell intrinsic.

Morphogenesis of segmental mesoderm

Mesoderm segmentation is evidenced by iterated morphologically distinct clusters of about a dozen cells, each of which corresponds to a single m blast cell clone, as early as about 48 hours after the birth of the corresponding sm cell (hereinafter designated as clonal age 48 hours), and well before any morphologically distinct units can be discerned within the ectoderm (Zackson, 1982). These clusters, or hemisomites, are visible in the anterior segmental portion of the lineage as early as 72 hours after the birth of the DM" (Fig. 3.2F,G; Zackson, 1982). By mid-stage 8, anterior segmental clusters start to spread out medially to underlie all ectodermal lineages (Fig. 3.2H; Zackson, 1982).

By late stage 9, after the completion of germinal plate formation, segmental morphogenesis occurs progressively from the anterior to the posterior. The M kinship group, one set of the segmentally repeated pattern elements derived from the M lineage, includes neurons (mn), connective muscle, dorsoventral muscle, body wall muscle as well as segment specific

features such as nephridia as mentioned above (Fig. 3.2; Weisblat and Shankland, 1985; Gleizer and Stent, 1993). As previously mentioned, each sm cell contributes one segment's worth of mesoderm. It is the arrangement of repeated blast cell clones along the body axis that results in morphological segmentation. During morphogenesis, clones derived from primary blast cells, which originally formed cohesive hemisomites, begin migrating posteriorly and interdigitating with neighboring clones (Fig. 3.1C-H; Zackson, 1982). Therefore, a kinship group in a morphological segment is made up of the progeny of more than one sm cell. Because of this interdigitation, a problem arises concerning the first several segments. Focusing on the M derived neurons for example, each mn cluster sits one segment posterior to the anterior boundary of the sm clone. Therefore, in the first segment, if there is not a more anterior sm cell to contribute mn neurons which lineage, if any, will complete the kinship group of the first segment? This problem will be addressed in subsequent sections.

DM" and M make major contributions anterior to the first segment

Several previous workers have noted that, in stage 7-8 embryos in which either the DM'' cell was injected with lineage tracer, or an individual M teloblast soon after the bilateral division of DM'', numerous labeled M-derived cells are visible in addition to the sm clones described above.

Specific examples of these seemingly non-segmental, M teloblast derivatives include: 1) a set of about 32 scattered migratory cells (freckle cells; Chi, 1996) lying beneath a micromere-derived epithelium between the germinal bands; 2) at the anterior lateral portion of the left and right germinal bands are pairs of conspicuous flat cells with large nuclei (Fig. 3.2G-J; Gline et al., 2009); 3) directly medial and posterior to these large flat cells are distinct populations of cells with different nuclear sizes and cell densities (Fig. 3.2I). Do these cells truly represent non-segmental mesoderm? If so, from which cells do they arise and to what tissues to they contribute their definitive progeny?

Using ectodermal lineages to define the anterior limits of segmentation

During stage 8, the progeny of the left and right hemisomites join at the prospective ventral midline from anterior to posterior forming the germinal plate, giving rise to all segmental mesoderm. Concurrently, overlying left and right complements of segmental ectoderm meet in a similar manner. Interestingly, the anteriormost portions of the left and right mesodermal lineages do not come in contact even while more posteriorly the left and right complements of the segmental lineage have already met to form the germinal plate (Fig. 3.2J). I therefore hypothesized that the anteriormost contact point in the germinal plate marks the anterior boundary of the segmental tissues (sm clones) at this stage.

It is already known that the OP lineage makes only segmental contributions (Kuo and Shankland, 2004). The first segment can thus be marked by injecting the OP teloblast with lineage tracer immediately after its birth. I therefore injected either DM" or an M teloblast soon after its birth with RDA, and the ipsilateral OP teloblast with FDA, then cultured the embryos to stage 9 or 10 to examine the distribution of fluorescently labeled cells. In these and all subsequent unilateral M injections described, only the M_L teloblast was injected as it is the most superficial of the two during early stages; M_R being buried deeper beneath the macromeres.

In stage 10 embryos resulting from these experiments, a large portion of RDA labeled M-derived cells lies anterior to the FDA labeled OP lineage (Fig. 3.5A), consistent with my hypothesis that the morphologically distinct anterior M-derived cells are non-segmental. The early N lineage makes two non-standard blast cells, which do not make segmental contributions (Zhang and Weisblat, 2005), so I also carried out similar experiments comparing the anterior boundaries of the M and N lineages. The germinal plates of embryos whose M teloblast was injected with RDA and N teloblast with FDA were dissected away from the yolk and analyzed. There were many RDA containing cells anterior to the FDA labeled N lineage, the anteriormost portion of which is already non-segmental. Additionally, portions of the anterior M lineage were seen crossing over the midline (Fig. 3.5B). In embryos whose DM" was injected with RDA and the left and right OPQ" with FDA, large anterior DM" contributions were also apparent (Fig. 3.5C). Together, these data confirms that the DM" lineage contributes to anterior non-segmental tissue.

Early morphogenesis of the anterior DM" lineage can be seen in ventral and dorsal projections of high-magnification confocal stacks of DM" injected embryos. Ventral projections reveal an anterior ring of cells, corresponding to the muscular sheath surrounding the proboscis of later stages (Fig. 3.5E). Deeper projections show medial anterior cells corresponding to the forming proboscis (Fig. 3.5F). More advanced morphogenesis in the DM" lineage can bee seen, in those embryos whose DM" cell was co-injected with RDA and pEF-H2B:GFP and cultured to stage 9; hundreds of DM" derived cells can be seen in the developing head including throughout the proboscis (Fig. 3.4).

Segmental blast cell production begins around the same time in the mesodermal and ectodermal lineages

Since the M teloblasts are born around 6.5 hours before the N teloblast and around 12.5 hours before the OP proteloblast and Q teloblast it was previously assumed that segmental blast cell production began earlier in the mesodermal lineage than in the ectodermal lineages. However it is now clear that the early mesodermal lineage makes major anterior non-segmental contributions and thus must begin sm production later than previously thought. In light of these results, I set out to test the hypothesis that segmental blast cell production begins at around the same time in all teloblast lineages.

For this purpose, I performed timed injections of separate tracers (RDA and FDA) into the mesodermal and ectodermal lineages. Embryos were grown up to early stage 9 and the germinal plate was then dissected off of the yolk and mounted for confocal imaging. The OP lineage makes only segmental contributions, therefore as expected when the M teloblast was injected at its birth with RDA and the OP teloblast at its birth (12.5hours later) with FDA, their anterior boundaries did not align (Fig. 3.6A). When the M teloblast and the OP teloblasts were both injected at the birth of the OP teloblast, in 19/26 (73%) of the embryos the anterior boundaries of the lineages aligned while in 7/26 (27%) of the embryos the anterior boundary of the M lineage sat one segment posterior to that of OP (Fig. 3.6B,C). Given slight differences in developmental timing across batches, delays between injections and natural asynchronies among teloblasts it is expected that minor offset in the timing of injection would occur in some embryos, but the M and OP lineages begin segmental blast cell production around a much narrower time window than previously thought.

Somewhat similar results were seen when N and OP were injected at the birth of OP or when M and N were injected at the birth of OP (Fig. 3.6D-F); 11/23 embryos with the N and OP teloblasts injected at the birth of OP had aligning anterior boundaries and 12/23 embryos had N lineage contributions anterior to that of OP. It has been previously shown that the N teloblast makes two non-segmentally contributing micromeres during its early divisions (Zhang and Weisblat, 2005). The N lineage also contributes extra neurons to the ganglia of the first segment, R1 (Zhang and Weisblat, 2005) therefore its anterior segmental boundary extends beyond that of the other ectodermal lineages. Therefore, even though the N teloblast is born prior to the other ectodermal teloblast lineages, it only starts producing standard segmental blast cells around the time when the other ectodermal teloblasts do (Zhang and Weisblat, 2005).

Identification and enumeration of the em cells

Having determined the timing of the onset of segmental blast cell production in the M lineage (after the start of stage 6b), I then sought on to determine how many "early mesoderm" (em) cells were born prior to that time point and to characterize their contributions; in fact previous work in the lab had already shown that two such em cells accounted for the freckle cells described earlier (Chi, 1996), but whether these cells accounted for all the non-segmental tissue was unknown. Additionally, because the early M lineages make non-standard contributions, I wanted to determine the early cell cycle durations of the M teloblasts (defined as the time interval between two cytokineses) to see if there was systematic variation in the teloblast cell cycle length during production of the postulated em cells and if the teloblast cell cycle duration during em production differed from that during sm production. I also wanted to correlate the birth of each em cell with landmark events in development in order to facilitate timed tandem injections as described below.

To ascertain all of the above points, timelapse movies were taken of embryos whose DM" proteloblast or early M_L teloblast was injected with RDA, starting soon after DM" divided into M_L and M_R. Darkfield and fluorescent time-lapse images were taken at a frame rate (0.2-0.5/minute) which was already known to be sufficient for revealing the rhythmic movements associated with cytokinesis of the teloblasts. Movies were also made starting at late stage 5 through stage 7 using darkfield only; by these stages the M_L teloblast is more superficial and fluorescent tracer is not required for its visualization. Timelapse imaging showed that six cells were born from the M teloblast prior to the beginning of stage 6b, when the first definitive sm cell is born (Fig. 3.6B, Fig. 3.7). I found no significant different in teloblast cell cycle durations during em production or between em and sm production; average cell cycle durations were calculated for the first ten divisions of the M teloblast after the birth of em1, with an overall average cell cycle of 120 minutes (Fig. 3.7). The minimum average was 116.6 minutes (em5) and maximum 127.6 minutes (em4). Students' T test revealed no significant difference between em4 and 5 (P=0.2795). Timelapse data also revealed that stage 5 lasted on average 5 hours 42 minutes and stage 6a lasted on average 6 hours in *Helobdella* sp. (Austin), compared to approximately 3 hours 45 minutes and 3 hours 30 minutes for stages 5 and 6a respectively in the faster developing *Helobdella robusta* (Huang and Weisblat, 2001). The cell cycle of the M teloblast during em1 production could not be determined directly from time-lapse recording since time had elapsed after the start of 4c and the beginning of imaging, but it can be

reconstructed by combining the time-lapse data and direct observation of the onset of stage 4c (i.e. the birth of M teloblast).

In addition to showing the invariance of early M teloblast cell cycle durations, this analysis also allowed me to identify easily observed developmental landmarks that correlated reliably with the birth of each em cell (Fig. 3.7).

Clonal proliferation and distributions in the early mesodermal lineages

To test the conclusion that the M teloblasts systematically generate six putatively non-segmental em cells prior to the first sm blast cell, and to visualize the clonal distributions and proliferation of the em cells, progeny of individual em or sm cells were uniquely labeled using timed tandem injections (Fig. 3.8). For this purpose, M teloblasts of carefully staged embryos were first injected with RDA and either pEF-H2B:GFP plasmid or *h2bgfp* mRNA. Two hours later the same teloblast was injected with Alexafluor 647 tracer. This two hour interval corresponds to the cell cycle length of the M teloblast, so that exactly one cell should be born between the two injections. If not imaged immediately, embryos were processed for anti-GFP immunostaining to preserve the GFP label. The time-lapse data described above were used to determine the timing of tandem injections. Starting at late stage 4c, this time window was shifted later into development to uniquely label individual em cells and sm cells. Definitive contributions of em cells to the stage 9 embryo were determined using similar timed tandem injections to those described above. In these injections, the left M teloblast was injected with RDA at a selected time point and then two hours later with FDA. Tandemly injected embryos were then grown to stage 9, fixed and processed for confocal microscopy.

The tandem injection experiments confirmed that six em cells (henceforth designated em1 through em6) are born prior to the first "normal" sm cell, and also revealed that these cells make distinct, predictable and (largely) non-segmental contributions to the embryo according to their birth order, as described in the following paragraphs:

em1 and em2

The progeny of em1 and em2 behave similarly throughout development; both undergo rounds of equal cell divisions to generate clones of morphologically indistinguishable, migratory cells, largely as described by Candace Chi (1996) for *H. robusta*. Despite these similarities, cell counts for em1 were on average lower than those for em2 at both two and three days clonal age. In *H.* sp. (Austin), at two days clonal age there are on average 1.7 cells (2 maximum) uniquely labeled born from em1 and 4.3 cells (6 maximum) born from em2 (Fig. 3.8A,B; Fig. 3.9). At three days clonal age, the progeny of em1, comprise on average 8.65 cells (14 maximum), and those of em2, 13.75 cells (16 maximum) (Fig. 3.8A',B'; Fig. 3.9). I have determined however that the M lineage during stage 4 in *H.* sp. (Austin) is sensitive to injections and development is delayed when injections are performed before stage 5. In those embryos with low counts for em1 at three days clonal age, counts for em2, visible as the migratory population of double-labeled cells, were also lower. There were however, several embryos with cell counts for em1 equivalent to those for em2 at 3 days clonal age. I therefore concluded that the proliferation differences between em1 and em2 were likely artifacts of injection. In comparable experiments in the closely related *H. robusta*, em1 and em2 were shown to have equivalent rates of proliferation by 50 hours clonal age. Development in *H. robusta* is similar to that of *H.* sp. (Austin) with several

notable differences, including acceleration of some stages of development relative to those of *H.* sp. (Austin), and proliferation of the em1 and em2 lineages is one example of this. By 50 hours clonal age, average cell counts for the progeny of em1 in *H. robusta* were 14.35 while those for em2 were 13.4 (Candice Chi honors thesis, 1996). These numbers were similar to those of 3-days clonal age in *H.* sp. (Austin) therefore the early proliferation rates in em1 and em2 are faster in *H. robusta* by a day than in *H.* sp. (Austin).

Progeny of em1 and 2 behave similarly throughout development and contribute to comparable populations of cells in the stage 9 embryo (Fig. 3.10A-C). Cells derived from em1 and em2 are flat, spread out and make little to no contact with one another. By five days clonal age, they are deeply localized (i.e. not physically associated with the body wall but with the endoderm, which can be readily identified by its autofluorescent yolk content; Fig. 3.10B-C). While there are clearly two separate populations that each derive from em1 and em2 respectively, there is some intermixing of the two populations as evidenced by double labeled flat mesenchymal cells mixed with singly labeled cells; in general, the em1 clone is the more posteriorly situated of the two (Fig. 3.10C).

em3

At two days clonal age, em3 comprises exactly two cells, which sit at the lateral anterior edge of the M lineage; the anteriormost cell being the larger of the two (Fig. 3.8C; Fig. 9). They form an arch-shaped cell cluster in the anterior of the M lineage (Fig. 3.8C). Little variation was seen in cell counts of the uniquely labeled progeny of all em and sm cells studied except for em3 (Fig. 3.9). At 3 days clonal age, the uniquely labeled progeny of em3 showed little variation in counts relative to those of the other cells analyzed (Fig. 3.9). By three days clonal age there are on average 4.3 cells derived from em3. Of this clone, the largest cell sits at the anterior of the lineage. Three to four smaller cells also derived from em3 are posterior to the larger cell. Progeny of em4 overlie some of the cells derived from em3.

In stage 9 embryos, em3 contributes to a small patch of cells at the lateral edge of the developing head (Fig. 3.10E,F). In all embryos the lineage tracer in this patch was bright with respect to the rest of the lineage suggesting that there had been fewer cell divisions in this sub-lineage (so that the tracer had remained more concentrated). Progeny of em3 also give rise to muscles within the proboscis (Fig. 3.10E,F).

em4

At two days clonal age em4 comprises an average of 4.6 cells, roughly equal in size (Fig. 3.8D; Fig. 3.9). By three days clonal age there is a distinct stereotyped morphology of the progeny of em4, which average 15.7 in number (Fig. 3.8D',D"; Fig. 3.9). At the anterior lateral portion of the clone is a curved column of cells. The rest of the uniquely labeled cells are more compactly clustered at a more medial position. All the cells derived from em4 at this stage have similar nuclear sizes (Fig. 3.8D'.D"). In stage 9 embryos, em4 contributes to scattered cells throughout the head including musculature within the proboscis (Fig. 3.10G,I,J). Additionally, em4 gives rise to a sparse population of cells with extended cellular processes amongst the provisional circumferential muscle fibers (3.10H). However, these cells are morphologically distinguishable from the sm cell-derived circumferential muscle fibers; they are not striated, nor are they always oriented in parallel to the muscle fibers and sometimes bridge several muscle

cells. These cells may be neurons innervating provisional circumferential muscle fibers, which start their coordinated rhythmic contraction at this stage.

em5

The progeny of em5 at two days clonal age, with an average clonal size of 7.4 cells, have exhibit a range of nuclear sizes and comprise a coherent cluster at the anterior of the M lineage (Fig. 3.8E; Fig. 3.9). By three days clonal age em5 comprises on average 22.7 cells, some of which are situated beneath the rest of the M lineage and therefore not visible in maximally projected confocal stacks (Fig. 3.8E',E"; Fig. 3.9). In many embryos at 3 days clonal age, there was cell debris containing RDA anterior to the labeled lineage, suggesting that cell death had occurred in em5 sublineage(s).

In the stage 9 embryo, most definitive progeny of em5 lie in anterior non-segmental tissue, including cells in the proboscis as well as a ring of cells around the opening of the proboscis, which will become the musculature of the proboscis sheath (Fig. 3.10K,M,N). In addition, like em4, em5 gives rise to a sparse population of cells amongst the provisional circumferential muscle fibers (Fig. 3.10L).

In marked contrast to the em1-em4-derived clones, however, em5 also gives rise to a small cluster of presumptive neurons on the ventral side of segmental ganglion of R1, ventral to the first forming coelom (Fig. 3.10N). Morphologically similar clusters of m derived neurons (mn), each arising from one sm cell, are found in every segmental ganglia (Kramer and Weisblat, 1985; Weisblat and Shankland, 1985; Huang and Weisblat, 2001). It is therefore likely that the cluster of cells in the ganglia of R1 derived from em5 is serially homologous to the other segmentally iterated mn along the AP axis. em5 is therefore a hybrid, both segmental (mn in segment R1), and non-segmental (major contributions to the head), in its contribution.

em6

Data from time lapse imaging, simultaneous injections of the M and OP cells, as well as the tandem injections described in this section, all indicate that the cell designated as em6 is born one cell cycle before sm1, the M teloblast daughter giving rise to the hemisomite that aligns with the first segmental complement of OP-derived ectoderm. And yet, the em6 clone already exhibits many features of the standard sm clones.

At two days clonal age, the progeny of em6 form a coherent cluster of cells with varying nuclear sizes, averaging 10.3 cells in number (Fig. 3.8F; Fig. 3.9). By this stage segmentation in the anterior of the M lineage is apparent; nearly isomorphic repeats representing progeny of individual sm blast cells form anteroposteriorly (hemisomites; Fig. 3.2F-H; Zackson, 1982). At this point, the em6 clone is morphologically similar to those of its posterior neighboring hemisomite. One day later, cells within the anterior hemisomites have begun migrating medially to underlie all ectodermal lineages, and this migratory behavior can also be seen in the uniquely labeled clone (Fig. 3.8F',F"). By three days clonal age, the progeny of em6 have undergone more extensive proliferation than em1-em5, with clones averaging 37 cells (Fig. 3.9).

Thus, em6 is the first cell born from the M teloblast to give rise to a nearly complete segment's worth of progeny spanning segments R1-R3 (Fig. 3.10O-Q). Deeper projections show uniquely labeled cells surrounding the walls of the forming coelomic cavity of R1, as well as to connective muscle, more superficial muscle, a small cluster of m derived neurons in segment R2, as well as a lateral patch of mesoderm in segment R3 (Fig. 3.10P-Q). However, in addition to a

largely normal complement of segmental progeny, this clone also gives rise to some non-segmental progeny, in the form of longitudinal muscles within the proboscis, and it does not give rise to a population of uniquely labeled provisional circumferential muscle fibers. These differences lead me to judge this cell as also being a hybrid between segmental non-segmental in character, and to designate it as an em cell rather than a standard segmental (sm) cell. By my criteria, the first purely segmentally contributing cell born from the M teloblast is the seventh cell born, now called sm1 (see below).

sm

Progeny of smx (any given sm cell) are very similar in both morphological appearance and proliferation rates at both 2 and 3 days clonal age, 10.1 and 41.5 cells respectively, to those of em6 (Fig. 3.8F-G"). Clonal sizes of em6 and smx were not distinguishable from each other at both two and three days clonal age (Student's t test, unpaired, unequal variance assumed, P=0.862 and 0.282 respectively), suggesting the proliferation rates of the progeny of these two cells are very similar (Fig. 3.9). Contributions of segmental m blast cells to the later stage embryo have been well characterized (Kramer and Weisblat, 1985; Weisblat and Shankland, 1985; Gleizer and Stent, 1993; Huang and Weisblat, 2001). My results here, following the progeny of individual sm cells, confirm previous findings. While there are segment-specific specializations in the M lineage (Gleizer and Stent, 1993), there are certain contributions that are invariant between sm cells and these include provisional muscle fibers, m derived neurons, connective muscle, dorsoventral muscle as well as other muscular contributions. Confocal images of embryos with uniquely labeled sm cells in varying positions of the bandlet give rise to progeny exhibiting nearly identical patterns of labeled cells at stage 9. Similar to the progeny of em6, progeny of any given sm cell contribute to musculature surrounding the coelom, connective ventral muscle and to a cluster of neurons one segment posterior to the majority of the clone (Fig. 3.10R-T). Circumferential muscle fibers descending from a segmental blast cell migrate both dorsally away from the germinal plate and posteriorly from the anterior boundary of the clone for a distance ranging from 1-5 segments (Fig. 3.10R).

Since the contributions of em6 were nearly identical to that of a standard sm cell, with the exception of contributions of longitudinal muscle fibers to the proboscis, I wanted to test the hypothesis that its initial division was similar to that of a typical sm cell. Despite segment specific specializations in their later development, in their first cell division, all primary segmental m blast cells divide equally and bilaterally and have similar cell cycle lengths. To visualize the first division of em6, timed injections of RDA into the M teloblast were performed. Embryos were then fixed approximately 20-24 hours later, processed for anti-histone antibody staining, cleared in BBBA and imaged using confocal microscopy. As predicted, em6, like all standard sm cells, undergoes a bilateral first division. Relative to the more posterior sm cells, em6 generally divided with respect to birth order (Fig. 3.11A), with the exception of one embryo where it was seen completing mitosis after an sm cell directly posterior to it (Fig 3.11B). This suggested em6 has a similar cell cycle length to the sm cells. With respect to more anterior em cells, however, em6 appears to have a significantly shorter cell cycle. In one embryo, em6 was seen completing mitosis while directly anterior to it, em5 and em4 had not yet divided, suggesting the cell cycle length of primary em cells differs as would be expected based on differences in proliferation and clonal distributions of em cells 1-6 at 2 and 3 days clonal age (Fig. 3.11C).

Interactions of mesodermal and ectodermal lineages during development

One puzzle in leech development is how the consegmental progeny of blast cells from the five separate lineages come into register with one another on the left and right sides of the embryo, given that the blast cell from which they arise are born at different times and places within the embryo (Weisblat and Shankland, 1985; Huang and Weisblat, 2001). It was originally assumed that segmental blast cell production in the mesodermal lineage began earlier than in the ectodermal lineages, and that the ectodermal lineages crawled along the mesodermal lineage towards the presumptive anterior to make up for this delay (Huang and Weisblat, 2001). From the work presented here, we now know that M_L and M_R do not begin purely segmental blast cell production until around the same time as when ectodermal teloblasts start their segmental blast cell production. The ectodermal lineages may therefore converge and crawl along the mesodermal lineage aligning not with the anterior of the M bandlets, but with the mesodermal progeny contributing to the first segment.

To investigate this process I injected a left M teloblast at its birth with RDA and an ipsilateral OP teloblast at its birth (12 hours after the M injection) with FDA. As mentioned in an earlier section, the OP teloblast was chosen because its progeny are only segmental in contribution. Moreover, unlike Q, it is more superficial and thus easier to inject. Embryos were fixed at various time points post injection (hours correspond to time elapsed after the second injection). By 30 hours post injection, the M and OP lineages were not yet in contact and the anterior ends of the m and op bandlets face one another (Fig. 3.12A). By two days post injection, the OP lineage has become lined up with the M lineage (Fig. 3.12B). At this moment, em1- and em2-derived cells have begun migrating away from the anterior end of the m bandlet. The anterior end of the OP lineage does not align with the anterior end of the M lineage (Fig. 3.12B). Three days after injection, the anterior non-segmental M lineage has become morphologically distinct. The OP lineage does not overlie this large population of morphologically distinct M derived cells. I interpret this as indicating that the ectodermal bandlets line up with the anteriormost segmental sm blast cell (Fig. 3.12C). The actual signals by which the ectodermal and M lineage communicate to coordinate this morphogenetic alignment remain unknown.

Contributions of DM" to the proboscis

The proboscis of *Helobdella* and all, rhynchobdellids or "jawless" leeches, is a specialized eversible feeding apparatus, which in *Helobdella* is used to penetrate between the foot of the snail and the shell, and suck out the soft body parts. Structurally, the adult proboscis is a muscular tube with a roughly tripartite lumen and comprising three sets of muscles, along with various accessory cells. First and most prominent are the radial muscles, which span the wall of the proboscis from the lumen to the outer surface and whose contraction increases the diameter of the lumen, sucking in material. Second, a band of circumferential muscles sits roughly at the midpoint of the radial muscles. Contraction of these muscles should decrease the lumen. Thus, the radial and circumferential muscles work in mutual opposition. Third, a ring of longitudinal muscles at the outer edge of the proboscis should serve to bend the proboscis (which when extended undergoes searching movements similar to those undertaken by an elephant's trunk)

and perhaps also to shorten it. Accessory cells include sheath cells, neurons and ductules that carry the salivary gland secretions (Sawyer, 1986; Kang et al., 2003). Development of this complex organ, becomes evident during stage 9; the proboscis forms in the everted position and soon becomes the most prominent structure at the anterior end of the embryo. By late stage 10, the proboscis retracts into the body mass. In the adult, it only becomes everted when feeding (Kang et al., 2003).

As the proboscis takes shape during stage 9/10, organized sets of cells with characteristic positions relative to one another become evident. Generally, the proboscis is organized into three morphologically distinct layers. The inner ring at this stage is not tripartite, but rather doughnut shaped, and appears as a continuous column of epithelial cells surrounding the lumen. Just outside of and hugging the inner ring is the middle ring comprised of circumferential muscle fibers. The outer ring made up of both radial muscles, which are oriented towards the lumen as well as longitudinal muscle fibers (Kang et al., 2003; Huang et al., 2001). The proboscis sits in a fluid filled cavity, which is encased by a bilayered sheath made up of both muscle and epithelium.

Multiple lineages contribute to the proboscis. Micromeres dm' and c''' were identified to give rise to a network of circumferential muscle fibers in the proboscis (Huang et al., 2002). Directly outside of and surrounding these circumferential muscle fibers, are presumptive longitudinal muscles derived from the primary quartet (micromeres a', b', c' and d') (Kang et al., 2003). At least three additional micromere lineages (a", c" and dnopq') also make contributions to the proboscis including to presumptive neurons, epithelia and muscle. Furthermore, at least five known lineages contribute to the proboscis sheath (Huang et al., 2002). Until my present experiments however, the major contributor of cells in other portions of the proboscis, such as the inner ring, and the majority of the outer layer, were still unaccounted for based on lineage tracing results (Huang et al., 2002; Kang et al., 2003). Here I show that in addition to mesoderm throughout the head, DM" makes major contributions to the inner and outer layers of the proboscis, to the musculature of the sheath as well as minor contributions to circumferential muscles in the middle layer as outlined below.

Contributions of DM" to the proboscis and its sheath were characterized in embryos whose DM" proteloblast was injected with RDA (stage 4b); the injected embryos were fixed at early stage 10 and counter-stained with DAPI, then embedded in plastic blocks and sectioned by hand using a razor blade, and observed by fluorescence microscopy. RDA-containing muscle fibers were seen throughout the sheath at all levels along the A-P axis of the proboscis. Sagittal sections near the surface of the head revealed an array of DM"-derived presumptive longitudinal muscle fibers radiating from the tip of the proboscis and are embedded in the sheath extending posteriorly toward the oral opening where another set of DM" derived circumoral muscle fibers run perpendicularly to these longitudinal fibers (Fig. 3.13A). The RDA-labeled muscle fibers in the sheath and the inner ring of the proboscis are visible in the anteriormost transverse sections. The inner ring appears as a continuous ring of RDA containing cells, indicating that it is completely derived from DM" at the level of this section (Fig. 3.13B-B"). At this stage, the inner ring exhibits the morphology of a simple columnar epithelium in which cells are tightly packed with individual cells exhibiting a wedge shape to form a perfect ring (Fig. 3.13B-B"); the definitive fate of this inner ring remains to be determined. Perhaps it thins to become the inner lining of the proboscis lumen. Directly surrounding the inner ring were several RDA containing circumferential muscle fibers. The majority of the contributions from DM" to the outer ring,

however, were presumptive radial muscles with their processes extending towards the lumen (Fig. 3.13C-C"). However, these muscle fibers did not extend across the middle and inner layers to the lumen as in the adult.

Sectioning was also performed on stage 10 embryos with unilateral RDA injections into early M_L teloblasts. In these embryos, cells in the sheath, inner, middle and outer layers all showed variable amounts of midline crossing (Fig. 3.13D-F"). This is unlike in the segmental portion of the lineage in which progeny of sm cells strictly respect the midline boundary (Fig. 3.6; Weisblat et al., 1980). Also relative to one another, the medial boundaries of RDA-labeled cells within the three layers of the proboscis and the sheath often did not align (Fig. D-F"). Because of this, RDA labeled circumferential muscle fibers in regions where the inner ring cells were not labeled, were especially apparent (Fig. 3.13D-D" and F-F").

Conundrum of the proboscis

Extrapolating from the morphology the adult proboscis using data from sections, false assumptions were previously made concerning the cells of the inner ring of the stage 10 embryo (Kang et al., 2003). It has been well documented that in the proboscises of adult leeches across diverse species, radial muscle fibers extend from the basal lamina of the lumen to the outer periphery of the proboscis (Fig. 3.13A',A"; Sawyer, 1986; Kang et al., 2003). These radial muscles fibers are opposed by a belt of circumferential muscle fibers midway along the radius of the proboscis dividing them into inner and outer layers. The radial muscle fibers are therefore a uniform population of cells, and thus the distinction between radial muscles of the inner and outer layers is somewhat false (Fig. 1.2; Fig. 3.13A',A"). However it is now clear through DM" and M lineage tracing experiments, that at early stage 10 the inner and outer rings are distinct. At this stage, the M derived inner ring looks morphologically dissimilar from the radial muscle fibers in the outer ring, and there is little to no contact between the two (Fig. 3.13).

The discovery that the inner ring of the stage 10 leech embryo is distinct from the outer layer, and that neither layer extends across the radius of the proboscis, poses a new problem. If the inner and outer layers of the adult proboscis include radial muscles spanning from the lumen to the outer edge, what becomes of the cells of the inner layer of the stage 10 embryo? Do they eventually form projections and extend to the outer edges of the proboscis while the outer radial muscles extend inwards? Or do the cells of the inner ring become compressed towards the lumen to form a thin layer of epithelium between the lumen and the radial muscle fibers? Or are they dispersed among radial muscle fibers that have extended from the outer layer across to the lumen? Sections of DM" and early M RDA-injected embryos at stages intermediate between 10 and adult are necessary to solve this morphological problem.

4d lineage in the oligochaete annelid Tubifex

Tubifex tubifex is an oligochaete relative of the leech, which undergoes nearly identical early development to that of *Helobdella* (Shimizu, 1982; Goto et al., 1999a; Goto et al., 1999b; Nakamoto et al., 2000). Differences between these worms however, include the ability of *Tubifex* to elongate their body axis by adding new segments posteriorly throughout their lifetime and their capability to regenerate following amputation. Additionally, *Tubifex* worms feed by ingesting mud and selectively digesting the bacteria and other nutrients that come along with it

(hence their common name, the sludge worm). Therefore, *Tubifex* does not have an eversible proboscis as does *Helobdella* and thus has a different head structure. Despite many developmental and morphological differences, embryonic cell lineages and their fate maps are similar between the two. *Tubifex* is therefore a useful model system with which to compare segmentation and development to that of leeches.

Contributions from segmental m blast cells to the late stage *Tubifex* embryo are nearly identical to those in *Helobdella*, with only a few segment-specific differences (Goto et al., 1999a). As in *Helobdella*, m blast cells in *Tubifex* give rise to circular and longitudinal muscles, muscle surrounding the coelomic walls, m-derived neurons in the ventral ganglion as well as segment specific features. Species-specific segmental specializations include the presence of nephridia, in segments 7 and 8 of *Tubifex* as opposed to midbody segments 2-5 and 8-18 of *Helobdella*, and primordial germ cells in segments 10 and 11 of *Tubifex* as opposed to segments 6 and 8-18 of *Helobdella* (Weisblat and Shankland, 1985; Goto et al., 1999a). These segmental differences in the M lineage between *Helobdella* and *Tubifex* already indicate disparities in the developmental program of the M teloblasts between the two (Gleizer and Stent, 1993; Goto et al., 1999b).

Given the major differences in the head structures between *Tubifex* and *Helobdella*, I wanted to first test the hypothesis that the 4d lineage in *Tubifex* makes anterior non-segmental contributions, and secondly to determine the extent to which these contributions differ from those of the 4d lineage in *Helobdella*. To determine the anterior non-segmental contributions of the 4d lineage in *Tubifex*, it was first necessary to define the anterior boundary of the first segment. *Tubifex* is an oligochaete, a worm with bundles of chitinous bristles (chaetae) segmentally distributed along their body axis. There are four bundles of chaetae per segment in *Tubifex tubifex*, one dorso-lateral pair and one ventro-lateral pair (Fig. 3.14; Bouche et al., 1999). While there are numerous photoreceptor chaetae in the prostomium, it is devoid of the normal segmentally repeating pattern of chaetae, as is the peristomal "segment". The first segmentally repeated chaetae only appear immediately posterior to peristome (Bouche et al., 1999). However, in this segment there is not a segmental ganglia; the anterior end of the first segmental ganglion is in the adjacent posterior segment (data not shown). Therefore, depending on how a segment is defined, the first true segment may correspond to the second chaetae containing body segment, referred to as segment III in Bouche et al. (1999).

To visualize the mesodermal lineage in *Tubifex*, the precursor cell, 4d (homologous to DM" in leech), was injected with RDA and embryos were cultured for various amounts of time prior to fixation. Similar to leech, in *Tubifex*, the M teloblasts undergo highly asymmetric divisions to give rise to smaller blast cells, born towards the animal pole (Fig. 3.15A; Goto et al., 1999b). However, unlike in *Helobdella*, the left and right M bandlets in *Tubifex* do not make contact at the presumptive anterior (Fig. 3.15A,B). After three days of development the anterior of the 4d lineage is morphologically distinct from the more posterior segmentally contributing portions (Fig. 3.15C,C'). On each side of the bilateral axis, there is a distinct anterior cell or cell cluster projecting with fine branching on the cellular processes. This cell or cell cluster extends posteriorly along the dorsal side of the embryo. A portion of the branches associated with this structure extend anteriorly beyond the anterior end of the germinal band (Fig. 3.15C,C'). In *Tubifex*, as in the early embryo of *Helobdella*, injected cytoplasmic tracers such as RDA, become concentrated over the nuclei of cells (Weisblat et al., 1984; Goto et al., 1999a; Goto et al., 1999b). Using this as a fortuitous marker of nuclei, the anteriorly extending projection appears to

be made up by a single cell whose large nucleus sits at the lateral anterior portion of the lineage (Fig. 3.15C'). By 4 days post injection, the projection has continued to extend posteriorly and still appears to be composed of one single cell at the anterior of the lineage (Fig. 3.15D,D'). As the segmental lineage beings migrating dorsally, M derived circumferential fibers come in contact with the long projection, which is running perpendicular to them. These bilateral cell processes also continue to extend posteriorly between 6 and 7 days post injection (Fig. 3.15F,G). At this stage it is apparent that the 4d lineage labels cells up to and including the mouth as well as an array of thin muscle fibers that extend across the head, with each individual fiber attaching to a common anchor point on the left and right sides (Fig. 3.15F',G'). Despite the uncertainty in defining the anterior boundary of the first true segment (either segment II or segment III, see above), there is clearly a large amount of anterior non-segmental mesoderm derived from 4d in *Tubifex*. Therefore similar to *Helobdella*, in *Tubifex*, 4d contributes to anterior non-segmental mesoderm but gives rise to a morphologically distinct set of progeny to that in *Helobdella*.

Discussion

While morphologically diverse as adults, spiralian embryos exhibit conserved early cleavage patterns. The precursor of the bilateral mesoderm, traditionally designated as micromere 4d, has been considered one of the most obviously homologous cells in this group (Lambert, 2008). However, variations in its subsequent divisions and contributions across spiralians are becoming evident. The evolutionary plasticity of the 4d lineage thus reflects the diverse forms of mesoderm seen across Spiralia. In order to understand the developmental sources of change behind these morphological differences it is necessary to study this lineage in detail across spiralians. Here, our current findings are setting the stage for the long-term goal of understanding how changes in the 4d lineage translate to diversity among spiralians and asking when along the development of this lineage these changes arise.

Mesoderm of midbody segments of diverse clitellates are morphologically distinguishable and yet we know that early divisions and contributions of the segmental m lineage across clitellate embryos are nearly identical (Weisblat and Shankland, 1985; Goto et al., 1999a; Goto et al., 1999b). Therefore, we propose that the morphological segmental differences in these worms arise during the stages of terminal differentiation within the segmental progeny of the 4d lineage. How about the early non-segmental contributions of 4d? We know that the anterior mesoderm of clitellates also varies; there is huge diversity in head and foregut morphology across this group. Are these anterior differences due to early changes within the lineage, or to differences later on during anterior differentiation? Do all clitelates produce exactly 6 em cells, two of which are hybrid in contribution, or do the number of anterior non-segmental contributors born from the M teloblasts as well as their division patterns and fates vary within this group? The major difficulty in answering this question is that in general there is little data available on anterior non-segmental head regions in these worms and until this work the details of the anterior contributions from 4d were relatively unknown in any clitellate.

Comparisons of our results from *Helobdella* sp. (Austin) with work done in the leech *Helobdella triserialis* indicate similarities in the contributions of early M sublineages. There is evidence of both migratory mesoblasts, or freckle cells, and prostomial contributions, from the M lineage in *H. triserialis* (Zackson, 1982). A more complete analysis of the early progeny of the M teloblasts has been done in the leech *Theromyzon rude* (Gleizer and Stent, 1993). In *T. rude*,

m blast cells are large, born superficially and can be individually microinjected, allowing for the labeling of progeny of single m blast cells. Comparing our results with those from *T. rude* indicate significant differences and similarities in anterior contributions of DM" (Gleizer and Stent, 1993). For example, in *T. rude,* there is no evidence of migratory freckle cells (progeny of em1 and em2) as in *Helobdella* (Gleizer and Stent, 1993). In *T. rude*, the first two m blast cells (m1 and m2) contribute to the prostomium as well as to m derived neurons in the first two segments (Gleizer and Stent, 1993). This is unlike *H.* sp. (Austin) where em cells 1-4 only make non-segmental contributions while the later born em5 and em6 cells are hybrids. The number of additional anterior, non-segmentally contributing m blast cells in *T. rude* is unclear, but m3-m5 may also be hybrids making both segmental and prostomial contributions (Gleizer and Stent, 1993). A more detailed and careful analysis of the early m progeny in *T. rude* is necessary in order to begin to address whether and to what degree the early DM" sublineages are homologous among the Glossiphoniid leeches.

Outside of the Glossiphoniid leeches there is even greater morphological diversity especially in the anterior non-segmental regions. Within the Rhynchobdellida, or jawless leeches, there is variation in proboscis location; protrusion can be seen from the head, or from the rim or middle of the anterior sucker. Proboscis morphology also varies among this group including the extreme example of the Japanese *Ancyrobdella biwae*, which has a specialized proboscis with three hook-like structures at its anterior tip. The Gnathobdella or jawed leeches, do not have proboscises and instead use "teeth" to feed on their prey and therefore have different foregut morphology from the Rhynchobdellids. Barring issues such as extreme feeding and lifestyle requirements, it would be interesting to study and compare the anterior contributions of the DM" lineage across leeches in order to ask whether these early M sublineages are homologous with late divergence at the level of differentiation, or if there is already variation in the number, division patterns and fate of early non-segmental m cells.

I have shown here that in the more distantly related oligochaete worm *Tubifex*, the 4d lineage makes very different contributions to head mesoderm than in *Helobdella*, as would be expected given that their lifestyles and head and foregut morphology are distinct. I have not done a careful analysis of the early M sublineages in *Tubifex* so do not know how many em cells are made in this worm and whether or not they exhibit similar early division patterns to those in *Helobdella*. Nevertheless, there are some interesting differences and potential similarities in the anterior contributing M progeny in these two worms. In *Tubifex* there is no evidence of migratory early M progeny as in *Helobdella.* Intriguingly however, in *Tubifex*, there is a conspicuous cell with a large flat nucleus in a lateral position at the anterior of the left and right germinal bands is visible by three days after the birth of 4d. While this cell makes a long branching process which migrates posteriorly, unlike any cells in the anterior M lineage of *Helobdella*, it is compelling to ask whether it is homologous to the progeny of em3 in *Helobdella* which also makes a large flat prominent cell at the lateral anterior region of the left and right germinal bands. Work done in *Theromyzon* using blast cell ablations to study segment-specific idiosyncrasies in the segmental M lineage determined that blast cell fate is highly cell intrinsic and specified at or soon after the birth of primary blast cell (Gleiser and Stent, 1993). If this were also the case for the em lineages it would suggest that there are differences in the early developmental programs of the M teloblasts between *Helobdella* and *Tubifex* resulting in the production of cells of different fate.

4d lineage in more distantly related spiralians

The daughters of the 4d cell in most spiralians outside of the annelids are commonly known as mesentoblasts because they give rise to both the majority of the mesoderm as well as to endoderm. In mollusks, 4d typically contributes to larval musculature, heart, kidney and intestine. “Typical” mesodermal bandlets have been identified during development of the 4d lineages in diverse spiralians including mollusks and nemerteans (Henry and Martindale, 1998; Goto et al., 1999a; Hejnol et al., 2007). However, limits to the notion of the 4d lineage as highly stereotyped and conserved are starting to emerge as more details of divisions and sub-lineage contributions are analyzed. For example, careful analysis of the early divisions of the 4d lineage in the mollusk *Ilyanassa*, revealed that while there are a pair of large identifiable mesentoblasts undergoing iterated asymmetric divisions as in the 4d lineage of many other spiralians studied, the smaller daughter cells are not always born at the same position relative to the mesentoblast, therefore the stereotypical cohesive mesodermal bandlets are not formed (Rabinowitz et al., 2008). An understanding of the variation in mesoderm across Spiralia will likely come from discovering differences in the 4d lineage during development.

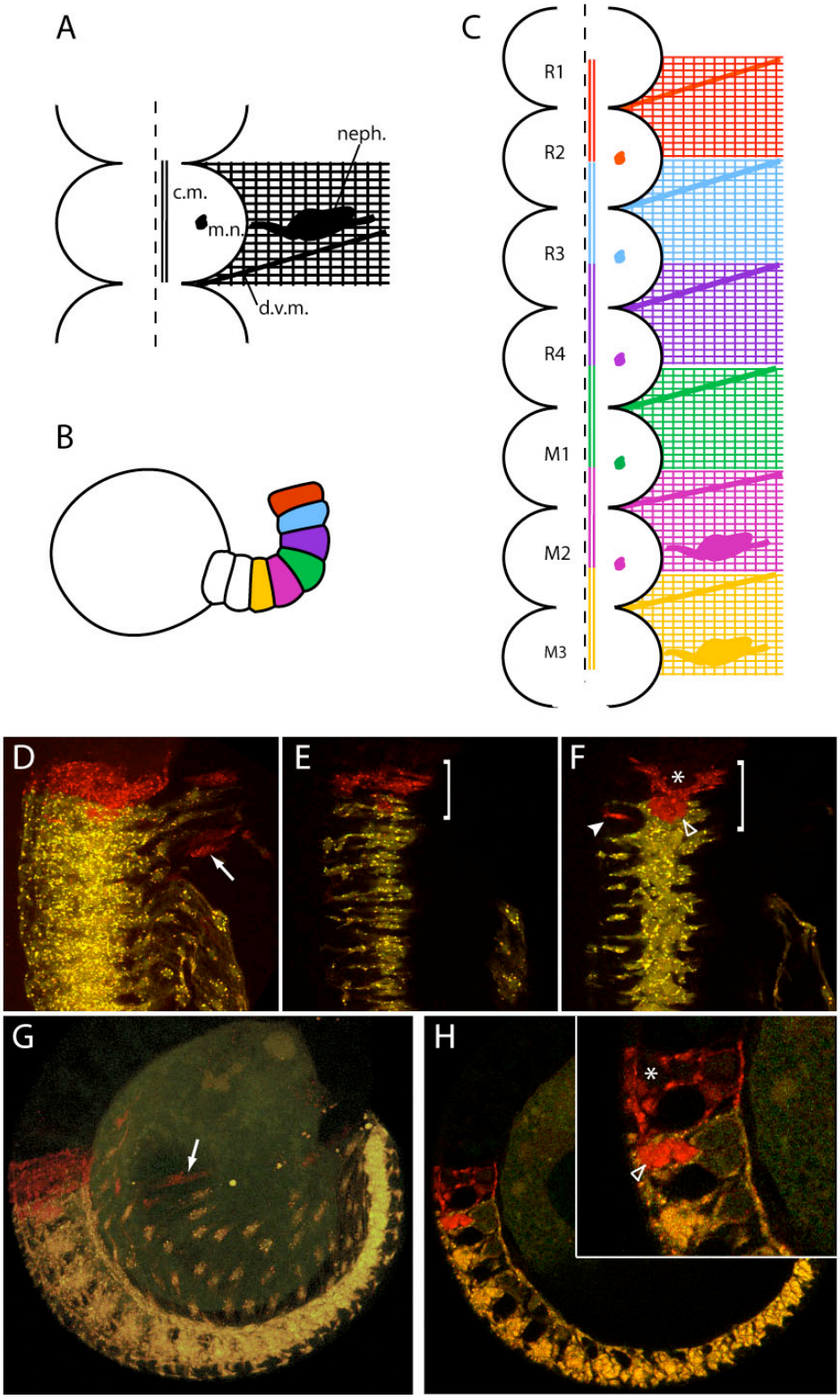


Figure 3.1. Distributions of individual sm cell clones.

Figure 3.1. Distributions of individual sm cell clones. A. Schematic of the M kinship group modified from Huang and Weisblat, 2001. Pattern elements indicated as follows; c.m., connective muscle, m.n., M-derived neurons, d.v.m. dorsoventral muscle, neph. nephridia, hatched lines represent circular and longitudinal muscles. Anterior is up in this and all subsequent figures unless otherwise noted. B. Schematic of an M teloblast and the column of primary sm cells born from it; sm1is labeled with red, sm2 blue, sm3 purple, sm4 green, sm5 pink and sm6 yellow. C. Distribution of pattern elements derived from individual sm cells across segments in the stage 9 embryo. Note, kinship groups of segments R1 and R2 are incomplete as there are no anterior contributing sm cells. Schematized elements are the same as those shown in A. D-F. Confocal projections of a dissected germinal plate showing clonal distributions of uniquely labeled progeny of sm cells in the stage 9 embryo. M_L was injected with RDA (red) during sm production, and re-injected with FDA two hours later, the time in which one sm cell was born. Uniquely labeled cells are shown in red, double labeled cells are in yellow. Embryos were fixed 4 days post injection. D. Complete projection. E. Ventral projection. F. Dorsal projection. Uniquely labeled structures include provisional circumferential muscle fibers (arrow in D), muscle (brackets in E and F) and migrating m derived neurons (arrowhead in F). A semi-circle of cells missing in the anterior patch of mesoderm (asterisk in F) is visible and contributed by the anterior unlabeled clone. The corresponding RDA labeled patch can be seen in the neighboring posterior segment (open arrowhead). G-H. Lateral projections of an undissected embryo similar to that in D-F. G. A large patch of segmental muscle as well as provisional circumferential muscle fibers (arrow) are uniquely labeled. H. Projection of medial slices showing coelomic cavitation. Inset, higher power image of the anterior clone highlighting a missing patch of mesoderm (asterisk), and muscle cells that migrated posteriorly to the neighboring segment (open arrowhead).

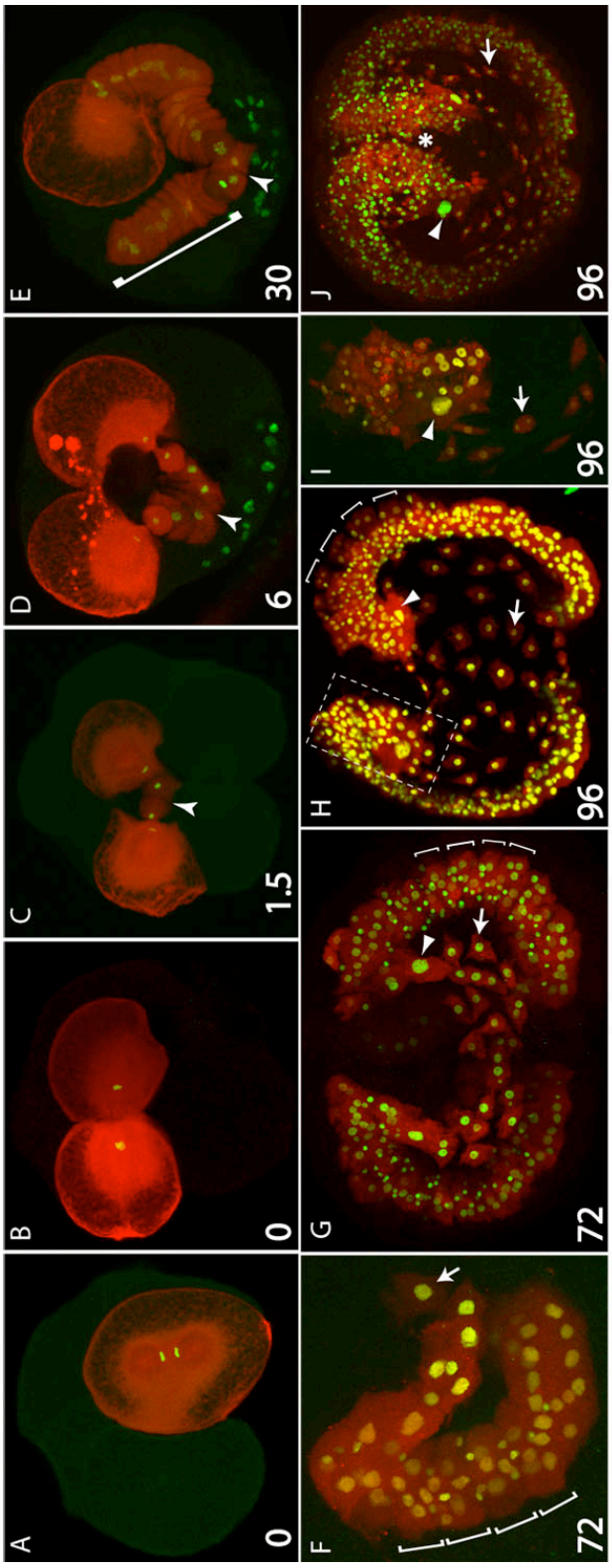


Figure 3.2. Mesodermal lineage during cleavage and segmentation stages.

Figure 3.2. Mesodermal lineage during cleavage and segmentation stages. A-E. To visualize the early mesodermal lineage, DM" was injected with RDA (red). Embryos were then cultured to different stages, processed for anti-histone antibody staining (green) and imaged using confocal microscopy. Numbers in lower left indicate the age of the labeled cell clone in hours. A. An embryo in which the DM" cell is undergoing mitosis. B. M_L and M_R soon after their birth. C. An embryo in which each M teloblast has given rise to one blast cell. The blast cells on the left and rights sides make contact at the presumptive anterior (arrowhead). This contact remains as subsequent cells are born (arrowhead in D) and as proliferation begins at the anterior of the lineage (arrowhead in E). Posteriorly, a column of blast cells is forming (bracket in E). F-J. The M lineage during stage 8 was visualized by co-injecting M_L or DM" with RDA (red) and pEF-H2B:GFP or *h2bgfp* mRNA (expression, green) and culturing embryos for 3-4 days. F. By three days post injection of M_L, segmentation is apparent in the M lineage (brackets). Migratory cells at the anterior of the lineage are beginning to detach (arrow). G. By three days post injection of DM", the anterior migratory progeny have spread out across the dorsal side of the embryo (arrow) and large cells at the anterior of the left and right germinal bands are apparent (arrowhead). H. By four days post injection of DM", medial migration of cells in the anterior hemisomites is visible (brackets). I. Animal view of boxed region in H in a sibling embryo. The large anterior lateral cell (arrowhead) and migratory cells are visible, one of which was captured dividing (arrow). J. A mid stage 8 embryo in which germinal plate formation has begun. Anterior ends of the left and right M lineages have become separated during stage 8. Anterior point of contact between left and right M lineages in the germinal plate is marked by an asterisk.

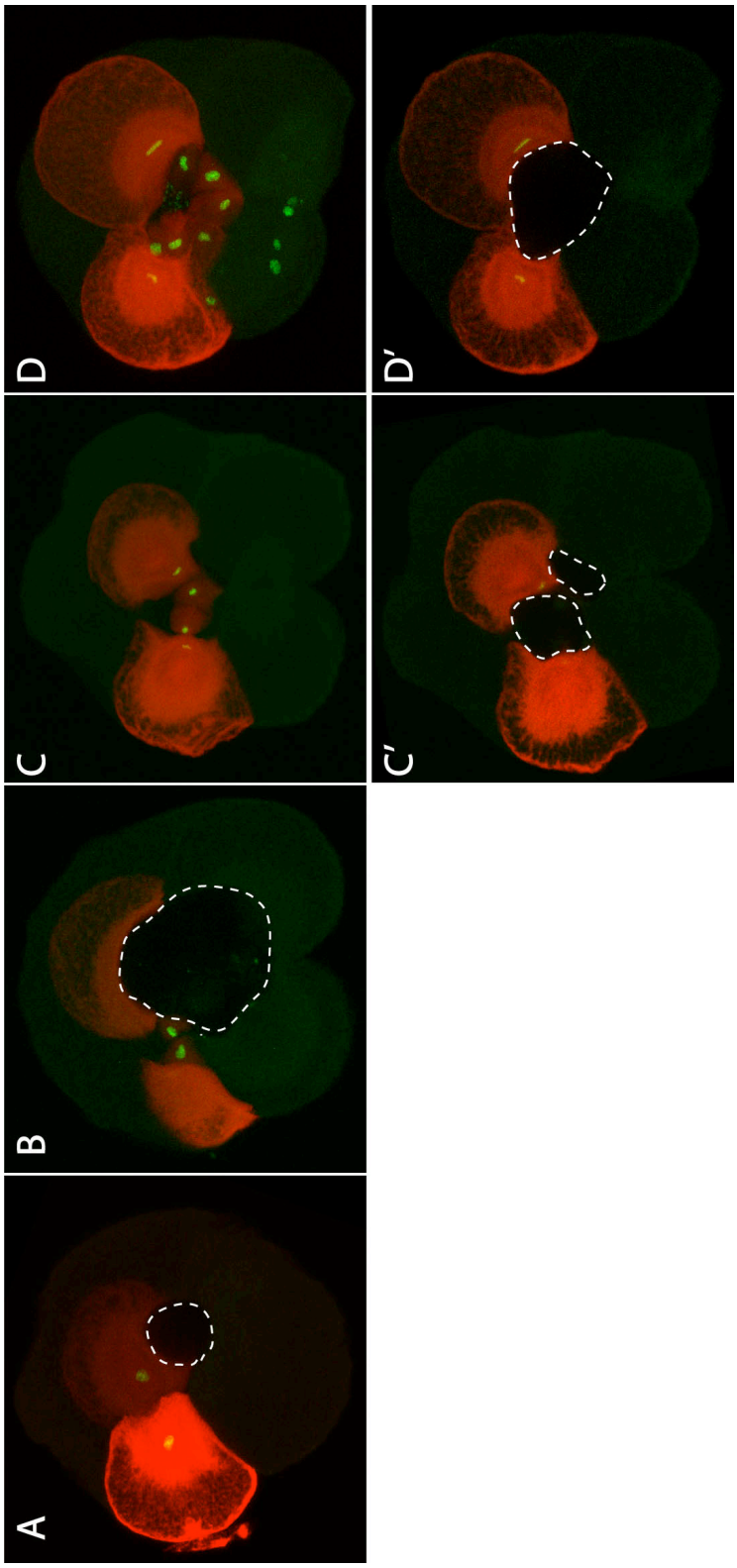


Figure 3.3. Blastocoel deformation of the M teloblasts during early blast cell production.

Figure 3.3. Blastocoel deformation of the M teloblasts during early blast cell production. A-D. Embryos fixed at various timepoints after injection of DM" with RDA (red), processed for fluorescent anti-histone immunostaining (green) and then imaged using confocal microscopy. Blastocoel outlined with white dashed line. A. Embryo fixed immediately after the birth of M_L and M_R. In this embryo, the blastocoel is only deforming the M_R teloblast. B. Embryo fixed 1.5 hours after injection, the large blastocoel is deforming the M_R teloblast. C. Animal projections and more vegetal projections (C') of the same embryo fixed 1.5 hours after injection. D. Animal projections and more vegetal projections (D') of the same embryo fixed 6 hours post injection. In this embryo the blastocoel is deforming both M teloblasts.

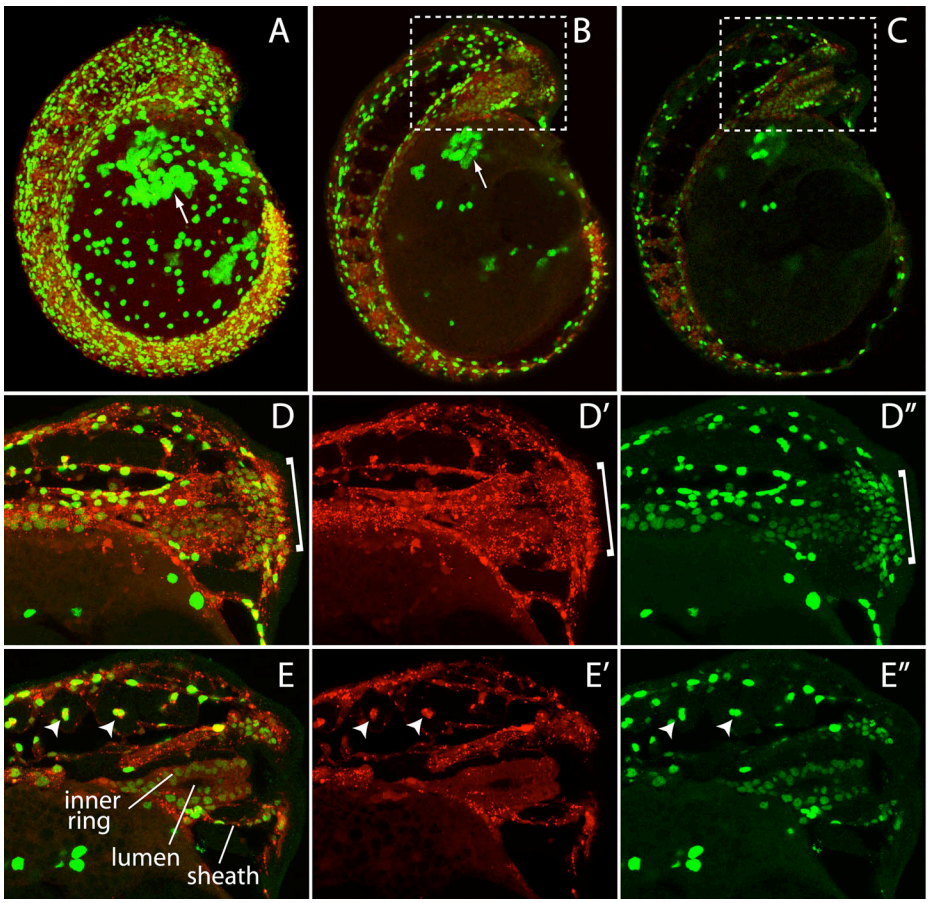


Figure 3.4. DM" makes large contributions to the prostomium of the late stage embryo. DM" was injected with RDA (red) and pEF-H2B:GFP (expression in green) to visualize anterior contributions to the late stage embryo. Embryos were fixed 5 days post injection and imaged using confocal microscopy. All images are lateral views. A-C. Projections of a confocal stack at different levels. A. Complete maximal projection. Strongly expressing clusters of cells in the yolk correspond to supernumerary blast cells (arrow). B Projection of more medial slices. Contributions to the proboscis and sheath are visible (boxed region). C. Projections of deep optical sections showing the lumen of the proboscis and layer of cells of the inner ring surrounding it (boxed region). D-E" High-power projected images of a similar embryo to that in A-C. D-D" Superficial projections of a region similar to boxed section in B, showing the anterior ring of cells that will become the muscular sheath of the proboscis (bracket). E-E" More medial projection of a region similar to the boxed section in C, showing cells of the inner ring surrounding the lumen of the proboscis. M derived clusters of neurons are visible in the ganglia (arrowheads).

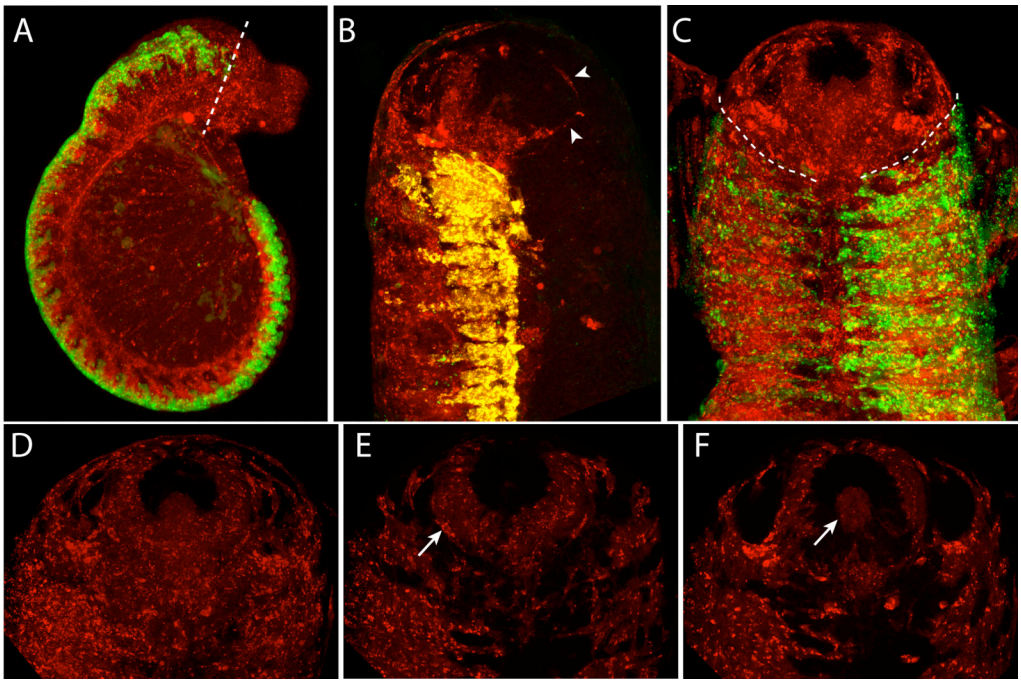


Figure 3.5. DM" contributions in relation to the body segments. To determine contributions from DM" anterior to the germinal plate, DM" or M_L was injected with RDA (red) and various ipsilateral ectodermal lineages with FDA (green). All teloblasts were injected soon after their birth. A. Lateral view of confocal projections of an embryo fixed 6 days 20 hours after injection of DM" with RDA and OP with FDA. Many RDA containing cells are seen anterior to the OP lineage (dotted line). B. Dissected germinal plate of an embryo fixed 4 days after injection of M_L with RDA and N_L with FDA. Although the anterior of the N lineage is non-segmental (Zhang and Weisblat, 2005), RDA containing cells were still seen anterior to its boundary. Additionally, some of these anterior cells crossed the midline (arrowheads). C. Dissected germinal plate of an embryo whose DM" cell was injected with RDA and OPQ"$_L$ and OPQ"$_R$ cells with FDA. There are many RDA containing cells anterior to the FDA containing lineages (dotted lines). D-F. Early morphogenesis of the anterior of the DM" lineage. High magnification confocal projections at different levels of the same embryo whose DM" cell was injected with RDA. Embryos were fixed 4 days post injection. D. Complete projection. E. Ventral projection in which the ring of cells corresponding to the developing sheath (arrow) is visible. F. More dorsal projection in which the cells of the developing proboscis are visible (arrow).

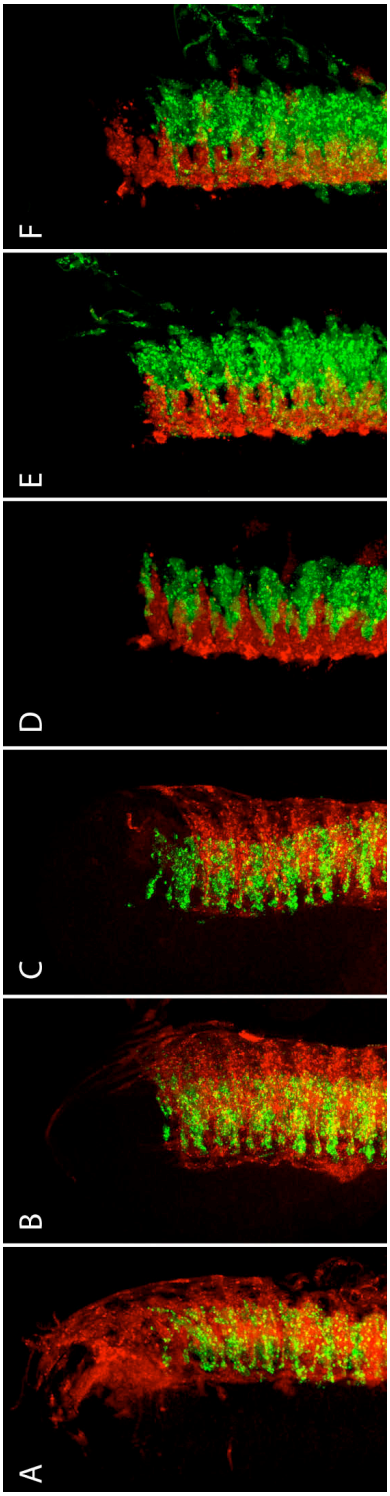


Figure 3.6. Mesodermal and ectodermal lineages begin segmental blast cell production at approximately the same time.

Figure 3.6. Mesodermal and ectodermal lineages begin segmental blast cell production at approximately the same time. Dissected germinal plates of embryos fixed 4 days post injection. A. An embryo whose M teloblast was injected with RDA (red) at its birth and the ipsilateral OP teloblast with FDA (green) at its birth. The anterior boundaries of the two lineages do not align. However, when M and OP are similarly injected at the birth of OP, their anterior boundaries either align (B) or the anterior boundary of the M lineage is posterior to that of OP (C). D. An example of an embryo whose N teloblast was injected with RDA and OP teloblast with FDA, both at the birth of OP. The anterior boundaries of both lineages in this embryo aligned. E. When the N and M teloblasts are injected at the birth of OP with RDA and FDA respectively there are embryos where the anterior boundaries of the injected lineages align (E), or where the anterior N boundary is anterior to that of M (F).

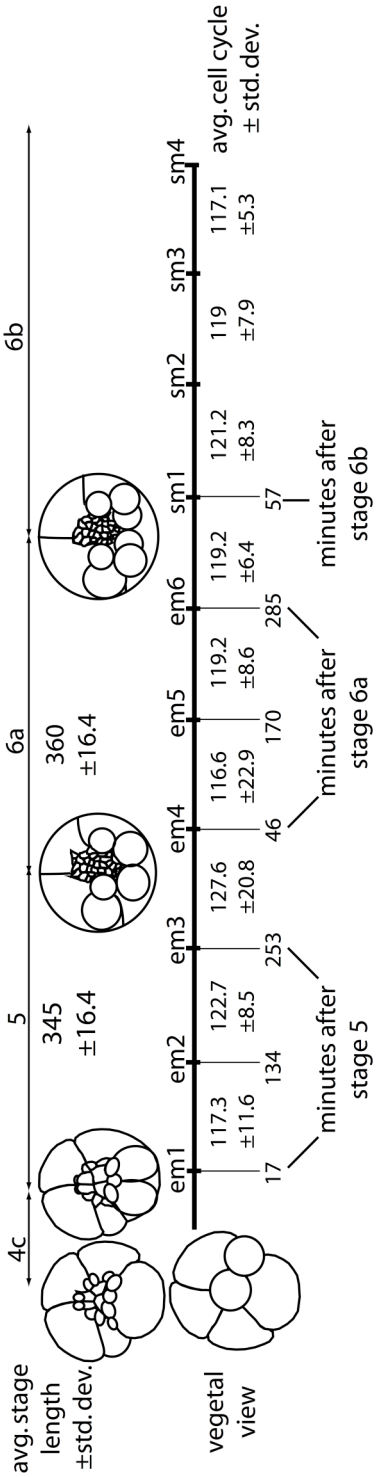


Figure 3.7. Six cells are born from each M teloblast prior to stage 6b.

Figure 3.7. Six cells are born from each M teloblast prior to stage 6b. Compiled data from time-lapse movies of the early divisions of the M teloblasts. Fluorescent and darkfield images were taken of embryos every 2-5 minutes. Cell cycles and stage lengths were calculated and averaged across all experiments. All averages are in minutes.

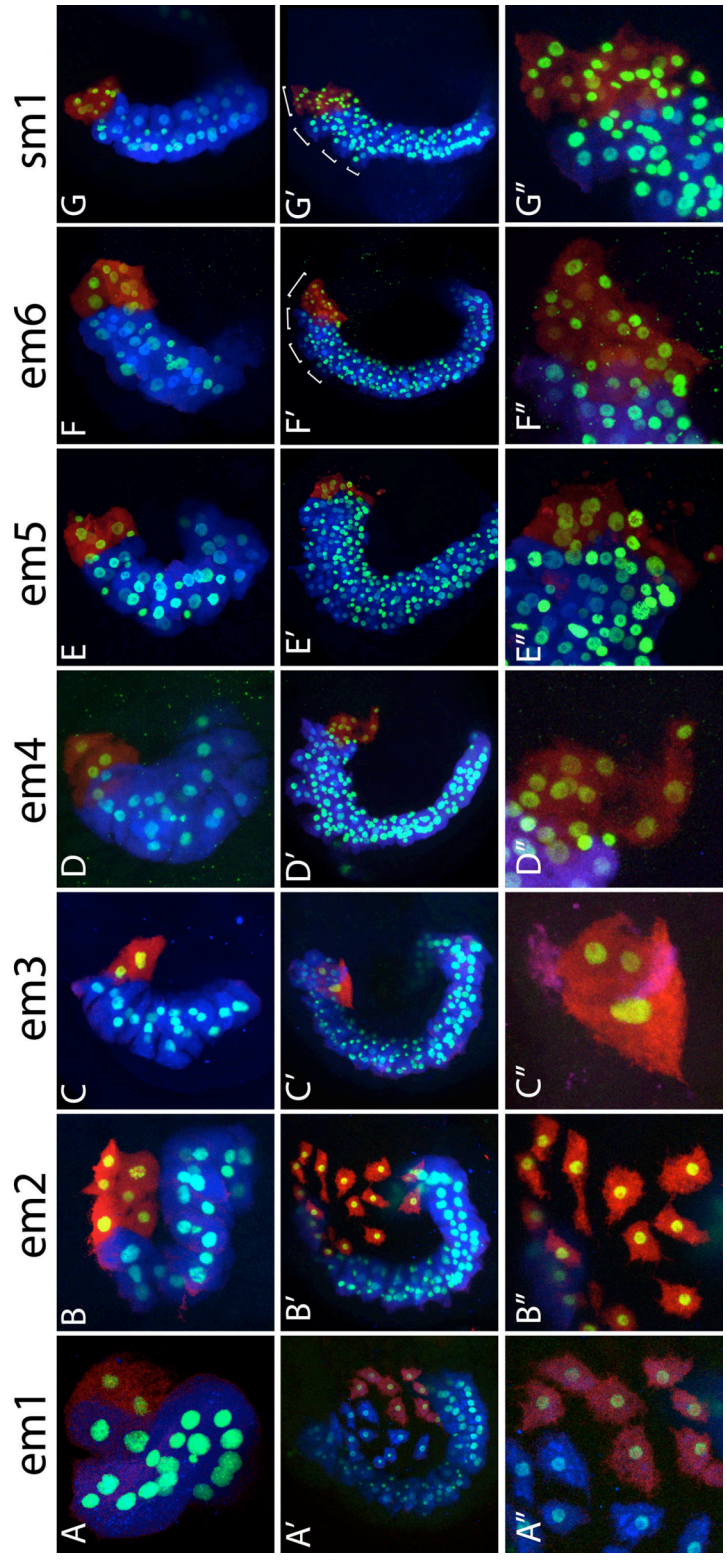


Figure 3.8. Clonal distributions of early m lineages.

Figure 3.8. Clonal distributions of early m lineages. Timed tandem injections were performed in order to uniquely label the progeny of em cells 1-6 and sm cells. M_L teloblasts were first injected with RDA (red) and either *h2bgpf* mRNA or pEF-H2B:GFP (expression shown in green) and then two hours later with the second tracer, alexa fluor 647. Double labeled cells (RDA and alexa fluor 647) are shown in blue. Embryos were cultured for 2 (top row) to 3 (middle and bottom rows) days post injection, fixed and then imaged using confocal microscopy. Bottom panels show close-up views of the uniquely labeled clones in the middle panel. The cell from which the uniquely labeled clone is derived is labeled above the row. Brackets in F' and G' mark migrating clones in hemisomites.

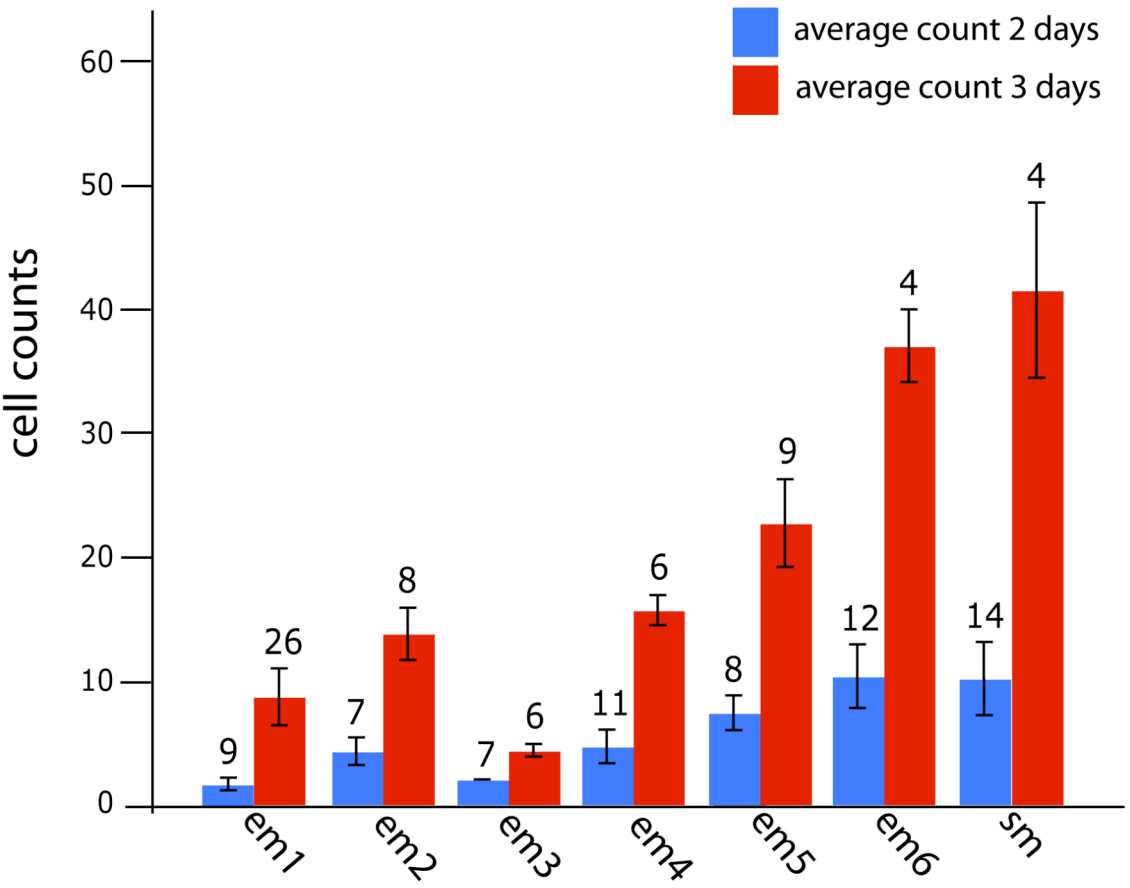


Figure 3.9. Proliferation rates of early mesodermal lineages at 2 and 3 days clonal age. Uniquely labeled cells from timed tandem injections shown in Figure 7 were counted at 2 and 3 days clonal age. Standard deviation is plotted in black over the bars. Numbers of embryos included in the cells counts are indicated above each bar.

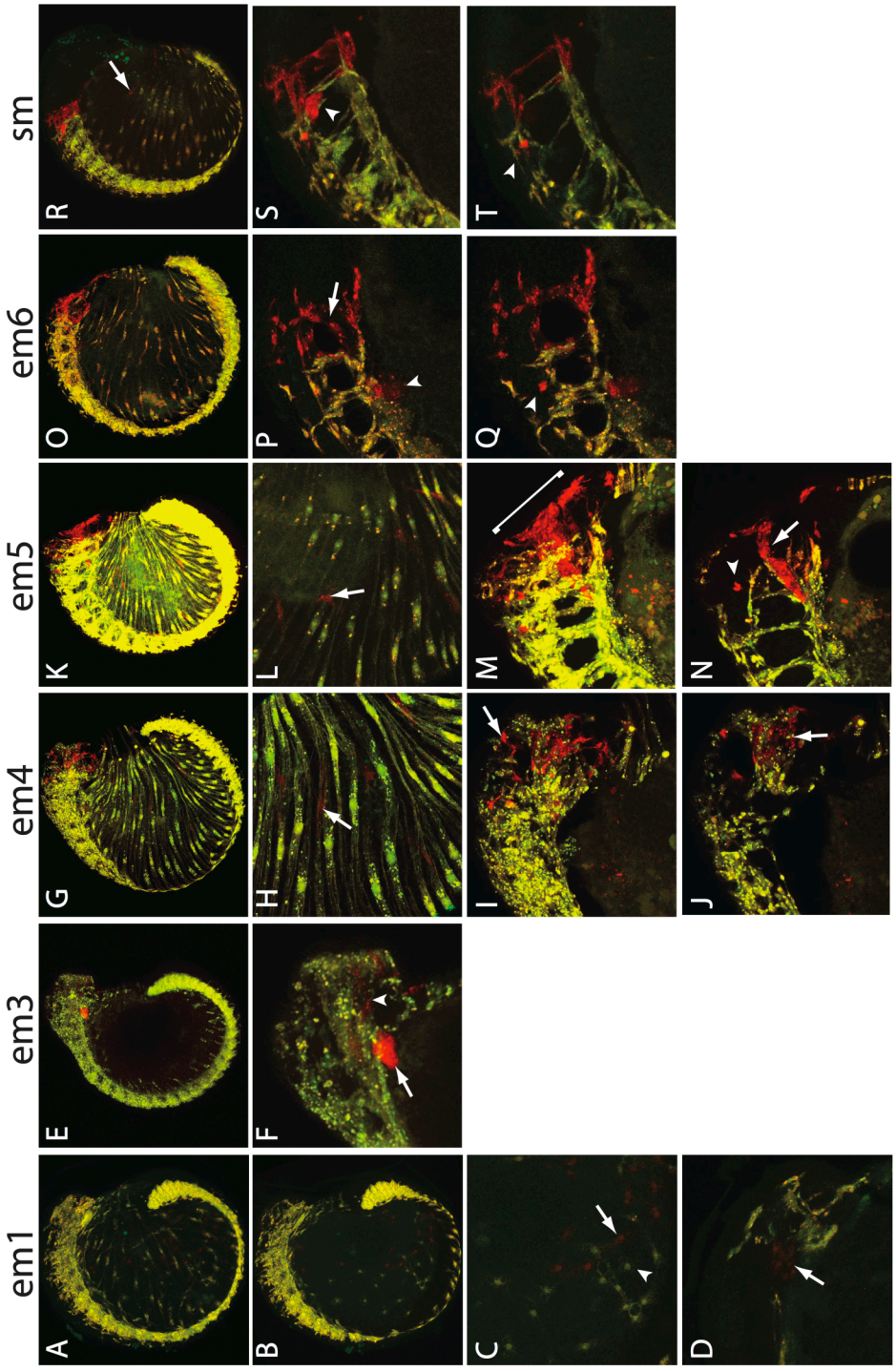


Figure 3.10. The early mesodermal lineages make unique definitive contributions.

Figure 3.10. The early mesodermal lineages make unique definitive contributions. Timed tandem injections were performed to uniquely label the progeny of the early mesodermal lineages. The left M teloblasts of timed embryos were injected with RDA (red) and then, two hours later, with FDA. Doubled labeled cells are yellow. Embryos were cultured to stage 9, fixed and then imaged using confocal microscopy. All images are lateral confocal projections. The top row is of complete maximal projections, subsequent rows focus on the anterior uniquely labeled clones and are projections made of either more superficial or medial regions. A-C. The progeny of em1 are beneath the superficial circumferential muscle fibers and line the endoderm. C. There is some intermixing of the progeny of em1 (arrow) and em2 (arrowhead). D. In deep projections, additional RDA only containing cells derived from em1, were seen in the prostomial region (arrow). F. Em3 contributes a brightly labeled patch of cells lateral to the developing head (arrow) and muscle fibers within the proboscis (arrowhead). G-J. Em4 contributes superficial cells amongst the circumferential muscle fibers (arrow in H), scattered cells in the prostomium (arrow in I) and musculature in the developing proboscis (arrow in J). K-N. Em5 makes major anterior contributions, including superficial cells amongst the circumferential muscle fibers (arrow in L), muscle fibers of the presumptive proboscis sheath (bracket in M), musculature throughout the proboscis (arrow in N) and a cluster of neurons in the ganglia of R1 (arrowhead in N). O-Q. Em6 contributes mesoderm to the proboscis as well as to the first segment. Em6 gives rise to longitudinal muscle fibers in the proboscis (arrow in P). Q. The progeny of em6 also contribute mesoderm surrounding the first forming coelom, a cluster of neurons in the ganglia of R2 (arrowhead in Q) as well as to a lateral patch of cells in segment R3 (arrowhead in P). R-T. Example of contributions of an sm cell to a stage 9 embryo. Sm cells give rise to provisional circumferential muscle fibers (arrow in R), mesoderm surrounding the coelom, a patch of mesoderm to the posterior neighboring segment (arrowhead in S) and a cluster of neurons in the ganglia (arrowhead in T).

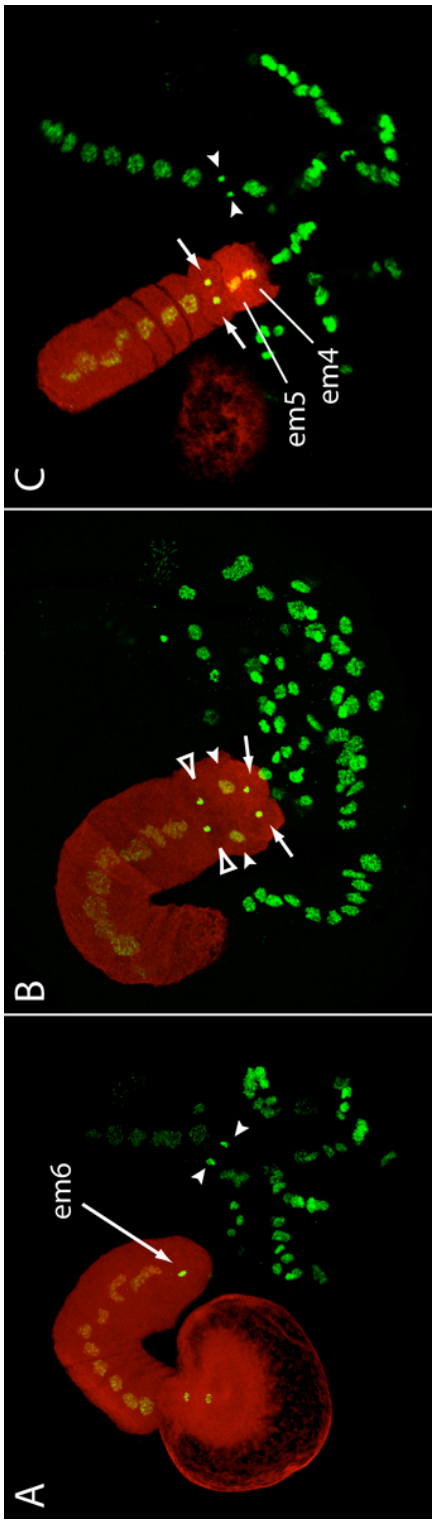


Figure 3.11. Similar to that of sm cells, the primary division of em6 is bilateral.

Figure 3.11. Similar to that of sm cells, the primary division of em6 is bilateral. To determine the primary division pattern of em6, timed RDA (red) injections into M_L were performed. Embryos were then fixed between 18.5-24 hours post injection, processed for anti-histone antibody staining (green) and imaged through confocal microscopy. A-B. Embryos whose M_L teloblast was injected 3.5 hours after 6a, labeling em6 and all subsequent cells. A. Embryo cultured for 20 hours at 23°C, post injection. Em6 was captured rounding up during mitosis (arrow). No other RDA containing cells had yet divided, however a pair of recently born cells in the unlabeled contralateral M bandlet, most likely corresponding to the progeny of em6, are visible (arrowheads). B. Embryo cultured for 24 hours at 25°C post injection. The anteriormost cell, corresponding to em6, in the labeled lineage, is undergoing its first division (arrows). The pair of cells directly behind it correspond to the progeny of sm1 (arrowheads). Posterior to the progeny of sm1, sm2 is undergoing its primary bilateral division (open arrowheads). C. Embryo whose M_L teloblast was injected at 6a, thus labeling all cells born after em3, cultured for 18.5 hours at 28°C. In this embryo, the two anterior labeled cells, em4 and em5 have not divided, but em6 is undergoing its first bilateral division (arrows). In the contralateral bandlet, a cell is also completing mitosis and most likely corresponds to the em6 cell in the right mesodermal lineage.

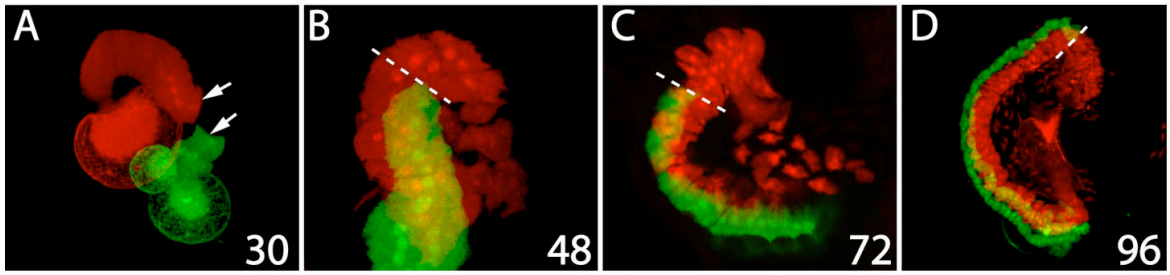


Figure 3.12. Alignment of segmentally contributing ectodermal and mesodermal lineages during development. Maximal projections of stacks of confocal images taken of embryos whose M_L teloblast was injected with RDA (red) at its birth and OP_L teloblast with FDA (green) at its birth. Numbers indicate hours the embryos were cultured post injection. A. Early M and OP lineages are born far apart, with their presumptive anteriors facing one another (arrows). No contact between the M and OP lineage is made by 30 hours post injection. B-D. Dashed lines indicate the anterior of the OP lineage. Note in D the anterior of the OP is curved where it enters the germinal plate.

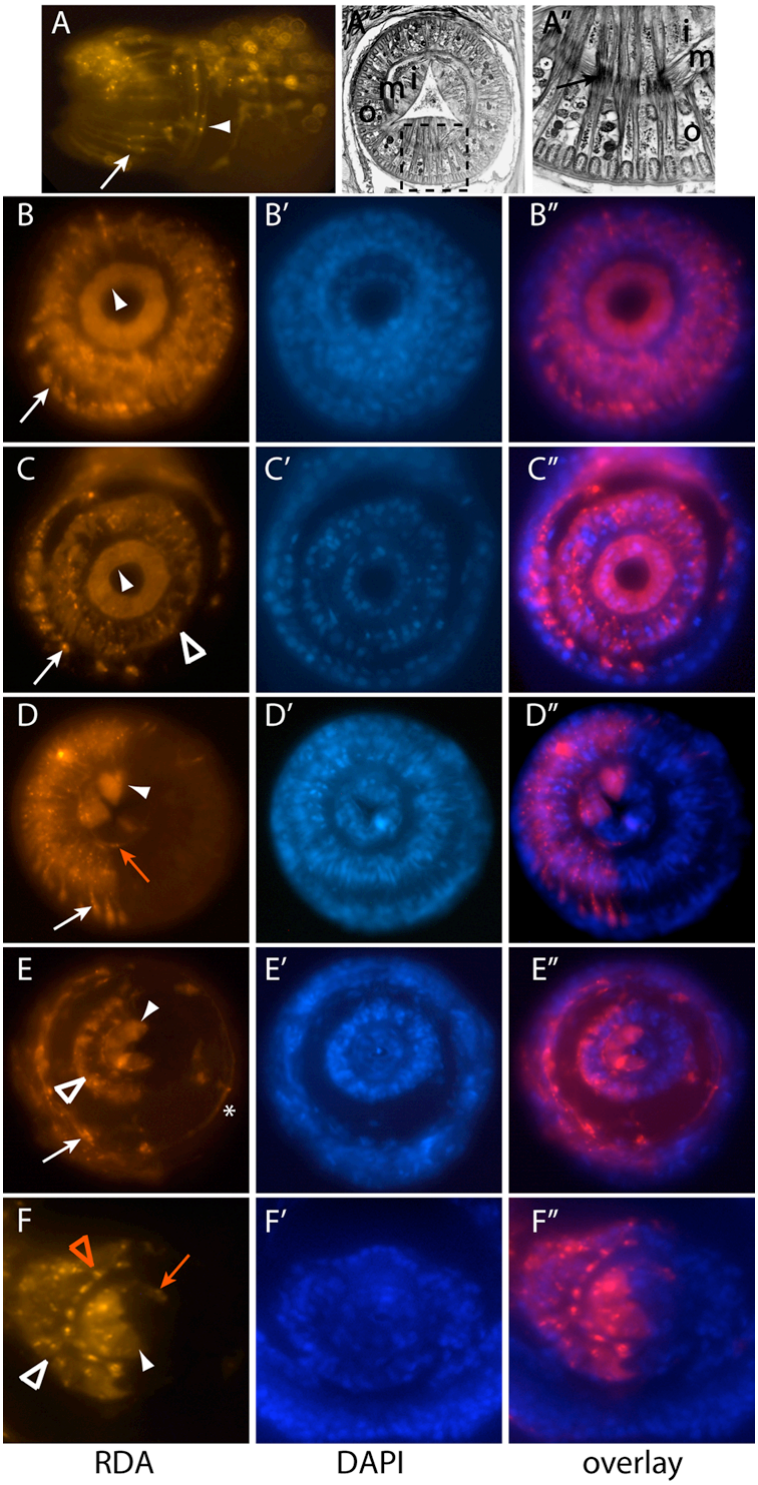


Figure 3.13. The DM" lineage contributes to the proboscis as well as to musculature throughout the proboscis sheath.

Figure 3.13. The DM" lineage contributes to the proboscis as well as to musculature throughout the proboscis sheath. Embryos whose DM" proteloblast (A and B-C") or M_L teloblast (D-F") was injected with RDA (red) and were then fixed at early stage 10, counterstained with DAPI (blue), embedded in plastic blocks and sectioned by hand. A. Sagital superficial section showing contributions of two populations of muscle fibers in the sheath; one running parallel to the long axis of the proboscis (arrow), the other running along the circumference of the proboscis at its base (arrowhead). Anterior is to the left. A-A". Brightfield confocal images of a transverse cross-section of an adult proboscis. Layers labeled; i, inner, m, middle and o, outer. A". High-power image of boxed region in A'. Radial muscle fibers extending from the outer layer across the middle and inner layers are visible (arrow). B-B" Anteriormost transverse cross-section illustrating contributions to muscle fibers of the sheath (arrow) and inner ring (arrowhead). C-C" In a more posterior section, contributions are visible in the sheath (arrow), inner ring (arrowhead) and radial muscle fibers of the outer layer (open arrowhead). D-D" Anteriormost transverse cross-section illustrating unilateral contribution of M to the sheath (arrow), circumferential muscle fibers in the middle layer (red arrow), and cells of the inner ring (arrowhead). Note the medial boundaries of the M derived cells in the different layers do not align. E-E". More posterior transverse cross-section of a M_L injection, showing contribution to the sheath (arrow), outer layer (open arrowhead) and inner ring (arrowhead). Note contributions to the sheath on the contralateral side (asterisk). F-F". Transverse cross-section of the posterior portion of the proboscis, focusing on the inner, middle and outer layers. M_L makes contributions to the radial muscle fibers of the outer layer (open arrowhead), longitudinal muscle fibers of the outer layer (red open arrowhead), circumferential muscle fibers in the middle layer (red arrow) and cells of the inner layer (arrow head). Medial boundaries of the contributions in each layer do not align.

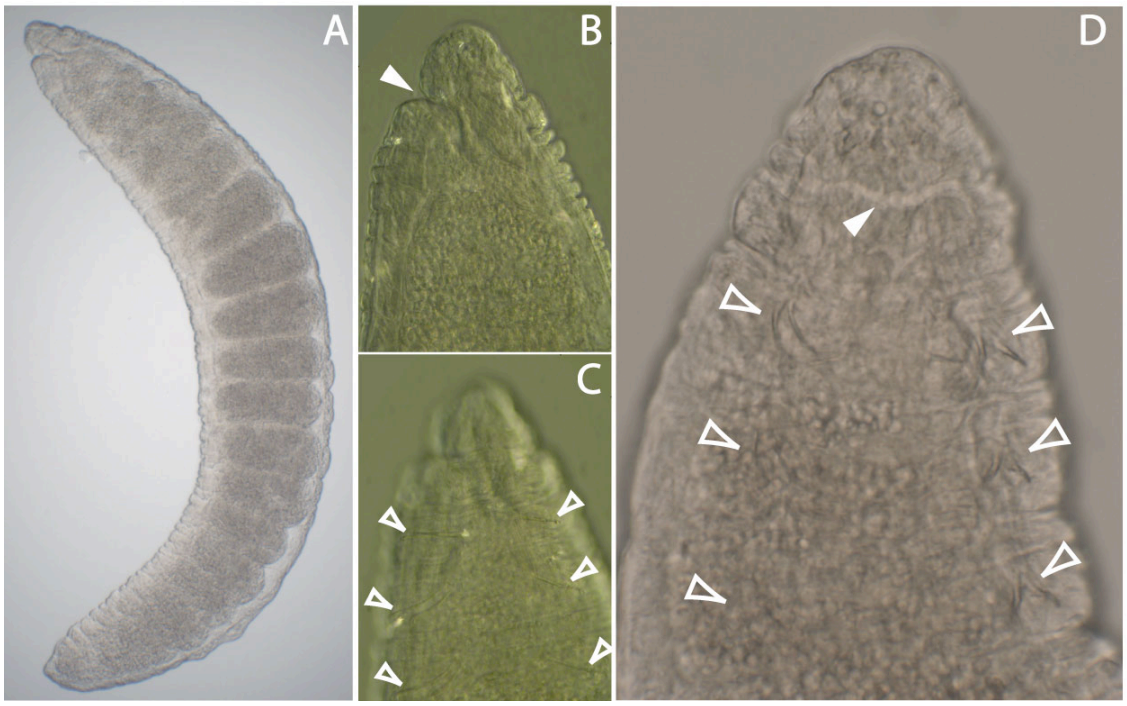


Figure 3.14. Morphology of late stage *Tubifex* embryos. Brightfield images of *Tubifex* embryos cultured for 7 days after the birth of 4d. A-C. Lateral views with dorsal is to the right and ventral to the left. B. Close-up view of the head showing the mouth opening (arrowhead) into the foregut. C. Superficial focal plane showing pairs of chaetae along the dorsal and ventral aspects (open arrowheads). D. Ventral view; mouth opening (arrowhead) and pairs of chaetae (open arrowheads) are visible.

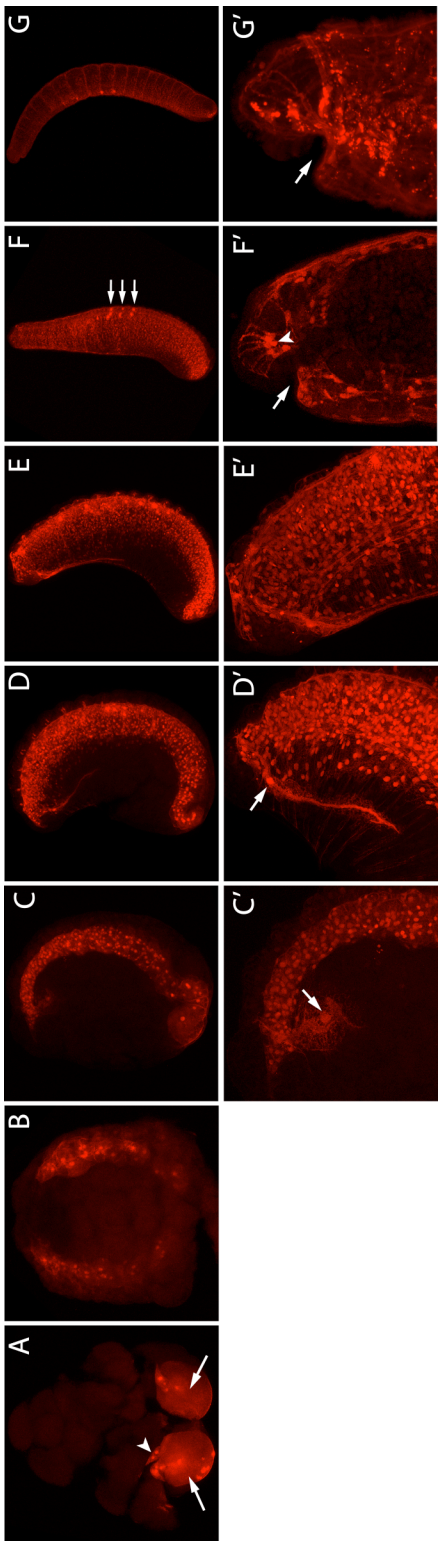


Figure 3.15. 4d lineage in *Tubifex* throughout development.

Figure 3.15. 4d lineage in *Tubifex* throughout development. 4d was injected soon after its birth with RDA (red). Embryos were cultured for 1-7 days post injection and imaged using confocal microscopy. A. Animal view of an embryo, 1 day post injection. M_L and M_R are visible (arrows) as are recently born blast cells (arrowhead). B. Animal view of an embryo 2 days post injection. Left and right germinal bands are visible and do not make contact at the presumptive anterior. C-G' Lateral views. C-C'. An embryo 3 days post injection. C'. Anterior region of the embryo in C. The long branching process extending posteriorly on the dorsal side appears to be formed by a single cell whose RDA concentrated in the nucleus (arrow). D-D'. An embryo 4 days post injection. Posterior extension of the anterior branching process continued, however the nuclei as judged by nuclear accumulation of RDA remains at the anterior of the lineage (arrow). E-E'. An embryo 5 days post injection. F-F'. An embryo 6 days post injection. PGCs are visible as three bright clusters of RDA containing cells (arrows). F'. RDA labels cells up to and including the mouth (opening indicated by arrow). At this stage, a thin fan of muscle fibers branch across the head out of a common anchor point (arrowhead). G-G'. At 7 days post injection the network of muscle fibers in the head and RDA containing cells within the mouth (arrow) are visible.

CHAPTER FOUR

Notch signaling during leech development

Introduction

Notch signaling is an evolutionarily conserved intercellular signaling pathway that plays an important role in multifarious aspects of metazoan development from single-cell tube morphogenesis in the *C. elegans* pharynx (Rasmussen et al., 2008) to patterning of the *Drosophila* eye (Roignant and Treisman, 2009). Briefly, Notch signaling is initiated through the binding of a membrane-bound ligand (Delta, Serrate or Jagged) to the receptor (Notch) of the neighboring cell. This allows for subsequent cleavages of the Notch receptor and liberates its intracellular domain (NICD) from the membrane. NICD then enters the nucleus and binds to Supressor of Hairless [Su(H)]. In the absence of the NICD, Su(H) normally occupies promoters of Notch target genes and functions as a transcriptional repressor. Upon binding to NICD, however, Su(H) together along with other co-factors, serves as a transcriptional activator (Bray and Furriols, 2001). Conserved Notch target genes include members of orange domain-containing subfamily of the bHLH transcriptional repressors (bHLH-O genes) such as *hairy* and *Enhancer of split* related genes (Giudicelli and Lewis, 2004). bHLH-O genes can target themselves and thus are involved in autoinhibitory feedback loops often resulting in their own dynamic, oscillating expression (Davis and Turner, 2001; Hirata et al., 2002; Gratton et al., 2003; Giudicelli and Lewis, 2004).

One well-known role of Notch signaling is its involvement in vertebrate segmentation. In vertebrate embryos, the paraxial mesoderm becomes segmented into transient structures called somites, which arise sequentially in rostrocaudal progression as partially epithelialized balls of cells, from the anterior end of the presomitic mesoderm (PSM). This process was at first theoretically explained by the "clock-and-wavefront" model proposed by Cooke and Zeeman in 1976, and is now supported by abundant molecular evidence (Lewis, 2003). Discovery of oscillations of the putative Notch target gene *hairy*, a transcriptional repressor, in the chick PSM, gave molecular backing to the concept of the "segmentation clock" (Palmerim et al., 1997). Various Notch pathway members have since been shown to oscillate in the PSM of multiple vertebrates. Functional data from multiple vertebrates additionally support the critical role of Notch signaling in vertebrate segmentation (Lewis et al., 2009).

The question of whether the bilaterian ancestor was segmented or whether segmentation has evolved multiple times remains open. Molecular phylogenies show that the three main segmented taxa (arthropods, annelids and vertebrates) are interspersed with unsegmented taxa in their respective super-phyla (Ecdysozoa, Lophotrochozoa and Deterostomia) and are thus more closely related to unsegmented taxa than they are to each other (Aguinaldo et al., 1997; Dunn et al., 2008). Parsimony, and the seeming unlikelihood of losing what is presumed to be an evolutionarily advantageous trait, favor a scenario in which segmentation evolved independently in each of the three major phyla (annelids, arthropods and chordates), as opposed to one in which the ancestral bilaterian was already segmented and this feature was then lost multiple times (Scholtz, 2002). On the other hand, apparent similarities in molecular patterning mechanisms of

segmentation favor the interpretation of segmentation as an ancestral bilaterian trait. In particular, recent work has indicated that Notch signaling plays a role in segmentation in both arthropods (Chipman and Akam, 2008; Stollewerk et al., 2003), and annelids (Rivera and Weisblat, 2008; Thamm and Seaver, 2008), as in vertebrates.

Further investigations into **how** Notch signaling functions in the embryological and cellular context of segmentation in various representatives of the three super-phyla is needed to shed further light on this controversy. *Helobdella* is a tractable annelid model and thus a useful candidate for studying lophotrochozoan segmentation. In *Helobdella,* segmentation is driven by a posterior growth zone (PGZ) comprised of five bilateral pairs of individually identified segmentation stem cells (teloblasts). Teloblasts and to a more limited extent their blast cell progeny are well characterized, and amenable to microinjections of lineage tracers, plasmids, mRNAs and morpholinos. Previous work has been done characterizing the expression and function of several Notch pathway members in the leech *Helobdella robusta* (Song et al., 2004; Rivera et al., 2005; Gonsalves and Weisblat, 2007; Rivera and Weisblat, 2008). Through in situ hybridization analysis, the leech homolog of a *hairy* and *Enhancer of split* (*hes*) related gene, *Hro-hes*, was shown to be strongly expressed during production of the segmental precursors (Song et al., 2004) as was the leech homolog of the Notch receptor *Hro-notch* (Rivera et al., 2005). To test the function of the Notch pathway in development, functional studies were performed targeting knock down of *Hro-hes* through injection of antisense morpholino oligomers (AS-MO) into the neurogenic N lineage. In conjunction with drug treatments of DAPT, an inhibitor of Notch signaling that prevents proteolytic processing of the Notch receptor, the AS-MO injected N lineage failed to undergo normal morphological segmentation at the stage where the control mis-match injected lineage developed normally (Rivera and Weisblat, 2008).

Recently, the genome of *Helobdella robusta* was sequenced, which allows for a more complete inventory of all signaling pathway members than previously possible (Cho et al., 2010). I took advantage of the available genome data to take a broader look at the Notch signaling pathway during leech development and further explore its involvement in segmentation. After mining the genome, many homologs of Notch pathway members were uncovered (Table 4.1). Those disussed in this work include a homolog of the ligand Serrate, *Hau-ser*, a homolog of the DNA binding factor, suppressor of Hairless *Hau-Su(H)* as well as more potential bHLH Notch target genes including one *Hey* family member *Hau-hey*, and another *hairy* and *Enhancer of split* related gene, *Hau-hes2*.

These candidates were cloned from cDNA of *Helobdella* sp. (Austin) and their expression patterns were analyzed across many stages of development using both in situ hybridization as well as developmental RT-PCR. Gene sequences for *H.* sp. (Austin) are typically >95% identical at the nucleotide level to their orthologs from *H. robusta* (for which the whole genome sequence is available). For precision, all genes identified in the *H. robusta* genome with be designated with the prefix *Hro-*, but if the orthologous sequences is then cloned from *Helobdella* sp. (Austin), that sequence will have the prefix *Hau-* instead. As part of this work I re-examined the expression of previously cloned Notch members in parallel with the new genes. Surprisingly, many of the Notch pathway members showed strongest expression in anterior non-segmental lineages. Additionally, the potential target genes showed expression patterns suggestive of their role in pattern formation independent of regulation by Notch signaling.

Results

Expression patterns of Notch pathway members in stages 7-9 in *Helobdella* sp. (Austin)

bHLH-O genes (potential targets)

In vertebrates, there are four known subfamilies of DNA binding proteins, related to the *Drosophila* hairy and Enhancer-of-split proteins. (Davis and Turner, 2001). Generally these transcriptional repressors are called bHLH-O proteins because all family members found in vertebrates have a bHLH domain followed by an orange domain. bHLH-O genes also have a conserved C-terminal tetrapeptide domain characteristic of their particular gene family (ex. WRPW, YRPW; Davis and Turner, 2001). In *Drosophila*, the bHLH and orange domains were shown to repress transcription of activators such as Scute and the C-terminal tetrapeptide was shown to be necessary for binding the co-repressor Groucho for repression of other targets (Paroush et al., 1994; Dawson et al., 1995). bHLH-O proteins can form dimers via their HLH domain (reviewed in Davis and Turner, 2001). Additionally it has been proposed that the orange domain plays a role in regulating formation of bHLH-O heterodimers (Dawson et al., 1995; Taelman et al., 2004) Four families of bHLH-O proteins have been described in vertebrates, Stra13, Hey, Enhancer of Split, and Hairy, all of which have been shown to function through the recruitment of transcriptional co-repressors to inhibit target gene expression, including bHLH-O genes themselves (Davis and Turner, 2001; Hirata et al., 2002; Gratton et al., 2003; Giudicelli and Lewis, 2004). Distinguishing them from other bHLH proteins, the Hairy and Enhancer of split related members have a conserved proline in the basic region, while Hey family members have a conserved glycine in the same position (Davis and Turner, 2001). Many bHLH-O proteins have been shown to be downstream targets of Notch signaling (Giudicelli and Lewis, 2004). Homologues of these gene families in segmented taxa outside of the vertebrates usually have a conserved bHLH domain, an orange domain as well as a conserved C-terminal tetrapeptide motif (Damen et al., 2000; Stollewerk et al., 2003; Kadner and Stollewerk, 2004; Aranda et al., 2008; Thamm and Seaver, 2008).

Interestingly, while the previously published *Hro-hes* gene family member contains a conserved WRPF domain and a bHLH domain particular to the *hairy* and *Enhancer of split* related family of genes, it appears to lack the characteristic orange domain (Fig. 4.1; Song et al., 2004). Previous experiments showed that *Hro-hes* was expressed most strongly during blast cell production (stages 7 through 8), with transcripts showing cell cycle dependent localization to mitotic chromatin (Song et al., 2004). I cloned the full length coding portion of this gene in *Helobdella* sp. (Austin) to use as an in situ probe. The coding sequence between these two leeches was nearly identical. Surprisingly, however, I saw a drastically different expression pattern using my *Hau-hes* probe on *Helobdella* sp. (Austin) embryos. During stage eight, *Hau-hes* transcripts were seen in a subset of cells in the O and P lineages in the left and right germinal bands (Fig. 4.2). This staining pattern, which appears segmental, most likely corresponds to expression in particular sublineages at precise clonal ages. Additionally, cellular localization of transcripts appeared cytoplasmic rather than nuclear, as previously described (Song et al., 2004). I have confirmed previous developmental RT-PCR results for *Hau-hes* in *Helobdella* sp. (Austin), and saw a similar increase in expression beginning at stage 7. Transcripts were

detectable through stage 10 (Fig. 4.3; Song et al., 2004). Under the circumstances, I conclude that the difference between these two sets of results is more likely to reside in yet-to-be-determined discrepancies in the in situ protocols used than in real and significant differences in gene expression between the closely related species, but the latter possibility cannot be excluded. A direct comparison between *Hro* and *Hau* is called for; unfortunately, *Hro* has not been available for the past year or so, due to problems with re-collecting that species in the wild and maintaining it in laboratory culture.

In my investigation of the *Hro* genome, I identified and cloned a second *hes* family member that also lacks an identifiable orange domain, designated *Hau-hes2* (Fig. 4.1; Fig. 4.4). *Hau-hes2* did have a bHLH domain similar to those of other *hairy* and *Enhancer of split* related genes, which interestingly had a longer loop region than the other family members, as well as a conserved C-terminal WRPW tetrapeptide motif (Fig. 4.1; Fig. 4.4). Through developmental RT-PCR analysis it was observed that unlike *Hau-hes*, whose expression peaks at stage 7/8, strong *Hau-hes2* expression was not seen until late stage 8 and continued through stage 10 (Fig. 4.3). Additionally, unlike *Hau-hes*, *Hau-hes2*, was expressed in anterior non-segmental populations of cells (Fig 4.5). At mid-stage 8, a bi-lobed population of *Hau-hes2* expressing cells was visible anterior to the germinal plate. Anterior to this population of cells was another sparse group of cells expressing *Hau-hes2* (Fig. 4.5A). By stage 9 these two populations were more distinct; there was one cohesive superficial, ventral cluster of expressing cells anterior to the germinal plate and an additional anterior circle of expressing cells around what appears to be the developing mouth (Fig. 4.5B-E). Staining was cytoplasmic and excluded from the nucleus.

The third bHLH-O gene cloned, *Hau-hey*, had a conserved bHLH domain, a conserved orange domain, as well as a conserved C-terminal YRPW motif, characteristic of Hey family members (Fig. 4.1, Fig. 4.6; Leimeister et al., 1999). Developmental RT-PCR for *Hau-hey* showed strong expression from stages mid-8 through 10 (Fig. 4.3). The earliest expression of *Hau-hey* detected using in situ hybridization, was at late stage 7 in a single cell at the anterior of the left and right germinal bands (Fig. 4.7A). At the start of stage 8, which is marked by the meeting of the left and right germinal bands at what becomes the anterior end of the germinal plate, there were bilateral pairs *Hau-hey* expressing cells (Fig. 4.7B). As the germinal plate continued to form, pairs of cells expressed *Hau-hey* in a clonal age-dependent fashion; at each time point examined, the most posterior pair of expressing cells were located at the point where the left and right lineages meet (Fig. 4.7C). Lineage tracing analysis confirmed these early-expressing paired cells in the germinal plate were in the N lineage (Fig. 4.8C). At this stage, the anterior-most cells expressing *Hau-hey* appear to be anterior to the germinal plate, i.e., in non-segmental portions of the head (Fig. 4.8A,B). As epiboly proceeds, *Hau-hey* is expressed in subsets of cells in all four ectodermal lineages (Fig. 4.7D-I). There is an additional subset of *Hau-hey*-expressing cells anterior to the germinal plate (Fig. 4.7D). By stage 9, all ectodermal lineages express *Hau-hey* in a complex dynamic pattern along the AP axis (Fig. 4.7G-I and Fig. 4.8 D-F).

Hro-Notch expression re-examined at stages early 8 through 9 in *Helobdella* sp. (Austin)

Previous experiments in *Helobdella robusta*, characterized *Hro-notch* in situ staining during stages 7 and early 8. In these experiments, expression was seen in all segmental lineages (proteloblasts, teloblasts, blast cells and blast cell progeny) (Rivera et al., 2005). Developmental

RT-PCR for *Hro-notch* showed highest expression levels at stages 7-10 (Rivera et al., 2005). Here I re-examined *Hro-notch* in situ staining patterns during stages late 7 through 9 in the closely related *Helobdella* sp. (Austin). Again the in situ expression pattern I saw differed from that published for *Helobdella robusta*, for the few time points overlapping between my work and previously published data on *H. robusta*. In brief, as for *Hau-hes*, the major difference between my results (using *Hau*) and previously published results (using *Hro*) is that I did not detect expression in the teloblasts or undivided blast cells. At late stage 7, just before the germinal plate starts to form, staining was seen in clusters of cells near the anterior of the left and right germinal bands (Fig. 4.9A,B). By mid stage 8, the anterior clusters of expressing cells resolved into paw-shaped circles of expressing cells (Fig. 4.9C). Additionally, at this stage, pairs of ectodermal cells in the germinal plate near the midline express *Hro-notch* (Fig. 4.9C). As germinal plate formation continued, the pairs of expressing cells in the ectoderm extended posteriorly, while expression in the anterior "paws" persisted. By early stage 9, expression in rows of cells anterior to the "paws" of expression became apparent (Fig. 4.9D-F).

To test the hypothesis that the anterior paws of expressing cells were anterior to the germinal plate and thus non-segmental, I performed Notch in situ hybridization on embryos whose OP teloblast was injected with RDA immediately after its birth. The contribution of the OP lineage is purely segmental and thus the anteriormost RDA containing cells should mark the first segment. The *Hau-notch* expressing circles of cells were anterior to the RDA containing OP lineage (Fig. 4.9H,I). However, there are extra N derived contributions to the first segment, therefore the anterior boundary of the segmental OP lineage is posterior to that of N (Zhang et al., 2005) so it can not be ruled out that some or all of the *Hau-notch* expressing cells are derived from early N progeny. Developmental RT-PCR for Notch in *Helobdella* sp. (Austin) showed expression gradually increasing starting at mid-stage 8, extending though stage 10 (Fig. 4.1).

Hau-suH and *Hau-serrate* are strongly expressed in populations of cells anterior to the germinal plate during stages 7 and 8

Expression of the leech homolog of *Suppressor of Hairless* was characterized during late stage 7 through early stage 8. At stage 7 *Hau-suH* showed broad expression throughout the germinal bands with increased expression in clusters of cells at the anterior of the germinal bands (Fig. 4.10A). These clusters of anterior expressing cells persisted through mid-stage 8 (Fig. 4.10B,C). Developmental RT-PCR for *Hau-suH* showed low levels of expression as early as stage two, and bands were detectable throughout development with expression increasing starting at mid-stage 8 continuing through stage 10 (Fig. 4.1).

Due to difficulties in cloning this gene from cDNA, *Hau-ser* a homolog of *Serrate*, in situ probe was made from a fragment cloned from genomic DNA and thus contained several short introns. Similar to late stage 7 expression patterns for *Hau-notch*, and *Hau-suH*, *Hau-ser* expression was seen in clusters of cells near the anterior of the left and right germinal bands (Fig. 4.10D). These groups of expressing cells persist during stage 8 as the germinal plate is formed (Fig. 4.10 E,F). Unlike the anterior *Hau-notch* expression, *Hau-serrate* expressing cells do not resolve into circles of fewer expressing cells and instead remain as bilateral cohesive clusters (Fig. 4.10F). Judging from the results of the experiment in which both Notch and Serrate probes were added together for in situs on stage 8 embryos, the *Hro-notch* expressing cells were within the larger domains of *Hau-serrate* expressing cells (Fig. 4.10G,H).

Discussion

The overlap of *Hro-notch*, *Hau-serrate*, and *Hau-suH* expression in clusters of cells just anterior to the left and right germinal bands suggests that canonical Notch signaling is taking place in these cells; ligand must be expressed in cells adjacent to those expressing the receptor in order for the cell-cell signaling network to take place. While most of the cells anterior to the OP lineage are derived from micromeres, the N lineage makes an early non-standard blast cell which gives rise to anterior non-segmental progeny, as well as extra contributions to the first segmental ganglia, R1 (Zhang et al., 2005). Unlike the other segments, the first segment, R1, must make connections to the supraesophageal ganglia. A subset of the anterior *Hro-notch* expressing cells could thus be derived from the early N progeny. Preliminary data is supportive of this hypothesis. Expression of several homologs of intermediate filaments, which usually mark differentiated neurons in older embryos, is seen in the anterior ventral region, likely in a subset of the cells expressing Notch signaling components (Dian-Han Kuo, data not shown). It is therefore possible that the anterior Notch signaling presented here could be involved in specification of a ventral neural tissue (e.g. sensory organ) that is as yet uncharacterized.

In these anterior ventral populations of cells there is broad expression of the ligand and co-activator, with only a subset of cells expressing the receptor. However, none of the potential Notch downstream targets examined in this work exhibit expression patterns indicative of their regulation by Notch signaling. One would expect Notch targets to be expressed in those cells also expressing the Notch receptor, or a subset of them. While there is likely overlap between some *Hro-notch* expressing cells and those expressing potential bHLH targets, the majority of potential target expression lies outside the domains of *Hro-notch* expression. Therefore, most of the expression of potential Notch targets cannot be accounted for through regulation by Notch signaling.

The expression patterns of both *Hau-hes* and *Hau-hey* are suggestive of involvement in cell fate specification in the ectodermal lineages. *Hau-hes* appears to be expressed in particular sublineages within the O and P lineages in the germinal bands. Expression is seen in a segmentally iterated pattern, likely representing homologous cells between blast cell clones expressing at precise clonal ages (Fig. 4.2). The complex and dynamic late expression pattern of *Hau-hey* is suggestive of its involvement in neurogenesis in all of the ectodermal lineages (Fig. 4.7). There are many examples of bHLH-O related genes involved in neural development, often in the maintenance of neural stem cells, which is necessary to regulate the timing of neurogenesis, as well as in boundary formation within the nervous system (Leimeister et al., 1999; Gratton et al., 2003; Sakamoto et al., 2003; Baek et al., 2006; Kageyama et al., 2008). Similar to *Hau-hes* and *Hau-hes2*, *Hau-hey* expression appears independent of Notch signaling; the majority of *Hau-hey* expressing cells were outside of regions of possible overlap with the Notch receptor. Other examples of bHLH-O genes whose transcription is presumably independent of Notch signaling have been found (Leimeister et al., 1999; Kageyama et al., 2007; Thamm and Seaver, 2008). However, until the expression patterns of the other Notch receptors and ligands are characterized, the possibility can not be ruled out that *Hau-hes*, *Hau-hes2* and *Hau-hey* are regulated by Notch signaling members not yet characterized.

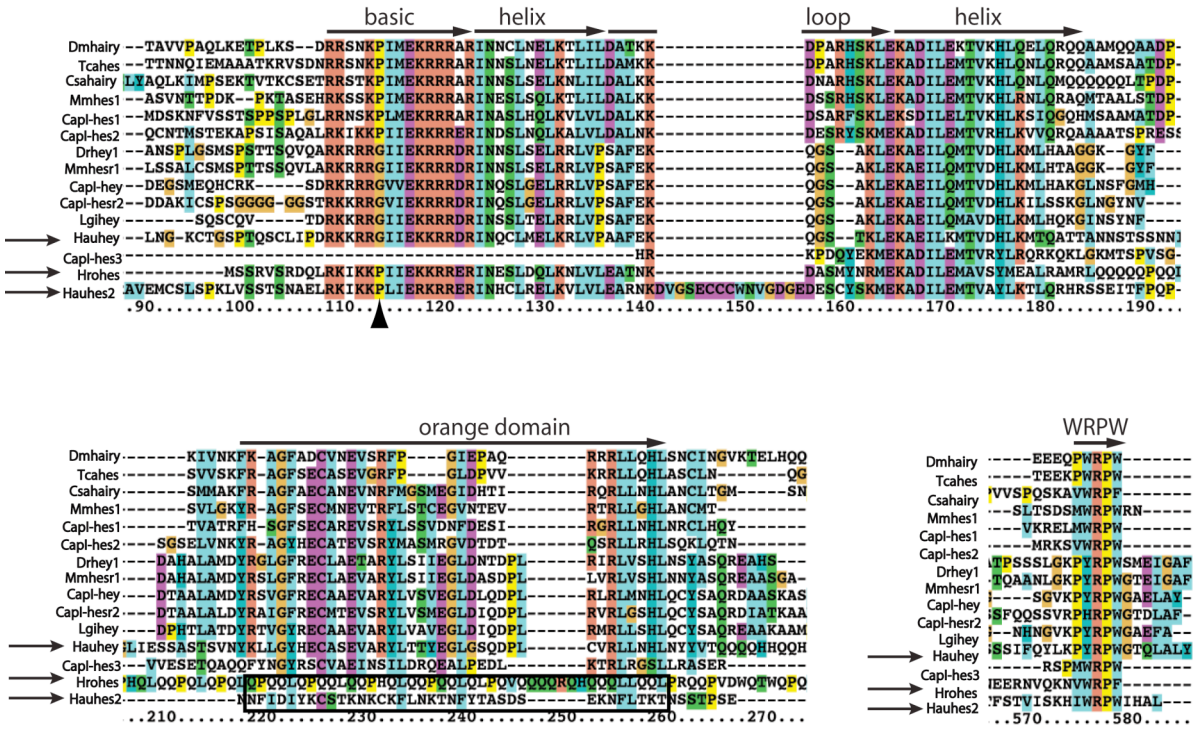


Figure 4.1. Alignment of conserved domains of hairy and Enhancer of split related family members. ClustalX alignment of protein sequences (see materials and methods for accession numbers of sequences used). Conserved domains are labeled above the alignment. Arrows on the left indicate sequences from *Helobdella*. Box highlights the regions in Hrohes and Hauhes2 that do not align with the conserved orange domain of the other family members. Arrowhead indicates conserved proline in hairy and Enhancer of split related family members, and conserved glycine in the Hey related subfamily. CapI; *Capitella* sp. I, Csa; *Cupiennius salei*, Dm; *Drosophila melanogaster*, Mm; *Mus musculus*, Lgi; *Lottia gigantea* Tca; *Tribolium castaneum.*

Table 4.1 Notch pathway members found in the *H. robusta* genome sequence.

Notch pathway member	Scaffold	Protein ID
Notch1 (Rivera et al., 2005)	16	75318; 75352; 75164
Notch2	11	72015
Serrate	17	190972
Delta1	19	77153
Delta2	13	109730
SuH1	22	186992
SuH2	14	190647
Hes1 (Song et al., 2004)	32	175137
Hes2	4	162289
Hey	17	190988

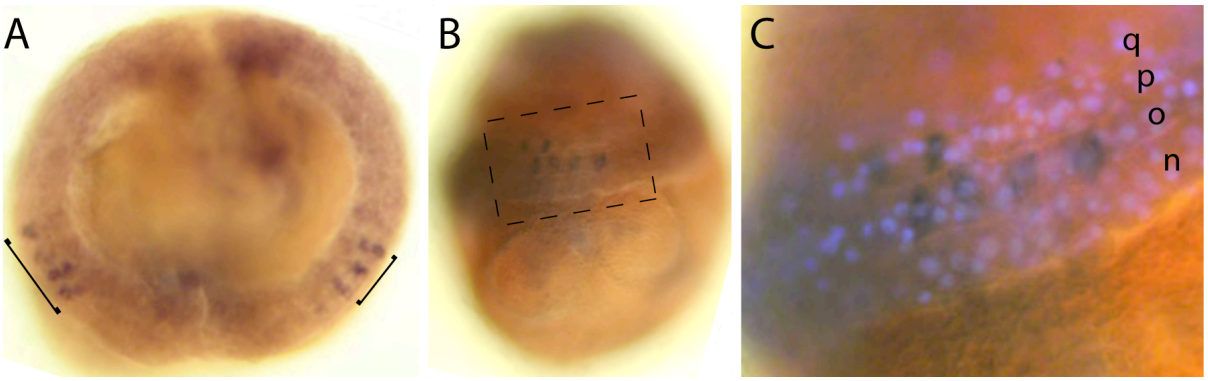


Figure 4.2. *Hau-hes* expression during stage 8. A. Animal view of a mid-stage 8 embryo. Expression is seen in a subset of cells in the O and P lineages in the left and right germinal bands (brackets). B. Lateral view of the right germinal band. C. Close-up view of boxed region in B. DAPI staining is in blue.

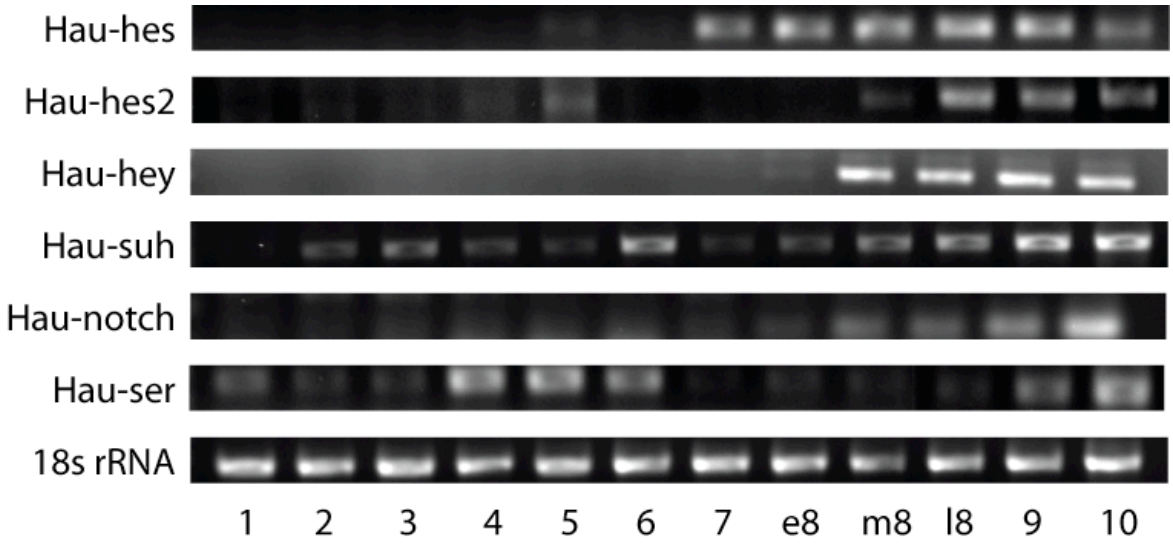


Figure 4.3. Developmental RT-PCR for Notch pathway members at stages 1-10. 18s rRNA was used as an internal control for variations in RNA extraction. Ethidium bromide stained gels show indicated transcripts across developmental stages. See materials and methods for details on RNA extraction, cDNA production and PCR amplification of Notch pathway members.

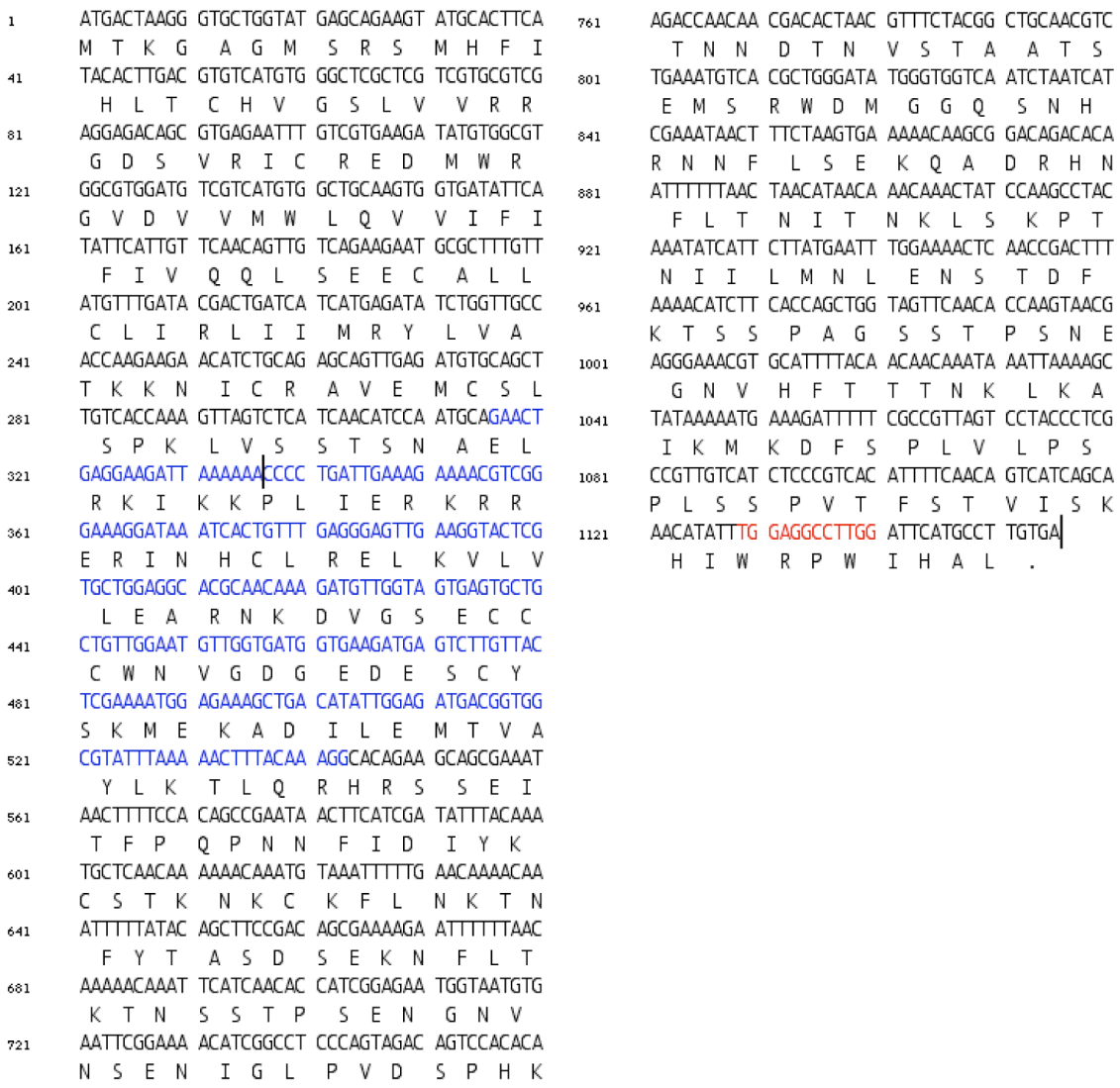


Figure 4.4. Nucleotide and protein sequence of *Hau-hes2*. Full-length coding sequence for *Hau-hes2* extrapolated from gene models in *H. robusta* genome sequence data. Nucleotide numbers are indicated on the left. Labeled domains; Helix loop helix (blue), C-terminal WRPW (red). Vertical black lines mark the boundaries of the region used to make in situ hybridization probe.

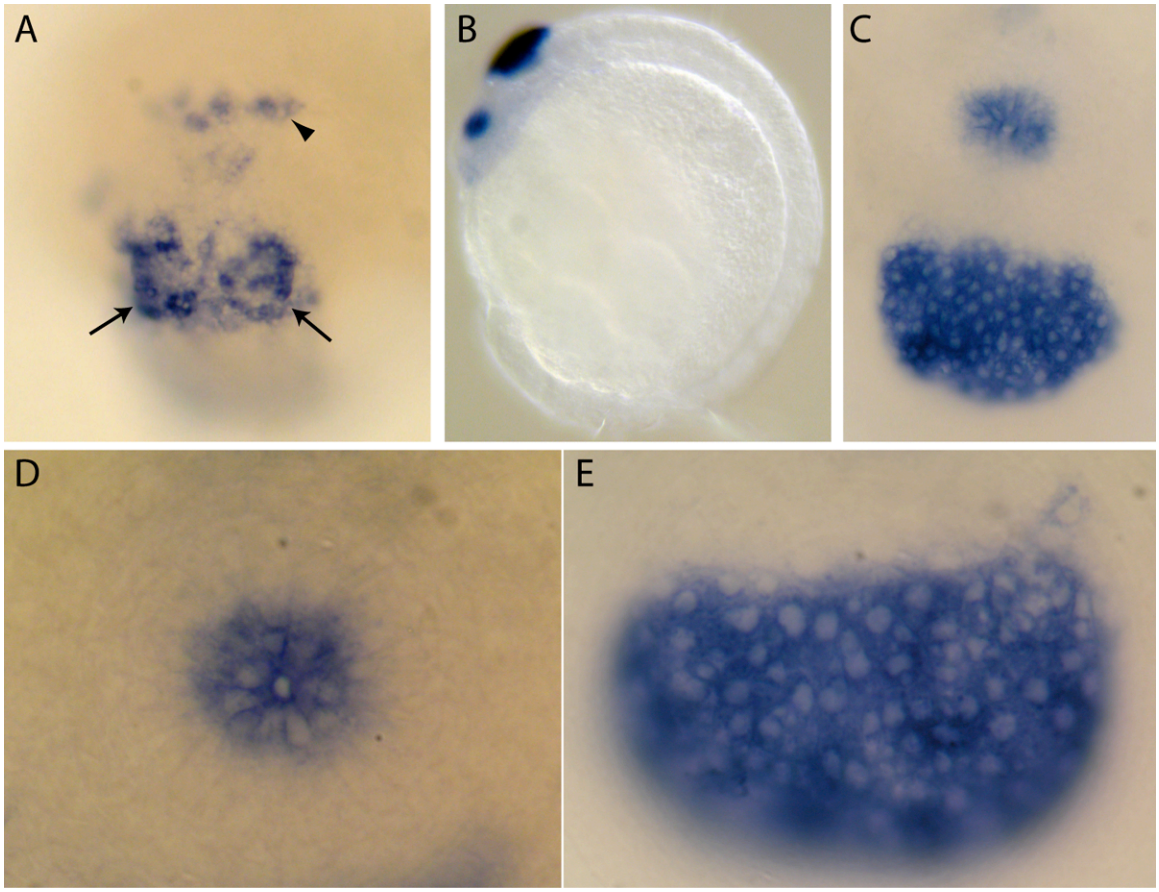


Figure 4.5. Expression of *Hau-hes2* during stages 8 and 9. A. Animal view of a mid-stage 8 embryo focusing on the region anterior to the germinal plate. Bilateral lobes of expressing cells at the anterior of the germinal plate (arrows) and a smaller population of more anterior expressing cells (arrowheads) are visible. B. Lateral view of a stage 9 embryo. C. Dorsal anterior view of expressing cells in embryo pictured in B. D. Close-up view of the anteriormost expressing population which forms a circle of cells in the prostomium. E. Close-up view of ventral posterior population of expressing cells anterior to the germinal plate, which form a cohesive semi-circle shape.

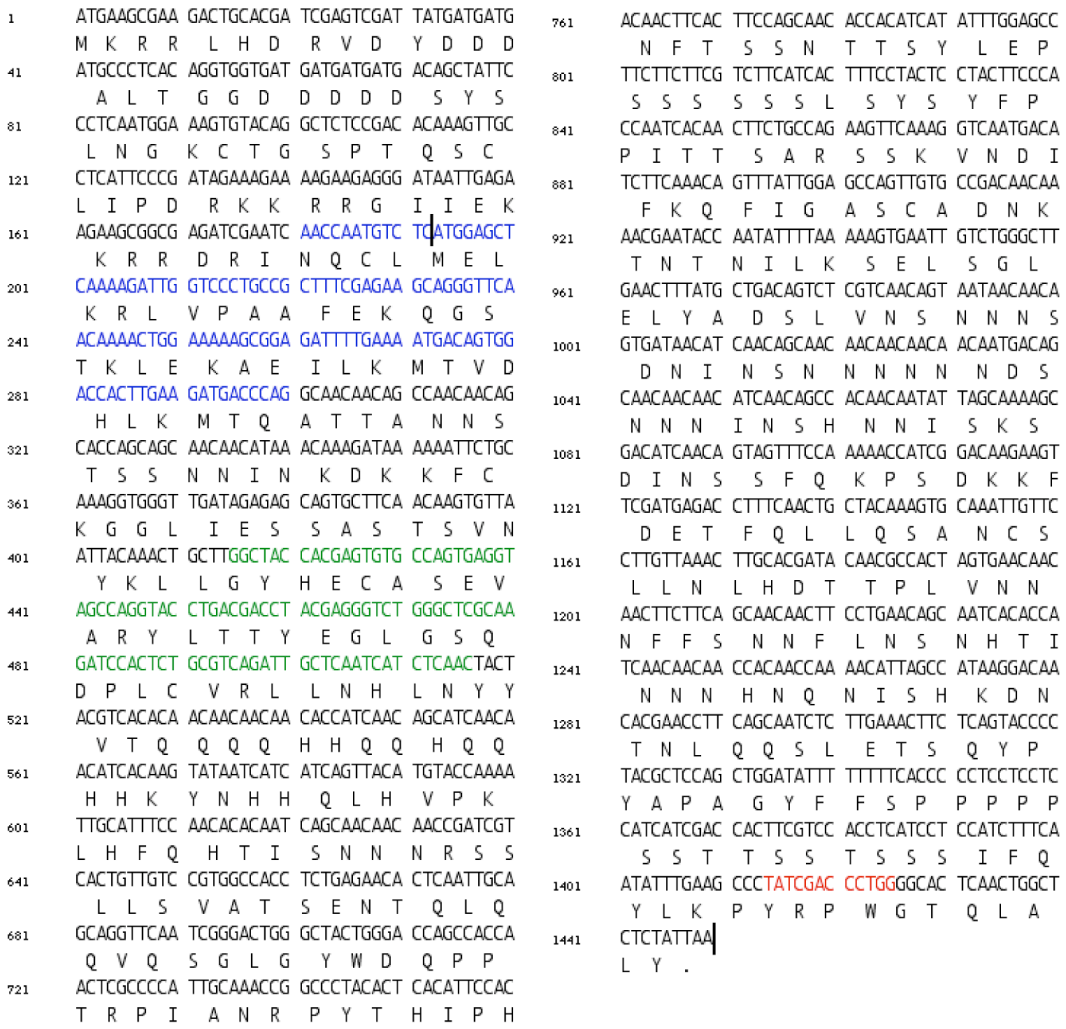


Figure 4.6. Nucleotide and protein sequence of *Hau-hey*. Full-length sequence extrapolated from gene models in the *H. robusta* genome annotation. Nucleotide number indicated on the left. Labeled domains; Helix-loop-helix (blue), orange domain (green), C-terminal YRPW (red). Vertical black lines mark the boundaries of the region used to make in situ hybridization probe.

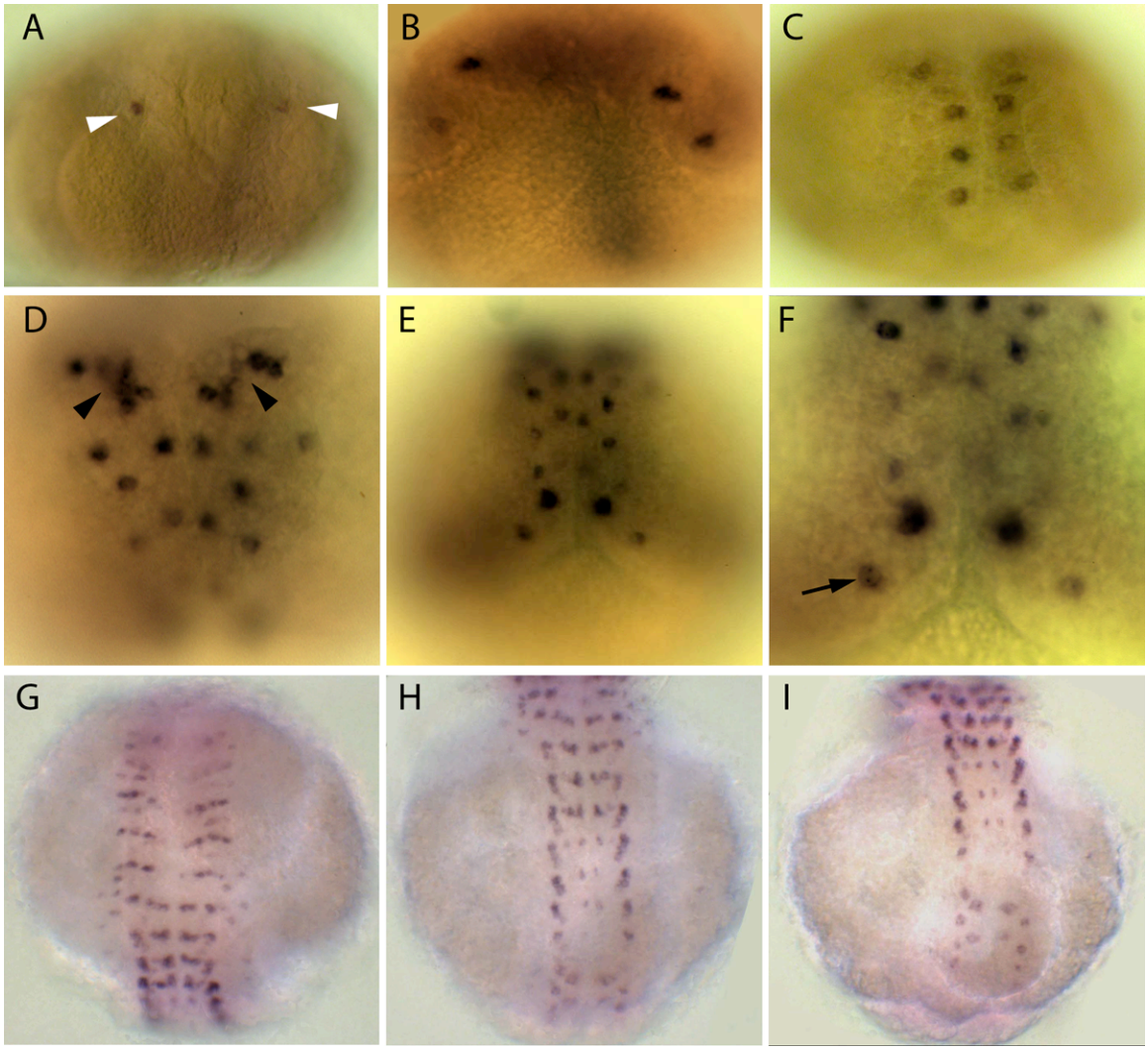


Figure 4.7. Expression of *Hau-hey* during development. A. Animal view of a late stage 7 embryo. Expression is seen in a single cell at the anterior of each of the left and right germinal bands (arrowheads). B. Vegetal view of the left and right germinal bands at late stage 7. There are two pairs of expressing cells. C. Germinal plate of a stage 8 embryo. There are pairs of expressing cells near the midline. D. Anterior portion of the germinal plate of a mid-stage 8 embryo. There are expressing populations of cells anterior to the germinal plate (arrowheads) as well as expressing cells throughout the ectodermal lineages. E. Posterior view of the germinal plate of the embryo shown in D. F. Close-up view of the germinal plate pictured in E. Note the cell with two dots in the nucleus representing active transcription (arrow). G-I. Different regions of the germinal plate of a stage 9 embryo. Dynamic expression is seen throughout the ectodermal lineages at anterior (G), middle (H) and posterior (I) regions.

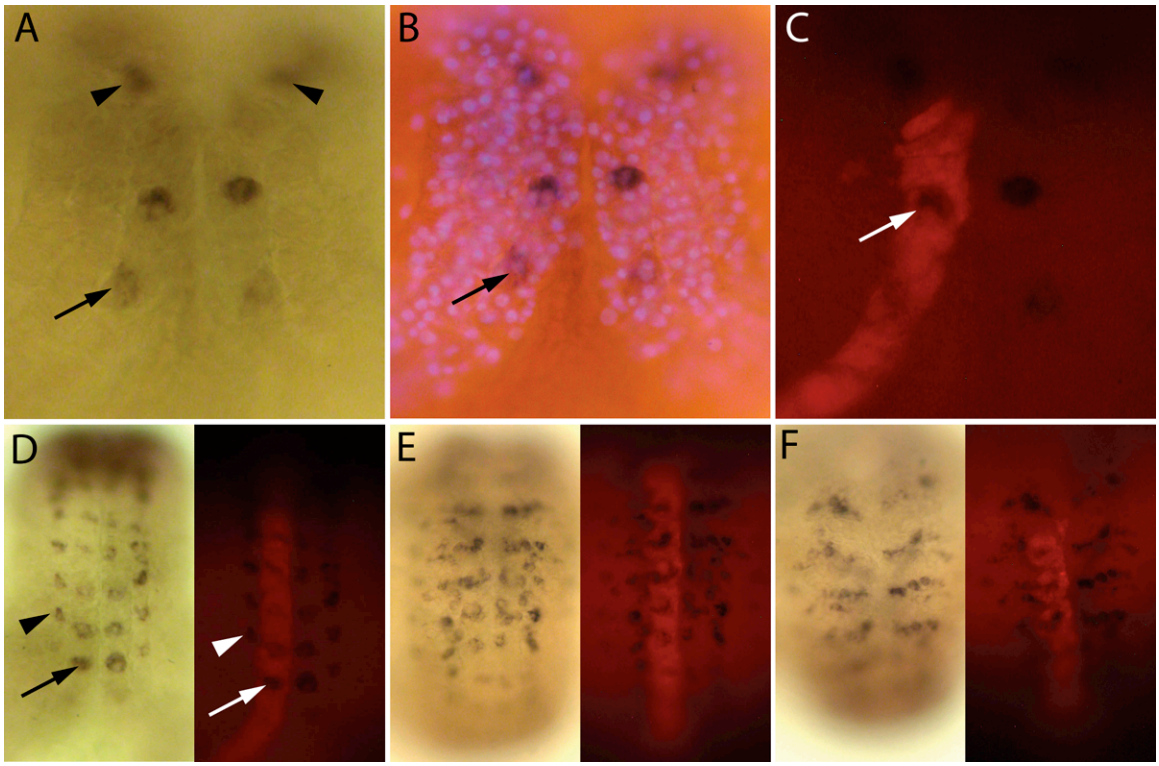


Figure 4.8. Early *Hau-hey* expression in the segmental precursors is first restricted to the N lineage and then expands to the other ectodermal lineages during stage 8-9. A left N teloblast was injected with RDA (red), embryos were cultured to early stage 8 (A-C) and late stage 8 (D-F) and processed for *Hau-hey* in situs. A-C. Forming germinal plate of a mid-stage 8 embryo. Cells anterior to the germinal plate express *Hau-hey* (arrowheads in A). Additionally, pairs of cells begin to express *Hau-hey* as they enter the germinal plate (arrow in A). Based on DAPI staining (blue in B) and lineage tracing (RDA, red in C), it is clear that these pairs of expressing cells are derived from the N lineage (arrow in C). D-F. Different regions of the germinal plate of a late stage 8 embryo. D. Posterior view of the germinal plate. Expressing cells in the N lineage (arrow) and neighboring O lineage (arrowhead) are visible. Middle (E) and anterior (F) views of the germinal plate; expression is seen in the RDA containing N lineage as well as in the other ectodermal lineages.

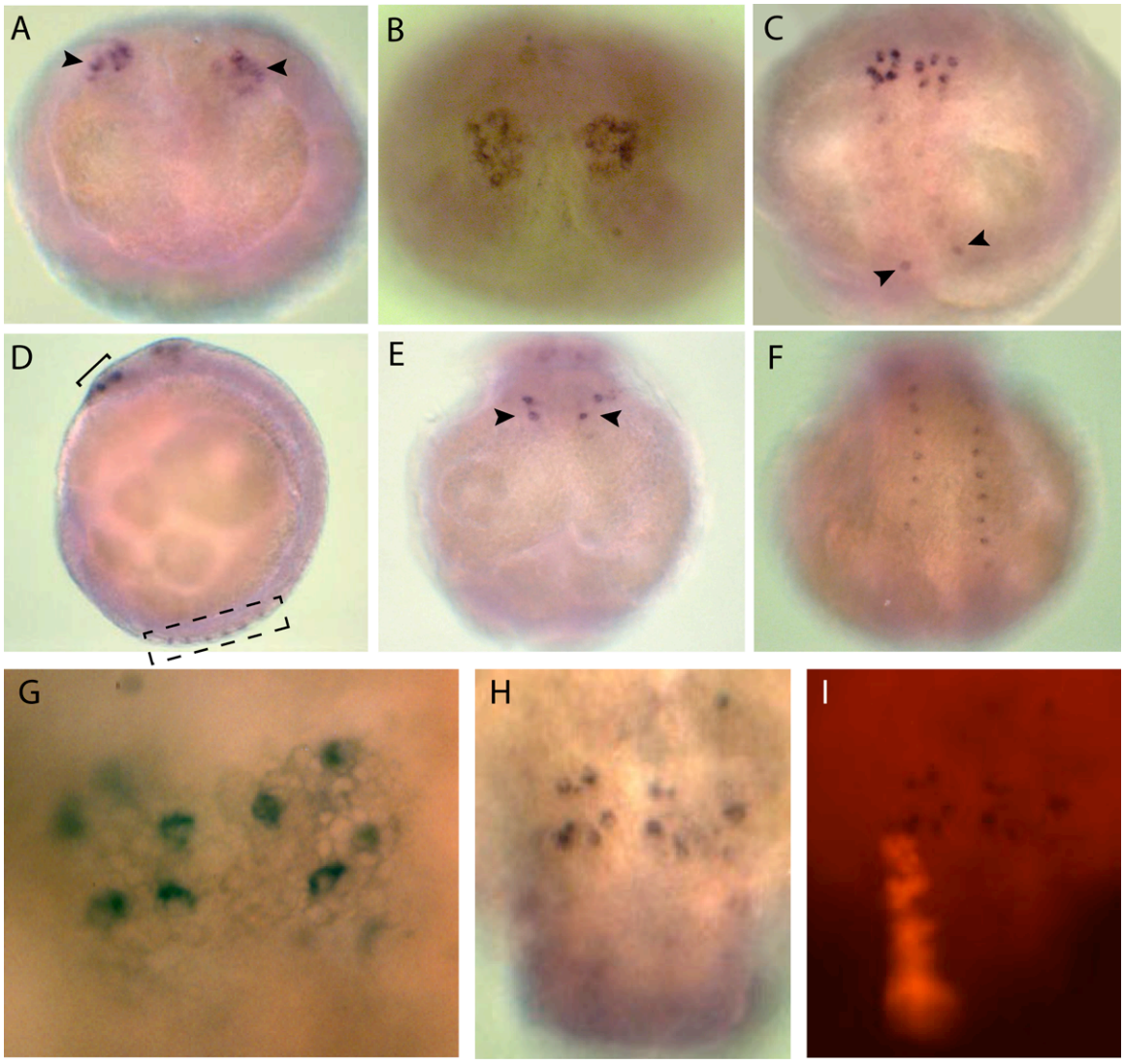


Figure 4.9. Expression of *Hro-notch* during stages late 7 to late 8. A. Animal view of a late stage 7 embryo. Clusters of cells are located at the anterior of the left and right germinal bands (arrowheads). B. View of the left and right germinal bands as they are about to join to form the germinal plate. Bilateral clusters of expressing cells are at the presumptive anterior. C. Germinal plate of a mid stage 8 embryo. Anterior "paws" of expressing cells are visible as are pairs of expressing cells along the midline (arrowheads). D. Lateral view of a late stage 8 embryo, in which germinal plate formation is nearly complete. E. Dorsal view of the embryo in D. Arrowheads indicate anterior expressing cells in the region marked by brackets in D. F. Posterior view of the germinal plate (boxed region in D) showing pairs of expressing cells near the midline. G. Close-up of anterior "paws" of expression in a mid-stage 8 embryo. Brightfield (H) and fluorescent (I) images of a stage 8 embryo whose OP lineage is labeled with RDA (red). *Hau-notch* expressing cells are anterior to the labeled OP lineage.

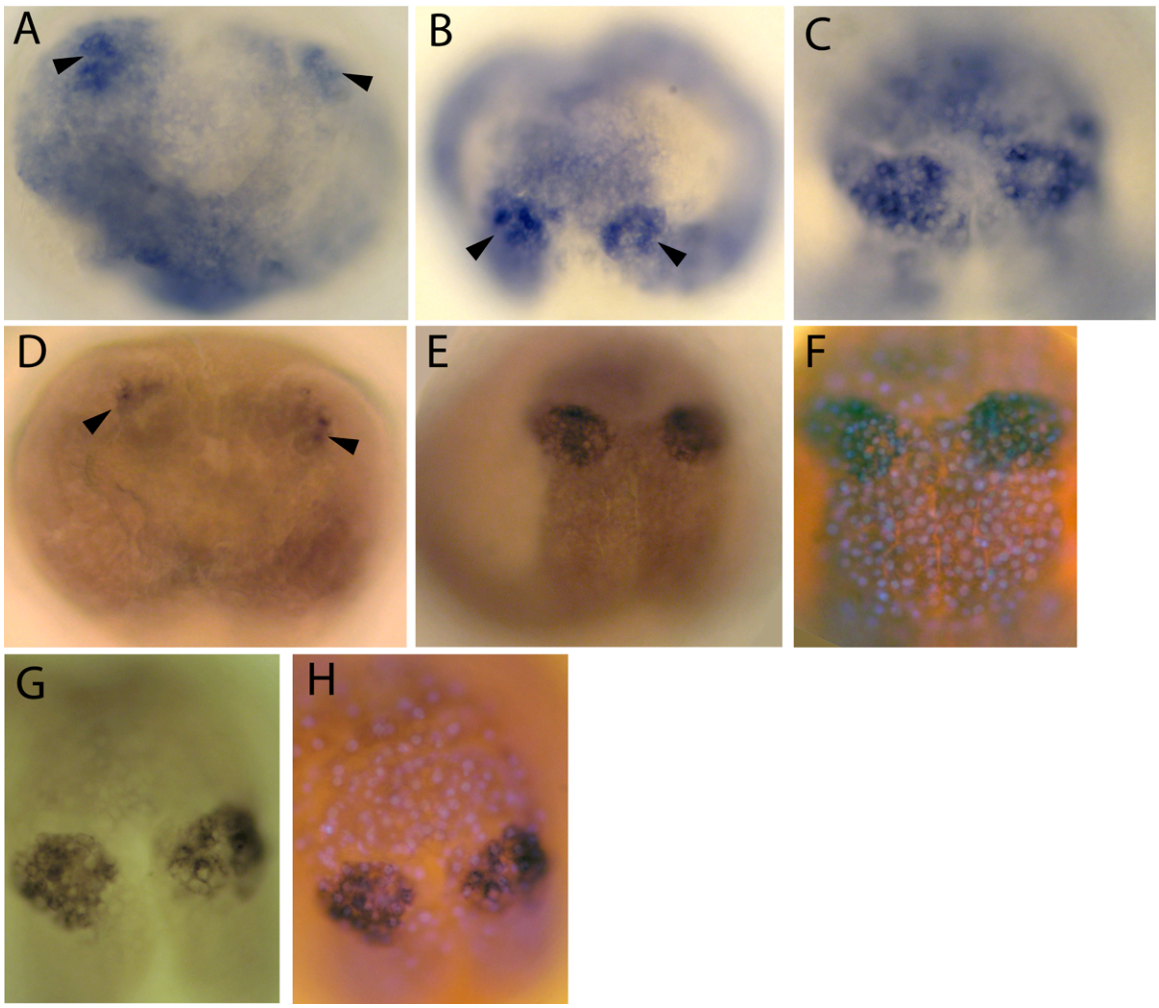


Figure 4.10. ***Hau-suH*, *Hau-ser* and *Hau-notch* show similar domains of expression during late stage 7 through stage 8.**

Figure 4.10. *Hau-suH*, *Hau-ser* and *Hau-notch* show similar domains of expression during late stage 7 through stage 8. A-C. Expression patterns of *Hau-suH*. A. Animal view of a late stage 7 embryo. *Hau-suH* is broadly expressed throughout the left and right germinal bands, with clusters of anterior cells (arrowheads) exhibiting stronger expression. B. Forming germinal plate of an early stage 8 embryo; *Hau-suH* is broadly expressed in the segmental precursors at low levels with stronger expression in anterior clusters of cells (arrowheads). C. Close-up view of anterior clusters of *Hau-suH* expressing cells at the anterior of the germinal plate of a stage 8 embryo. D-F. Expression of *Hau-ser* during late stage 7 and mid-stage 8. D. Animal view of a stage 7 embryo, in which anterior clusters of *Hau-ser* expressing cells are visible (arrowheads). E. Germinal plate of a mid-stage 8 embryo, *Hau-ser* expressing cells are at the anterior of the germinal plate. F. Embryo counterstained with DAPI (blue) to show that ventral clusters of *Hau-ser* expressing cells are anterior to the germinal plate. G-H. Anterior of the germinal plate of an embryo processed for both *Hau-notch* and *Hau-ser* in situs. It can be inferred that the *Hau-notch* expressing cells sit within the larger domain of *Hau-ser* expression, as there are not two separate expressing clusters of cells on each side of the embryo. H. Same embryo as in G showing DAPI (blue) counterstain.

Materials and methods

Embryos

Embryos of *Helobdella* sp. (Austin) collected from Austin, Texas, were obtained from a laboratory breeding colony. Embryos were cultured in HL saline and maintained at 23° C as described in Song et al. (2002). Staging and cell nomenclature are as defined previously (Weisblat and Huang, 2001) for *H. robusta* but there are species differences in the cell cycle rates (Zhang and Weisblat, 2005; Gonsalves and Weisblat, 2007).
Embryos of *Tubifex tubifex* were collected as previously described in (Shimizu, 1982). All *Tubifex* injections were done by Ayaki Nakamoto, who then shipped the fixed embryos to me for imaging.

Isolation of a *Helobdella* histone 2B homolog

A 228 base-pair DNA fragment encoding a portion of histone 2B was amplified by PCR from a commercially prepared, nondirectional cDNA library representing stage 7-10 embryos of *H. robusta* (Stratagene, La Jolla, CA), using degenerate primers (fwd = 5'-CARGTICAYCCIGAYCANGG-3'; rev = 5'-GTRTAYTTIGTIACNGCYTT-3'). This cDNA fragment was cloned into the pGEM-T Easy vector (Promega, Madison, WI) and sequenced. Additional coding sequence of *Hro-h2b*was amplified from the cDNA library using either a 3' or 5' extension primer (3' extension = 5'-GGCTTCTCGCCTCGCCCACTACAACA-3'; 5' extension = 5'-GTTGGCCAACTCGCCGGGTAACAGAA-3') paired with a vector-specific primer (5'-CACTATAGGGCGAATTGGGTACC-3'). Amplicons from these PCR reactions were isolated, cloned into pGEM-T Easy and sequenced. The *Hro-h2b* cDNA sequence was then assembled from the sequences of individually cloned amplicons (Genbank accession #GQ280381) and the *Hro-h2b* DNA fragment to be introduced into pCS107 (Gift from Richard Harland) was amplified from the cDNA library (fwd = 5'-TGGATCCAATGCCACCAAAGCCTGCCAGCAAGGGA-3'; rev = 5'-GGGTCGACCTTTGAGCTGGTGTACTTGGTGACGGC-3'. A BamHI restriction site was introduced at the 5' end of the start codon and the 3' stop codon was replaced with a SalI restriction site.

Construction of pCS107-H2B-eGFP

pCS107-H2B-eGFP was used as the template for in vitro synthesis of mRNA. To construct pCS107-H2B-eGFP, a DNA fragment containing eGFP coding region was first PCR-amplified from pCS2P-eGFP-X/P (Zhang and Weisblat, 2005) using the following primer pair: fwd = 5'-AGCGGCCGCTAGAAGGTGGCGGAATGG-3'; rev = 5'-CTCGAGTTACTTGTACAGCTCGTCCAT-3'. The resulting DNA fragment contains the coding sequence of eGFP flanked by a NotI site and XhoI site at the 5' and 3' ends, respectively. The *egfp* DNA was introduced between the NotI and XhoI sites in the polylinker region of pCS107. *Hro-h2b* DNA was then introduced between the BamHI and SalI sites in the pCS107 polylinker.

Plasmid Constructs

A ~2.3 kb genomic DNA fragment that lies immediately upstream to the EF1alpha coding region was excised from pEF1NASS (Pilon and Weisblat, 1997) using EcoR1 and Xba1, and then purified by electrophoresis and gel extraction. pBSMN, a modified version of pBluescript, with I-SceI sites flanking its multi-cloning sites (Ogino et al., 2006), was digested using EcoR1 and Xba1, treated with phosphatase and then purified by electrophoresis and gel extraction. The EF1alpha promoter fragment was then inserted into the digested pBSMN to create pBSMNEF1P.

pBSMNEF1P was first linearized with the restriction enzyme SalI. The ends of linearized pBSMNEF1P were then blunted by Klenow fragment treatment. The blunted linear pBSMNEF1P was next digested with the restriction enzyme ApaI, yielding 20 bp and 5.3 kb fragments. The 5.3 kb fragment was treated with phosphatase and purified by electrophoresis and gel extraction.

To prepare the insert, the forward primer originally designed for cloning the coding region fragment of *Hro-h2b1* (5'-TGGATCCAATGCCACCAAAGCCTGCCAGCAAGGGA-3') was paired with T3 primer (5'-ATTAACCCTCACTAAAGGGAA-3') to amplify the DNA fragment containing the coding region of H2B:eGFP and SV40 polyadenylation sequence. The PCR reaction was carried out using *Pfu* DNA polymerase (Stratagene), which generates blunt-end PCR products. The PCR product was then digested with ApaI. The ApaI digestion yielded 40 bp and 1.4 kb fragments. The 1.4 kb DNA fragment, containing the H2B:eGFP construct and the SV40 polyadenylation sequence was treated with polynucleotide kinase and purified by electrophoresis and gel extraction. The H2B-eGFP-SV40 DNA fragment was then inserted into the processed pBSMNEF1P to create pEF-H2B:GFP.

pEF-nGFP was built using the same strategy for constructing pEF-H2B:GFP. The nls:eGFP-SV40 fragment was PCR-amplified from pCS2P-nls-eGFP (Zhang and Weisblat, 2005) using *Pfu* DNA polymerase. Forward primer corresponding to the area around the start codon of nls-eGFP (5'-AATGGCTCCAAAGAAGAAGCGT) and T3 primer were used in the PCR reaction. The PCR product was then digested with ApaI, treated with kinase, purified, and inserted into the processed pBSMNEF1P. Hence, the cloning strategy described here appears to be a convenient and widely applicable way for transferring pCS-based molecular constructs into pBSMNEF1P backbone.

Plasmid purification, plasmid injection, mRNA synthesis, and mRNA injection

nGFP mRNA and h2bGFP mRNA were both transcribed in vitro from PCR amplicons generated from pCS2p-nls-eGFP (Zhang and Weisblat, 2005) and pCS107-H2B-eGFP plasmids, respectively, using SP6 and T3 primers. For this application, proofreading *Pfu* DNA polymerase was used for the PCR reaction. mRNA was transcribed from the amplicons using mMESSAGE mMACHINE SP6 kit (Ambion, Austin, TX). The concentration of mRNAs in the needle was 0.5 mg/ml with 8 mg/ml tetramethylrhodamine dextran (RDA; Molecular Probes, Eugene, OR). The final concentration of the plasmid in the injection needle was 96 mg/ml with 3 mg/ml RDA. Plasmids were purified using Qiagen MIDI Prep kits (Qiagen, Germantown, MD). Both mRNA and plasmid were co-injected with RDA lineage tracer. Alexa fluor 647 was injected at a concentration of 1 mg/ml.

Co-injection of plasmid with I-SceI

116 ng/ul of plasmid was preincubated with 0.5 units/ul of I-SceI in 1X buffer (New England Biolabs, Ipswich, MA) at 37° C for 40 minutes in a volume of 5 ul. After incubation, 1 ul of 18 mg/ml RDA solution was added to the digest and the resultant mixture (with a final plasmid concentration of 96 ng/ul) was loaded into glass micropipets for injection.

Microscopy

For time-lapse fluorescence microscopy injected embryos were allowed to develop to desired stages, mounted in HL saline, then examined and photographed using a Nikon E800 epifluorescence microscope equipped with a cooled CCD camera (Princeton Instruments, Trenton, NJ), controlled by MetaMorph software (Molecular Devices, Sunnyvale, CA). For confocal microscopy, embryos were fixed for 1 hr at RT or o/n at 4° C in 0.75x PBS in 4% paraformaldehyde. Images were acquired on a Leica SMRE microscope equipped with a TCS SL scanning head. Stacks of confocal images were processed using Image J (NIH) for color merging, 3D- and Z-projections.

In situ hybridization and immunostaining

Antisense GFP probe was synthesized from linearized pCS2p-nls-eGFP using MEGAscript T7 kit (Ambion, Austin, TX) and hybridization as previously described (Song et al., 2002). All Notch pathway member probes were similarly made using either MEGAscript T7 or SP6 kit as per manufactures instructions (Ambion, Austin, TX). H2B:GFP was visualized by immunostaining of GFP. In short, specimens were first relaxed with relaxation buffer (4.8 mM NaCl, 1.2 mM KCl, 10 mM $MgCl_2$ and 8% EtOH) at 4° C, fixed with 4% formaldehyde in 0.5X phosphate buffered saline at 4° C overnight, washed with 1% Tween-20 in PBS (PBT) several times, and then blocked with 5% normal goat serum and 2% bovine serum albumin in PBT at room temperature for two hours. A rabbit anti-GFP polyclonal antibody (Invitrogen, Carlsbad, CA) was added at a 1:1000 dilution in the blocking solution, and incubated at 4° C overnight. Following several washes with PBT at room temperature, the specimens were placed in blocking solution, and Alexa Fluor 488 conjugated goat anti-rabbit secondary antibody (Invitrogen, Carlsbad, CA) was added at 1:600. The specimens were incubated at 4° C overnight, washed in PBT at room temperature for at least six hours with frequent buffer changes. Immunostaining against histone H1 was done as for GFP with the following changes; mouse monoclonal antibody against histone H1 (Chemicon, MAB052) was used at 1:1000 and alexa fluor 488 conjugated goat anti-mouse secondary was used at 1:500.

Embedding and sectioning

Embryos were stained with DAPI (1:1000) during fixation, then dehydrated through an ethanol series. Dehydrated embryos were washed briefly in ppo then incubated overnight in ppo: poly/Bed 812 1:1 then transferred to Poly/Bed 812. Embryos were then embedded in a modified epoxide embedding resin; a mixture of Poly/Bed 812, 13.5 ul dodencenyl succinic anhydride 27.5 ul and DMP-30 0.7 ul and sectioned by hand using a razor blade.

Cloning of Notch pathway members

To clone the complete coding sequence for *Hau-hes* I amplified the first and second halves of *Hau-hes* separately, with some overlap. Then I chose a restriction site in the overlapping region, digested the amplicons and then ligated the two halves together and PCR amplified the full

length transcript from the ligation. Primers used to amplify the first half :TXRTF ATGTCCTCCAGAGTTTCGCGAG and hesgenR1 TGAGCTTTGTTCGTCATTGC
Primers used to amplify the second half: hestxf2 CTCCGAAACAACCCATCTTCC and TXRTR TTAAAACGGCCTCCAGACGTTC
Both amplicons were digested with BSSHII and then ligated together with T4 DNA ligase high concentration. Primers used for PCR amplification of the full-length *Hau-hes*: TXRTF ATGTCCTCCAGAGTTTCGCGAG and TXRTR TTAAAACGGCCTCCAGACGTTC

Hau-hes2 was cloned using the following primers, heswrpwF4 CCCCTGATTGAAAGAAAACGTCGG and heswrpwR1 GCAATGACGAACAAAGCTCA to clone a fragment around 800 bp in length.

Hau-hey was amplified using the primers heyF1 ATGGAGCTCAAAAGATTGGTCC and heyR1 TTAATAGAGAGCCAGTTGAGTGC. The resulting fragment was approximately 1.3 kb in length

Hau-suH was amplified using the primers suHFLF3 ATGGCCGAGTATTTGAGGTGTC and suHR5 CTGCAGGGGTTCTCTGA. The resulting amplicon was approximately 1100 kb in length.

Hau-serrate was cloned by Dian-Han Kuo from genomic DNA using the primer pair dhk255serratefw CGACAAAATTAAGCGGGGTAGTAA dhk256serratere CACAGACAATCAACGCTGAATAGA. The resulting amplicon was 2115 bp in length including introns.

All amplicons were ligated into pGEMT-Easy as per manufactures instructions (Promega).

Developmental RT-PCR
Each representative stage contained 50 embryos in 100ul of trizol. Tubes were stored at -80°C until all embryos were collected. Trizol was added to all tubes up to a volume of 500ul once thawed. RNA extraction protocol: Add 100ul choloroform, mix, incubate at RT for 10 minutes, centrifuge at 12,000 g for 15 minutes, transfer aqueous phase to new tube, add 1 ul glycogen, add 250 ul isopropanol, vortex 10 seconds, incubate at RT 10 min, spin at 12,000g for 8 min at 4°C, wash with 500 ul of 75% EtOH, spin at 7,500g for 5 min. Dissolve pellet in 19ul H_2O.
Reverse transcriptase reaction
19ul RNA, 2ul dNTPs, 4ul random hexamers. Incubate mixture at 75°C for three minutes then quickly chill. Then add 8ul 5x buffer, 4ul 0.1 M DTT, 2ul RNAsein and 1ul of Superscript II RT (Invitrogen, Inc.). Reaction was incubated at 42°C for 2 hours.
PCR on cDNA as follows:
All primers were designed to span an intron to control for contamination of genomic DNA. Primer pairs and length of expected amplicon are as follows:

Hau-notch:
NotchRTF1 AACAAACCCTTCCTACCTGGC NotchRTR1 CTTCGTGCTATGAGATTACAG 153 bp

Hau-hes:
hairy12RT ATCAAGAAGCCAATAATAGAG hairy 13 CTGTAATCTCATAGCACGAAG
183 bp

Hau-hes2:
heswrpwRTF1 CACTGTTTGAGGGAGTTGAAG heswrpwRTR1
GGTCTTGTGTGGACTGTCTAC 393 bp

Hau-suH:
F8 AGTTGGTTTGCGTTGAAACCG R4 GATCCACTCTGCGTCAGATTG
548 bp

Hau-hey:
heyF1 ATGGAGCTCAAAAGATTGGTCC
heyRTR1 CAATCTGACGCAGAGTGGATC 309 bp

Hau-ser:
serrateRTF1 GATGACTATCAGTGCCAGTGTC serrateRTR1
CATTGCGAGGGACAGATGCAC 546 bp
Cloning of *Hau-ser* was done by Dian-Han Kuo

For 18srRNA used classic primers 18s par "primer pair" and 18s competamers (Ambion, Inc.) 450bp

Cycling parameters for the amplification were: 95°C (10 min), 95°C (30 sec), 55°C (30 sec), 72°C (1 min) for 30 cycles.

Protein alignment
Protein sequences used for Clustal-X alignment (only those sequences are listed that were available through NCBI)
Drosophila melanogaster hairy, isoform A NP_523977 GI:24661088
Tribolium castaneum hairy NP_001107765 XP_971935 GI:166796106
Cupiennius salei hairy CAB89491.1 GI:7671520
Mus musculus hes1 NP_032261.1 GI:6680205
Capitella teleta hairy (hes1) ABD48946.1 GI:88698206
Capitella teleta hes2 ACD84803.1 GI:189212387
Danio rerio hey1 NP_997726.1 GI:47086903
Mus musculus hesr1 Q9WV93.1 GI:13124297
Capitella teleta hesr2 ACD84805.1 GI:189212391
Capitella teleta hes3 ACD84804.1 GI:189212389
Helobdella robusta hes AAN52160.1 GI:37720825

References

Aguinaldo AM, Turbeville JM, Linford LS, Rivera MC, Garey JR, Raff RA, Lake JA. 1997. Evidence for a clade of nematodes, arthropods and other moulting animals. *Nature* 387:489-493.

Aranda M, Marques-Souza H, Bayer T, Tautz D. 2008. The role of the segmentation gene hairy in Tribolium. *Dev Genes Evol* 218:465-477.

Baek JH, Hatakeyama J, Sakamoto S, Ohtsuka T, Kageyama R. 2006. Persistent and high levels of Hes1 expression regulate boundary formation in the developing central nervous system. *Development* 133:2467-2476.

Baker MW, Macagno ER. 2006. Characterizations of Hirudo medicinalis DNA promoters for targeted gene expression. *J Neurosci Methods* 156:145-153.

Baker MW, Macagno ER. 2007. In vivo imaging of growth cone and filopodial dynamics: evidence for contact-mediated retraction of filopodia leading to the tiling of sibling processes. *J Comp Neurol* 500:850-862.

Baker MW, Peterson SM, Macagno ER. 2008. The receptor phosphatase HmLAR2 collaborates with focal adhesion proteins in filopodial tips to control growth cone morphology. *Dev Biol* 320:215-225.

Bissen ST, Weisblat DA. 1989. The durations and compositions of cell cycles in embryos of the leech, Helobdella triserialis. *Development* 106:105-118.

Blair SS, Weisblat DA. 1984. Developmental interdeterminancy in embryos of the leech Helobdella triserialis. *Dev Biol* 101:326-335.

Bouche ML, Biagianti-Risbourg S, Vernet G. 1997. A light and scanning electron microscope study of the morphology of the chaetae of Tubifex tubifex in a non-polluted medium. *Hydrobiologia* 411:39-44.

Boyer BC, Henry JJ, Martindale MQ. 1998. The cell lineage of a polyclad turbellarian embryo reveals close similarity to coelomate spiralians. *Dev Biol* 204:111-123.

Bray S, Furriols M. 2001. Notch pathway: making sense of suppressor of hairless. *Curr Biol* 11:375-385.

Budd GE. 2001. Why are arthropods segmented? *Evol Dev* 3:332-42.

Chi C. 1996. *Freckle Cells, an Unique Population of Non-Segmental Mesoderm Found During Early Leech Development*. Berkeley, California: Thesis, Department of Molecular and Cellular Biology, University of Caifornia, Berkeley. 20 p.

Chipman AD, Akam M. 2008. The segmentation cascade in the centipede Strigamia maritima: involvement of the Notch pathway and pair-rule gene homologues. *Dev Biol* 319:160-169.

Cho SJ, Valles Y, Giani VC Jr, Seaver EC, Weisblat DA. 2010. Evolutionary dynamics of the Wnt gene family: a lophotrochozoan perspective. *Mol Biol Evol* ahead of print.

Clement AC. 1962. Development of Ilyanassa following the removal of the D macromere at successive cleavage stages. *J Exp Zool* 149:193–216.

Conklin EG. 1897. The embryology of Crepidula. *J Morph* 13:1-226.

Cooke J, Zeeman EC. 1976. A clock and wavefront model for control of the number of repeated structures during animal morphogenesis. *J Theor Biol* 58:455-476.

Costello DP, Henley C. 1976. Spiralian development: A perspective. *Amer Zool* 16:227-291.

Damen WG, Weller M, Tautz D. 2000. Expression patterns of hairy, even-skipped, and runt in the spider Cupiennius salei imply that these genes were segmentation genes in a basal arthropod. *Proc Natl Acad Sci* 97:4515-4519.

Dawson SR, Turner DL, Weintraub H, Parkhurst SM. 1995. Specificity for the hairy/enhancer of split basic helix-loop-helix (bHLH) proteins maps outside the bHLH domain and suggests two separable modes of transcriptional repression. *Mol Cell Biol* 15:6923-6931.

Desjeux I, Price DJ. 1999. The production and elimination of supernumerary blast cells in the leech embryo. *Dev Genes Evol* 209:284-293.

Dohle W. 1999. The ancestral cleavage pattern of the clitellates and its phylogenetic deviations. *Hydrobiologia* 402:267-283.

Dunn CW, Hejnol A, Matus DQ, Pang K, Browne WE, Smith SA, Seaver E, Rouse GW, Obst M, Edgecombe GD, Sørensen MV, Haddock SH, Schmidt-Rhaesa A, Okusu A, Kristensen RM, Wheeler WC, Martindale MQ, Giribet G. 2008. Broad phlyogenomic sampling improves resolution of the animal tree of life. *Nature* 452:745-749.

Fernandez J, Stent GS. 1980. Embryonic development of the glossiphoniid leech Theromyzon rude: structure and development of the germinal bands. *Dev Biol* 78:407-434.

Freeman, Lundelius JW. 1992. Evolutionary implications of the mode of D quadrant specification in coelomates with spiral cleavage. *J Evol Biol* 5:205-247.

Geling A, Steiner H, Willem M, Bally-Cuif L, Haass C. 2002. A gamma-secretase inhibitor blocks Notch signaling in vivo and causes a severe neurogenic phenotype in zebrafish. *EMBO Rep* 3:688-694.

Gimlich RL, Braun J. 1985. Improved fluorescent compounds for tracing cell lineage. *Dev Biol* 109:509-514.

Giudicelli F, Lewis J. 2004. The vertebrate segmentation clock. *Curr Opin Genet Dev* 14:407-414.

Gline SE, Kuo DH, Stolfi A, Weisblat DA. 2009. High resolution cell lineage tracing reveals developmental variability in leech. *Dev Dyn* 238:3139-3151.

Gleiser L, Stent, GS. 1993. Developmental origin of segmental identity in the leech mesoderm. *Development* 117:177-189.

Gonsalves FC. 2006. Signaling, Transcription and Trascript stability during early embryonic development of the leech, *Helobdella robusta*. Berkeley, California: Thesis, Department of Molecular and Cellular Biology, University of California, Berkeley. 130 p.

Gonsalves FC, Weisblat DA. 2007. MAPK regulation of maternal and zygotic Notch transcript stability in early development. *Proc Natl Acad Sci USA* 104:531-536.

Goto A, Kitamura K, Arai A, Shimizu T. 1999. Cell fate analysis of teloblasts in the Tubifex embryo by intracellular injection of HRP. *Dev Growth Differ* 41:703-713.

Goto A, Kitamura K, Shimizu T. 1999. Cell lineage analysis of pattern formation in the Tubifex embryo. I. Segmentation in the mesoderm. *Int J Dev Biol* 43:317-327.

Gratton MO, Torban E, Jasmin SB, Theriault FM, German MS, Stifani S. 2003. Hes6 promotes cortical neurogenesis and inhibits Hes1 transcription repression activity by multiple mechanisms. *Mol Cell Biol* 23:6922-6935.

Halanych KM, Bacheller JD, Aguinaldo AM, Liva SM, Hillis DM, Lake JA. 1995. Evidence from 18S ribosomal DNA that the lophophorates are protostome animals. *Science* 267:1641-1643.

Hejnol A, Martindale MQ, Henry JQ. 2007. High-resolution fate map of the snail Crepidula fornicata: the origins of ciliary bands, nervous system, and muscular elements. *Dev Biol* 305:63-76.

Hejnol A, Obst M, Stamatakis A, Ott M, Rouse GW, Edgecombe GD, Martinez P, Baguñà J, Bailly X, Jondelius U, Wiens M, Müller WE, Seaver E, Wheeler WC, Martindale MQ, Giribet G, Dunn CW. 2009. Assessing the root of bilaterian animals with scalable phylogenomic methods. Proc Biol Sci 276:4261-4270.

Henry JJ, Martindale MQ. 1998. Conservation of the spiralian developmental program: cell lineage of the nemertean, Cerebratulus lacteus. *Dev Biol* 201:253-269.

Henry JJ, Martindale MQ. 1999. Conservation and innovation in spiralian development. *Hydrobiologia* 402:255-265.

Henry J. 2002. Conserved mechanism of dorsoventral axis determination in equal-cleaving spiralians. *Dev Biol* 248:343-355.

Henry JJ, Perry KJ. 2008. MAPK activation and the specification of the D quadrant in the gastropod mollusc, Crepidula fornicata. *Dev Biol* 313:181-195.

Hirata H, Yoshiura S, Ohtsuka T, Bessho Y, Harada T, Yoshikawa K, Kageyama R. 2002. Oscillatory expression of the bHLH factor Hes1 regulated by a negative feedback loop. *Science* 298:840-843.

Huang FZ, Bely AE, Weisblat DA. 2001. Stochastic WNT signaling between nonequivalent cells regulates adhesion but not fate in the two-cell leech embryo. *Curr Biol* 11:1-7.

Huang FZ, Kang D, Ramirez-Weber F-A, Bissen ST, Weisblat DA. 2002. Micromere lineage in the glossiphoniid leech Helobdella. *Development* 129:719-732.

Isaksen DE, Liu NJ, Weisblat DA. 1999. Inductive regulation of cell fusion in leech. *Development* 126:3381-3390.

Kadner D, Stollewerk A. 2004. Neurogenesis in the chilopod Lithobius forficatus suggests more similarities to chelicerates than to insects. *Dev Genes Evol* 214:367-379.

Kageyama R, Ohtsuka T, Kobayashi T. 2007. The Hes gene family: repressors and oscillators that orchestrate embryogenesis. *Development* 143:1243-1251.

Kageyama R, Ohtsuka T, Kobayashi T. 2008. Role of Hes genes in neural development. *Dev Growth Differ* 50 Suppl 1:S97-103.

Kang D, Pilon M, Weisblat DA. 2002. Maternal and zygotic expression of a nanos-class gene in the leech Helobdella robusta: primordial germ cells arise from segmental mesoderm. *Dev Biol* 245:28-41.

Kang D, Huang F, Li D, Shankland M, Gaffield W, Weisblat DA. 2003. A hedgehog homolog regulates gut formation in leech (Helobdella). *Development* 130:1645-1657.

Kramer AP, Weisblat DA. 1985. Developmental neural kinship groups in the leech. *J Neurosci* 5:388-407.

Kuo DH, Shankland M. 2004. Evolutionary diversification of specification mechanisms within the O/P equivalence group of the leech genus Helobdella. *Development* 131:5859-5869.

Kuo DH, Shankland M. 2004. A distinct patterning mechanism of O and P cell fates in the development of the rostral segments of the leech Helobdella robusta: implications for the evolutionary dissociation of developmental pathway and morphological outcome. *Development* 131:105-115.

Lambert JD, Nagy LM. 2001. MAPK signaling by the D quadrant embryonic organizer of the mollusc Ilyanassa obsoleta. *Development* 128:45-56.

Lambert JD, Nagy LM. 2003. The MAPK cascade in equally cleaving spiralian embryos. *Dev Biol* 263:231-241.

Lambert JD. 2008. Mesoderm in spiralians: the organizer and the 4d cell. *J Exp Zool B Mol Dev Evol* 310:15-23.

Lambert JD. 2010. Developmental patterns in spiralian embryos. *Curr Biol* 20:R72-77.

Leimeister C, Externbrink A, Klamt B, Gessler M. 1999. Hey genes: a novel subfamily of hairy- and Enhancer of split related genes specifically expressed during mouse embryogenesis. *Mech Dev* 85:173-177.

Lewis J. 2003. Autoinhibition with transcriptional delay: a simple mechanism for the zebrafish somitogenesis oscillator. *Curr Biol* 13:1398-1408.

Lewis J, Hanisch A, Holder M. 2009. Notch signaling, the segmentation clock, and the patterning of vertebrate somites. *J Biol* 8:44.

Lyons DC, Weisblat DA. 2009. D quadrant specification in the leech Helobdella: actomyosin contractility controls the unequal cleavage of the CD blastomere. *Dev Biol* 334:46-58.

Macagno ER. 1980. Number and distribution of neurons in leech segmental ganglia. *J Comp Neurol* 190:283-302.

Martindale MQ. 1986. The organizing role of the D quadrant in an equal-cleaving spiralian, Lymnaea stagnalis as studied by UV laser deletion of macromeres at intervals between 3rd and 4th quartet formation. *Int J Invertebrate Reproduction* 9:229–242.

Muller K, Nicholls J, Stent G. 1981. *Neurobiology of the Leech*. Cold Spring Harbor, New York: Cold Spring Harbor Laboratory Press. 320 p.

Nakamoto A, Arai A, Shimizu T. 2000. Cell lineage analysis of pattern formation in the Tubifex embryo. II. Segmentation in the ectoderm. *Int J Dev Biol* 44:797-805.

Nardelli-Haefliger D, Shankland M. 1993. *Lox10*, a member of the *NK-2* homeobox gene class, is expressed in a segmental pattern in the endoderm and in the cephalic nervous system of the leech Helobdella. *Development* 118:877-892.

Nelson BH, Weisblat DA. 1991. Conversion of ectoderm to mesoderm by cytoplasmic extrusion in leech embryos. *Science* 253:435-438.

Nelson BH, Weisblat DA. 1992. Cytoplasmic and cortical determinants interact to specify ectoderm and mesoderm in the leech embryo. *Development* 115:103-115.

Nielson C. 2001. Animal Evolution: Interrelationships of the Living Phyla 2nd Edition. Oxford University Press. 1-578.

Noden DM, Schneider RA. 2006. Neural crest cells and the community of plan for craniofacial development: historical debates and current perspectives. *Adv Exp Med Biol* 589:1-23.

Ogino H, McConnell WB, Grainger RM. 2006. High-throughput transgenesis in Xenopus using I-SceI meganuclease. *Nat Protoc* 1:1703-1710.

Palmerim I, Henrique D, Ish-Horowicz D, Pourquie O. 1997. Avian hairy gene expression identifies a molecular clock linked to vertebrate segmentation and somitogenesis. *Cell* 91:639-648.

Paroush Z, Finley RL Jr, Kidd T, Wainwright SM, Ingham PW, Brent R, Ish-Horowicz D. 1994. Groucho is required for Drosophila neurogenesis, segmentation, and sex determination and interacts directly with hairy-related bHLH proteins. *Cell* 79:805-815.

Phillips AJ, Arauco-Brown R, Oceguera-Figueroa A, Gomez GP, Beltrán M, Yi-Te, L, Siddall, M. 2010. *Tyrannobdella rex* N. Gen. N. Sp. and the Evolutionary Origins of Mucosal Leech Infestations. *PLoS ONE* 5(4): e10057.

Pilon M, Weisblat DA. 1997. A *nanos* homolog in leech. *Development* 124:1771-1780.

Price AL, Modrell MS, Hannibal RL, Patel NH. 2009. Mesoderm and ectoderm lineages in the crustacean Parhyale hawaiensis display intra-germ layer compensation. *Dev Biol*

Rabinowitz JS, Chan XY, Kinglsey EP, Duan Y, Lambert, JD. 2008. Nanos is required in somatic blast cell lineages in the posterior of a mollusk embryo. *Curr Biol* 18: 331-336.

Rasmussen JP, English K, Tenlen JR, Priess JR. 2008. Notch signaling and morphogenesis of single-cell tubes in the C. elegans digestive tract. *Dev Cell* 14:559-569.

Ren X, Weisblat DA. 2006. Asymmetrization of first cleavage by transient disassembly of one spindle pole aster in the leech Helobdella robusta. *Dev Biol* 292:103-115.

Rivera AS, Gonsalves FC, Song MH, Norris BJ, Weisblat DA. 2005. Characterization of Notch-class gene expression in segmentation stem cells and segment founder cells in Helobdella robusta (Lophotrochozoa; Annelida; Clitellata; Hirudinida; Glossiphoniidae). *Evol Dev* 6:588-599.

Rivera AS. 2006. A role for Notch signaling during segmentation of the leech, *Helobdella robusta*, a lophotrochozoan. Berkeley, California: Thesis, Department of Molecular and Cellular Biology, University of California, Berkeley. 121 p.

Rivera AS, Weisblat DA. 2009. And Lophotrochozoa makes three: Notch/Hes signaling in annelid segmentation. *Dev Genes Evol* 219:37-43.

Roignant JY, Treisman, JE. 2009. Pattern formation in the Drosophila eye disc. *Int J Dev Biol* 53:795-804.

Sandig M, Dohle W. 1988. The cleavage pattern in the leech Theromyzon tessulatum (Hirudinea, Glossiphoniidae). *J Morphol* 196:217-252.

Sakamoto M, Hirata H, Ohtsuka T, Bessho Y, Kageyama R. 2003. The basic helix-loop-helix genes Hesr1/Hey1 and Hesr2/Hey2 regulate maintenance of neural precursor cells in the brain. *J Biol Chem* 278:44808:44815.

Sawyer R. 1986. Leech Biology and Behavior. Clarendon Press Oxford pg. 1-809.

Schnabel R, Hutter H, Moerman D, Schnabel H. 1997. Assessing normal embryogenesis in Caenorhabditis elegans using a 4D microscope: variability of development and regional specification. *Dev Biol* 184:234-265.

Scholtz G. 2002. The Articulata hypothesis-or what is a segment? *Org Divers Evol* 2:197-215.

Scholtz G, Edgecombe GD. 2006. The evolution of arthropod heads: reconciling morphological, developmental and palaeontological evidence. *Dev Genes Evol* 216: 395-415.

Shankland M. 1987a. Differentiation of the O and P cell lines in the embryo of the leech. I. Sequential commitment of blast cell sublineages. *Dev Biol* 123:85-96.

Shankland M. 1987b. Differentiation of the O and P cell lines in the embryo of the leech. II. Genealogical relationship of descendant pattern elements in alternative developmental pathways. *Dev Biol* 123:97-107.

Shankland M, Savage RM. 1997. Annelids, the segmented worms. In: Gilbert SF, Raunio AM, editors. *Embryology: Constructing the Organism*. Sunderland, MA: Sinauer. pp 219-235.

Shankland M, Weisblat DA. 1984. Stepwise commitment of blast cell fates during the positional specification of the O and P cell lines in the leech embryo. *Dev Biol* 106:326-342.

Shefi O, Simonnet C, Baker MW, Glass JR, Macagno ER, Groisman A. 2006. Microtargeted gene silencing and ectopic expression in live embryos using biolistic delivery with a pneumatic capillary gun. *J Neurosci* 26:6119-6123.

Shimizu T. 1982. Development in the freshwater oligochaete Tubifex. In: Harrison FH, Cowden RR (eds) Developmental biology of freshwater invertebrates. Liss, New York 283–316

Smith CM, Weisblat DA. 1994. Micromere fate maps in leech embryos: lineage-specific differences in rates of cell proliferation. *Development* 120:3427-3438.

Song MH, Huang FZ, Chang GY, Weisblat DA. 2002. Expression and function of an *even-skipped* homolog in the leech Helobdella robusta. *Development* 129:3681-3692.

Song MH, Huang FZ, Gonsalves FC, Weisblat DA. 2004. Cell cycle-dependent expression of a hairy and Enhancer of split (hes) homolog during cleavage and segmentation in leech embryos. *Dev Biol* 269:183-195.

Stent GS. 1999. Introduction to the leech. Cell lineage and fate determination. Edited by SA Moody. Academic press, San Diego. Pp. 173-184.

Stollewerk A, Schoppmeier M, Damen WG. 2003. Involvement of Notch and Delta genes in spider segmentation. *Nature* 423:863-865.

Sulston JE, Schierenberg E, White JG, Thomson JN. 1983. The embryonic cell lineage of the nematode Caenorhabditis elegans. *Dev Biol* 100:64-119.

Taelman V, Van Wayenbergh R, Sölter M, Pichon B, Pieler T, Christophe D, Bellefroid EJ. 2004. Sequences downstream of the bHLH domain of the Xenopus hairy-related transcription factor-1 act as an extended dimerization domain that contributes to the selection of the partners. *Dev Biol* 276:47-63.

Thamm K, Seaver EC. 2008. Notch signaling during larval and juvenile development in the polychaete annelid Capitella sp. I. *Dev Biol* 320:304-318.

van den Biggelar JA. 1977. Development of dorsoventral polarity and mesentoblast determination in Patella vulgata. *J Morphol* 154:157-186.

van den Biggelaar JA, Guerrier P. 1979. Dorsoventral polarity and mesentoblast determination as concomitant results of cellular interactions in the mollusk Patella vulgata. *Dev Biol* 68:462-471.

van den Biggelaar JA, Haszprunar G. 1996. Cleavage patterns and mesentoblast formation in the gastropoda: an evolutionary perspective. *Evolution* 50:1520-1540.

Weisblat DA, Blair SS. 1984. Developmental interderterminacy in embryos of the leech Helobdella triserialis. *Dev Biol* 101:326-335.

Weisblat DA, Harper G, Stent GS, Sawyer RT. 1980. Embryonic cell lineages in the nervous system of the glossiphoniid leech Helobdella triserialis. *Dev Biol* 76:58-78.

Weisblat DA, Huang FZ. 2001. An overview of glossiphoniid leech development. *Can J Zool* 79:218-232.

Weisblat DA, Kim SY, Stent GS. 1984. Embryonic origins of cells in the leech Helobdella triserialis. *Dev Biol* 104:65-85.

Weisblat DA, Harper G, Stent GS, Sawyer RT. 1980. Embryonic cell lineages in the nervous system of the glossiphoniid leech Helobdella triserialis. *Dev Biol* 76:58- 78.

Weisblat DA, Sawyer RT, Stent GS. 1978. Cell lineage analysis by intracellular injection of a tracer enzyme. *Science* 202:1295-1298.

Weisblat DA, Shankland M. 1985. Cell lineage and segmentation in the leech. *Phil Trans R Soc Lond B* 312:39-56.

Whitman CO. 1878. The embryology of Clepsine. *Q J Microsc Sci* 18:213-315.

Wilson EB. 1892. A cell-lineage of Nereis: a contribution to the cytogeny of the annelid body. *J Morph* 6:361-481.

Zackson SL. 1982. Cell clones and segmentation in leech development. *Cell* 31:761-770.

Zackson SL. 1984. Cell lineage, cell-cell interaction, and segment formation in the ectoderm of a glossiphoniid leech embryo. *Dev Biol* 104:143-160.

Zhang SO, Weisblat DA. 2005. Applications of mRNA injections for analyzing cell lineage and asymmetric cell divisions during segmentation in the leech Helobdella robusta. *Development* 132:2103-2113.